ROLE OF TNF-ALPHA IN SKELETAL MUSCLE ATROPHY IN OVARIECTOMIZED RATS: AN EXPERIMENTAL FUNCTIONAL, HISTOLOGICAL AND MOLECULAR BIOLOGY STUDY

A THESIS SUBMITTED TO
THE GRADUATE SCHOOL OF NATURAL AND APPLIED SCIENCES
OF
MIDDLE EAST TECHNICAL UNIVERSITY

BY

SEZİN DAĞDEVİREN

IN PARTIAL FULFILLMENT OF THE REQUIREMENTS
FOR
THE DEGREE OF MASTER OF SCIENCE
IN
BIOTECHNOLOGY

JUNE 2010

Approval of the thesis:

ROLE OF TNF-ALPHA IN SKELETAL MUSCLE ATROPHY IN OVARIECTOMIZED RATS: AN EXPERIMENTAL FUNCTIONAL, HISTOLOGICAL AND MOLECULAR BIOLOGY STUDY

submitted by **SEZİN DAĞDEVİREN** in partial fulfillment of the requirements for the degree of **Master of Science in Biotechnology Department, Middle East Technical University** by,

Prof. Dr. Canan Özgen
Dean, **Graduate School of Natural and Applied Sciences** _____

Prof. Dr. İnci Eroğlu
Head of the Department, **Biotechnology** _____

Prof. Dr. Feza Korkusuz
Supervisor, **Physical Education and Sports Dept.**, **METU** _____

Prof. Dr. Petek Korkusuz
Co-supervisor, **Histology a Dept., Hacettepe U Med. Fac.** _____

Examining Committee Members:

Assoc. Prof. Ayşen Tezcaner _____
Engineering Sciences Dept., METU

Prof. Dr. Feza Korkusuz _____
Physical Education and Sports Dept., METU

Assist. Prof. Dr. N. Dilara Zeybek _____
Histology and Embryology Department.,
Hacettepe University Medical Faculty

Assist. Prof. Dilek Keskin _____
Engineering Sciences Dept., METU

Prof. Dr. Bülent Gümüşel
Pharmacology Dept., Faculty of Pharmacy, _____
Hacettepe University

Date: 15.06.2010

I hereby declare that all information in this document has been obtained and presented in accordance with academic rules and ethical conduct. I also declare that, as required by these rules and conduct, I have fully cited and referenced all material and results that are not original to this work.

Name, Last name: Sezin Dağdeviren

Signature:

ABSTRACT

ROLE OF TNF-ALPHA IN SKELETAL MUSCLE ATROPHY IN OVARIECTOMIZED RATS: AN EXPERIMENTAL FUNCTIONAL, HISTOLOGICAL AND MOLECULAR BIOLOGY STUDY

Dağdeviren, Sezin

M. S., Department of Biotechnology

Supervisor: Prof. Dr. Feza Korkusuz

Co-supervisor: Prof. Dr. Petek Korkusuz

June 2010, 101 Pages

Skeletal muscle is defined to be atrophic in osteoporosis models and therefore is a potential target tissue for osteoporosis research. The aim of this longitudinal randomized controlled interdisciplinary study was to analyze the functional, histological, ultra-structral and molecular changes and the role of cachectic muscle atrophy inducer TNF-alpha in the skeletal muscles of the ovariectomized (OVX) rat model which mimics postmenopausal osteoporosis.

Female Sprague-Dawley rats were randomly assigned to the control, the OVX and the OVX+10μg/g/week TNF-alpha antagonist (Remicade) treated OVX-TNF groups. Maximum isometric and tetanic-twitch amplitudes were lower than the control group in the OVX group. Maximum isometric twitch amplitudes recovered in the fast-twitch extensor digitorum longus (EDL) muscles but not in the slow-twitch soleus muscles in the OVX-TNF group. The decrease in tetanic-twitch amplitudes recovered in the OVX-TNF group in both muscle types. Splitting and size variations of fibers, central nuclei and well-preserved overall ultrastructure were noted in the OVX and the OVX-TNF groups. Slow-twitch Type I fiber percentage, areas and diameters increased in EDL muscles of the OVX and the OVX-TNF group comparing to the control group. p65 and MyoD immune-labeling increased in OVX group whereas MyoD and C-Rel increased

and p50 decreased in OVX-TNF group. Expressions of 61 genes and 42 unidentified transcripts were significantly different between the control, the OVX and the OVX-TNF groups. To sum up TNF-alpha has a role in skeletal muscle dysfunction in OVX rats and TNF-alpha antagonist administration recovered it. But this modulation was not sufficient for total structural recovery.

Keywords: Osteoporosis, skeletal muscle, atrophy, TNF-alpha, ovariectomy

ÖZ

TNF-ALFANIN OVARİYEKTOMİZE SIÇANLARIN İSKELET KASI ATROFİSİNDEKİ ROLÜ: İŞLEVSEL, HİSTOLOJİK VE MOLEKÜLER BİYOLOJİ ÇALIŞMASI

Dağdeviren, Sezin

Yüksek Lisans, Biyoteknoloji Bölümü

Tez Yöneticisi: Prof. Dr. Feza Korkusuz

Ortak Tez Yöneticisi: Prof. Dr. Petek Korkusuz

Haziran 2010, 101 sayfa

İskelet kasları osteoporoz modellerinde atrofiye uğramış olarak tanımlanmıştır, bu yüzden osteoporoz araştırmalarında incelenmek üzere hedef alınabilecek bir dokudur. Bu disiplinlerarası, randomize, kontrol grubu içeren, ileriye yönelik ve uzunlamasına araştırmanın amacı postmenapozal osteoporozu taklit eden ovariyektomili (OVX) sıçan modelinin iskelet kaslarındaki işlevsel, histolojik, ince yapısal ve moleküler değişiklikleri ve bir kaşektik kas atrofisi uyaranı olan TNF-alfa molekülünün bu değişikliklerdeki rolünü araştırmaktır.

Çalışmada dişi Sprague-Dawley sıçanlar randomize olarak kontrol, OVX ve OVX+10μg/g/hafta TNF-alfa antagonisti (Remicade) uygulanmış OVX-TNF gruplarına ayrılmıştır. Maksimum izometrik ve tetanik kasılma değerleri OVX grubunda kontrol grubuna göre daha düşük bulunmuştur. Maksimum izometrik kasılma değerlerinin düşüşü OVX-TNF grubunda hızlı kasılan ekstensör digitorum longus (EDL) kasında engellenmiş ancak yavaş kasılan soleus kasında aynı şekilde engellenememiştir. Tetanik kasılma değerlerindeki düşüş OVX-TNF grubunda her iki kas tipi için de engellenmiştir. OVX ve OVX-TNF gruplarında fiberler arasında ayrılma ve ebat farklılıkları, merkezi çekirdekler ve iyi korunmuş ince yapıya rastlanmıştır. Yavaş kasılan Tip I fiber yüzdesi, alanları ve çapları OVX ve OVX-TNF grubunun EDL kaslarında kontrol grubuna göre artış

göstermiştir. p65 ve MyoD molekülü immün işaretlenmeleri OVX grubunda kontrole göre artarken OVX-TNF grubunda kontrole göre C-rel ve MyoD molekülü işaretlenmeleri artmış p50 molekülü işaretlenmeleri azalmıştır. Altmış bir genin ve 42 tanımlanmamış transkriptin ekpresyonu OVX ve OVX-TNF gruplarında anlamlı olarak farklılık göstermiştir. Sonuç olarak TNF-alfa'nın OVX sıçanların iskelet kaslarında gözlemlenen fonksiyon kaybında rolü olduğu ve TNF-alfa antagonisti (Remicade) enjeksiyonun bu kaybı engellediği gösterilmiştir. Fakat bu uygulama yapısal değişiklikleri engellemede yeterli olamamıştır.

Anahtar Kelimeler: Osteoporoz, iskelet kası, atrofi, TNF-alfa, ovariyektomi

To my parents, my grandmother and Korkusuz family

ACKNOWLEDGEMENTS

I would like to express my deepest gratitude to my supervisor Prof. Dr. Feza Korkusuz and co-supervisor Prof. Dr. Petek Korkusuz for their endless support , guidance, patience, encouragements and shared excitement through the study.

I want to express my thanks to examining comitee for their consideration, Berna Uysal for her valuable help, Ass. Prof. Dr. Dilara Zeybek for her great support during my work and Prof. Bülent Gümüşel and Ass. Prof. Dr. Burak Kandilci for pharmacological studies, Vet. Dr. Alper Çetinkaya for surgical operations. Also, I want to express my thanks to Ass Prof. Dr. Çetin Kocaefe, Uğur Akpulat and Yılmaz Yıldız for their effort in microarray studies.

Finally, I wish to thank my family for their moral support during my studies and throughout my whole life.

This research is approved by Hacettepe University Animal Ethics Comittee (14.05.2008-2008/7/40-8).

This research is supported by Hacettepe University Scientific Researches Unit (HUBAB: 08 01 101 003) and TUBITAK (109S344).

TABLE OF CONTENTS

LIST OF TABLES

TABLES

LIST OF FIGURES

FIGURES

ABBREVIATIONS

BMD	Bone Mineral Density
C°	Celcius degrees
cm	Centimeter
DXA	Dual-Energy X-Ray Absorptiometry
e.g.	Exempli gratia (For example)
EDL	Extensor Digitorum Longus
EDTA	Ethylenediaminetetraacetic acid
FDA	Food and Drugs Admisitration
g	Gram
g/cm^3	Gram per centimetercube
h	Hour
Hz	Hertz
IgG	Immuneglobulin G
KH	Krebs- Henseleit
kV	Kilovolt
M	Molar
mA	Miliamper
mA/s	Miliamper per second
mcg	Microgram
METU	Middle East Technical University
mg	Miligram
mg/kg	Miligram per kilogram
mg/kg	Miligram per kilogram
min	Minutes
ml	Mililiter
ml	Mililiter
mM	Milimolar
mm	Milimeter

ms	Miliseconds
NADH-TR	Nicotinamide Adenin Dinucletotide-Tetrazolium Reductase
NF-kB	Nuclear Factor-kappa B
nm	Nanometer
nm	Nanometer
OVX	Ovariectomy/Ovarectomized
P	P value
PBS	Phosphate Buffered Saline
SOL	Soleus
TNF-alpha	Tumor Necrosis Factor-Alpha
WHO	World Health Organization
µg/g	Microgram per gram
µg/ml	Microgram per mililiter
µm	Micrometer
μm^2	Micrometer square
ACOX2	Acyl coenzyme A oxidase 2
CSA	Cross sectional area
PKC	Protein kinase C
UbC	Ubiquitin C

CHAPTER 1

INTRODUCTION

Osteoporosis is characterized by decrease in bone mineral density (BMD), loss of skeletal micro-architecture and increase in fragility fractures [1]. The condition is mostly recognized in women after menopause, following the decrease in estrogen production [2]. Estrogen is a steroid hormone produced by the ovaries that normally increases BMD and reduces bone fracture risks [3]. One-in-three women over 50 years of age experiences osteoporotic fractures that may lead to fatal results [4].

Ovariectomy (surgical removal of ovaries) (OVX) of rodents is efficiently used to generate a well established model to mimic postmenopausal osteoporosis for research purposes. Ovariectomized rat is the most preferred model for postmenopausal osteoporosis studies [5].

Osteoporosis is an epidemic bone disease and current clinical view suggests that evaluation of skeletal diseases should always include an assessment of the musculature [6]. A decrease in mechanical stress on bones limits the osteoblast mediated bone formation and osteoclast mediated bone resorption [7]. We assume not only the bones but also the skeletal muscles are affected in this multifactorial metabolic musculoskeletal system disease. The structure and the function of skeletal muscles are rarely investigated in osteoporosis even their force is directly proportional to bone strength [8].

Muscle atrophy meaning the wasting of the muscle may lead to muscle weakness. Decrease in muscle strength is previously recorded in postmenopausal women [9]. Atrophy, declined contraction times and functional deterioration of

skeletal muscles are furthermore defined in OVX rats [10,11]. Estrogen administration recovered skeletal muscle size changes after OVX in rats in a previous study [12]. Myofiber growth, regeneration and extracellular matrix remodeling are recorded after estrogen replacement at recovery from disuse atrophy [13]. Skeletal muscle atrophy is also defined in senile osteoporotic rats [14]. Molecular mechanism and functional pathways of skeletal muscle atrophy after OVX however is rarely investigated.

Muscle atrophy may develop following two main mechanisms: (1) Disuse atrophy and (2) Cachectic atrophy. The situation can develop due to sedentary lifestyle that is developed postmenopausally following the disuse pathway or it may proceed by cachectic atrophy pathway involving inflammatory molecules. In both cases skeletal muscle atrophy follows a common final catabolic ubiquitin-proteosome pathway whose upper signaling mechanisms differ due to the cause of the state [15].

Tumor Necrosis Factor (TNF)-alpha is a muscle wasting cytokine that induces the nuclear factor-kappa beta (NF-kB) catabolic pathway in the cachectic but not in the disuse atrophy pathway [15,16,17,18]. It is a potent activator of the NF-kB pathway [19] and is an important triggering molecule of skeletal muscle atrophy and apoptosis [20]. Also the expression of different NF-kB pathway elements increases in both pathways. If the skeletal muscle atrophy and dysfunction in postmenopausal patients are developing because of cachexia, they must have been following the TNF-alpha and NF-kB pathway. The primary research question of this study was 'Does TNF-alpha antagonist administration recover skeletal muscle atrophy and dysfunction in OVX rats?' In this study we aimed to examine the effects of OVX on skeletal muscle function , histology and molecular biology and later on the effect of TNF-alpha antagonist [21,22] administration in skeletal muscles.

CHAPTER 2

BACKGROUND INFORMATION

2.1: The Bone and the Skeletal Muscle

The muscoskeletal system is composed of the bones, the cartilage, the skeletal muscle, the tendons, the ligaments and the peripheral nervous system. The bone is composed of inorganic and organic components and is a metabolically dynamic tissue. It is responsive to environmental forces. Bone has a balanced cycle of resorption and regeneration during its lifespan. It is that balance that determines the welfare of bone; if this balance is disturbed, diseases emerge. Factors that affect the bone metabolism are decreased calcium intake, sex hormones, growth hormones, steroids, sedatives, diuretics, lack of exercise and the process of aging [4,23].

Bone turnover is arranged due to the needs of the organism, as conveyed by mechanical stress that is transmitted by skeletal muscles. There is a correlation between muscle strength and bone formation. Wolff's law (1892) states that 'Bones are able to sense the loads on them and they can modify their structures to suit to these changes' [24]. Frost developed this theory to form 'mechanostat hypothesis' suggesting a mechanostat system that analyses bone deformations produced by muscular contraction and modulates bone strength by osteogenic cells and osteoclasts according to this outcome (Figure 2.1) [6,25]. According to this theory bone responses to physical and mechanical forces by remodelling.

Lack of mechanical stress on bone inhibits bone formation by osteoblasts and enhances bone resorption by osteoclasts [7,8]. Cortical bone loss is reported in

conditions where mechanical stress is decreased including anti-gravitational environment [8]. It is known that lack of mechanical stress induces loss of cortical bone at its unstressed regions [26]. It has been proposed previously that muscular disuse and weakness may contribute to osteoporotic changes and bone loss in trabecular bone that was previously associated with aging [27]. Hence the computational and animal models of gluteus muscular weakness were shown to be contributing to osteoporosis; mainly in trabecular bone [28].

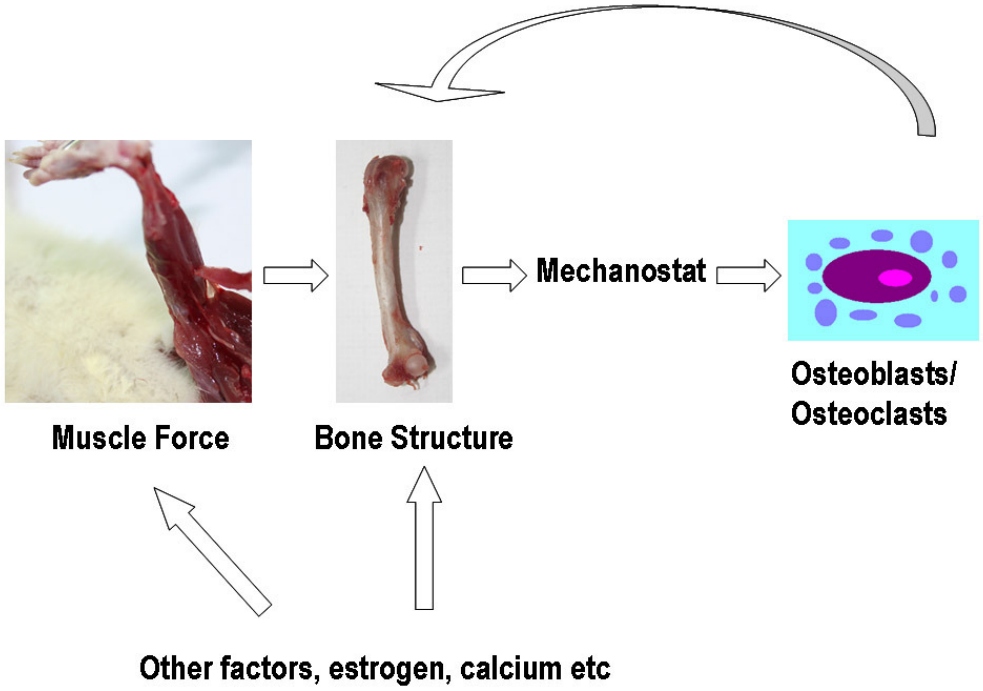

Figure 2.1: Scheme demostrating the mechanostat hypotehesis and regulatory circuit, between skeletal muscle contraction and bone homeostasis (adapted from Schönau et al. 2006).

The weakness of the muscles would not only increase risk of falling but also compromise bone formation. Biomechanical induction of bone by muscles, like in the duration of exercise is one of the main factors that triggers bone formation. A condition which deteriorates the function of muscle force units would certainly affect the bone. Therefore, the diagnosis of osteoporosis is a biomechanical matter relating both skeletal muscle and bone strength [4,6]. While dealing with bone diseases like osteoporosis much of the research is focused on bones, while there's only little research that focused on the other component of the musculoskeletal system including the skeletal muscles. This study is examining the skeletal muscles by developing postmenopausal osteoporosis in rats.

2.2: Osteoporosis, Ovariectomy and Animal Models

2.2.1: Osteoporosis

Bone is a living tissue. Human body constantly breaks down old tissues and generates new tissues to keep the bones strong. Osteoporosis, a disease literally meaning 'porous bone' in Latin, occurs when the bone formation and resorption turnover balance is disturbed. World Health Organization (WHO) defines osteoporosis as a skeletal disorder characterized by compromised bone strength predisposing a person to an increased risk of fracture [29].

Human beings reach their peak bone mineral density (BMD) in their early 20's and bone mass increase stops around the age of 30 years. The risk factors for osteoporosis can be female gender, family history, thin frame, old age, calcium deficient diet and ethnicity (Figure 2.2). Lack of exercise, or immobility or bed rest also weakens muscles and bones and can increase the risk of the development of osteoporosis [1, 30].

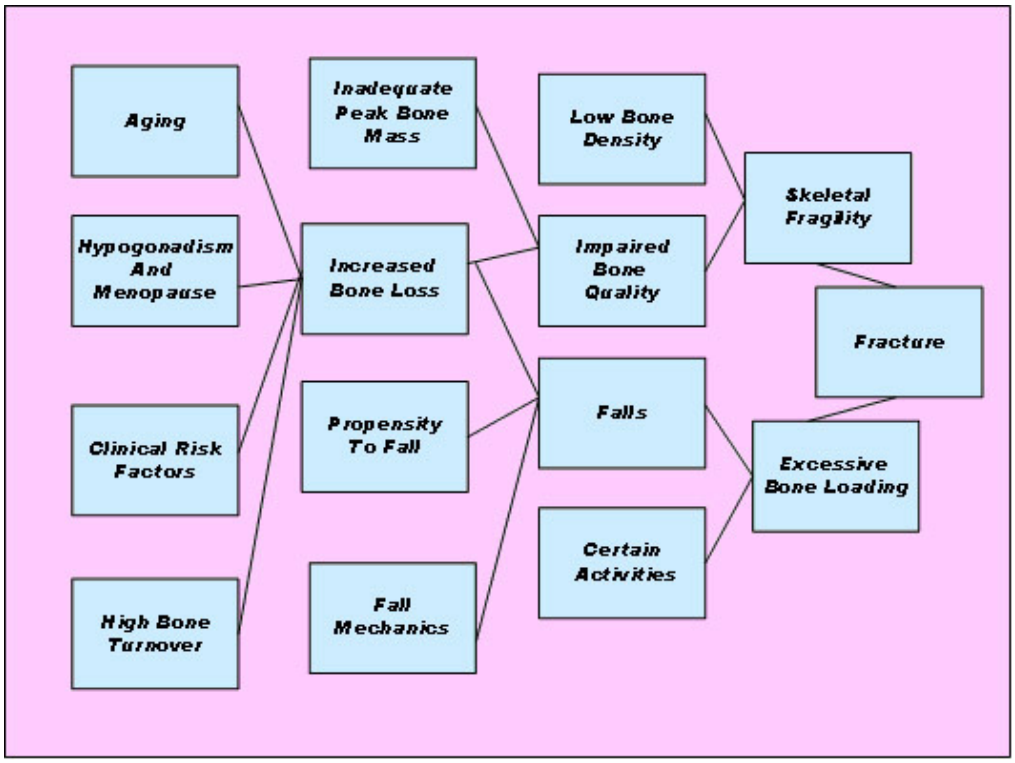

Figure 2.2: Pathogenesis of osteoporosis related fractures (adapted from NOF Clinician Guide 2009)

Osteoporosis is the most common bone disease in human kind and it represents a major public health problem [31]. Osteoporosis has been estimated to affect 75 million people in Europe, the United States and Japan [30]. The condition affects 45% of women over 50 years of age. It is estimated that hip fracture numbers worldwide will double by the year 2025 [1]. It is a problem that should not be under-estimated because hip fractures caused by osteoporosis alone cause more death than combination of cervix, ovary and uterus cancers all together [4].

Osteoporosis is referred as a 'silent disease', because it reveals itself when a fracture occurs; until that time no physical symptoms are observed. The resorption takes place mostly in the hip, spine and wrists. The diagnosis of osteoporosis relies on

Dual Energy X-Ray Absorptiometry (DXA), which gives quantitative accurate results of BMD [32]. Femurs and vertebrae are the common sites of BMD analysis for diagnosis. The measurement is carried out in computerized environment (Figure 2.3).

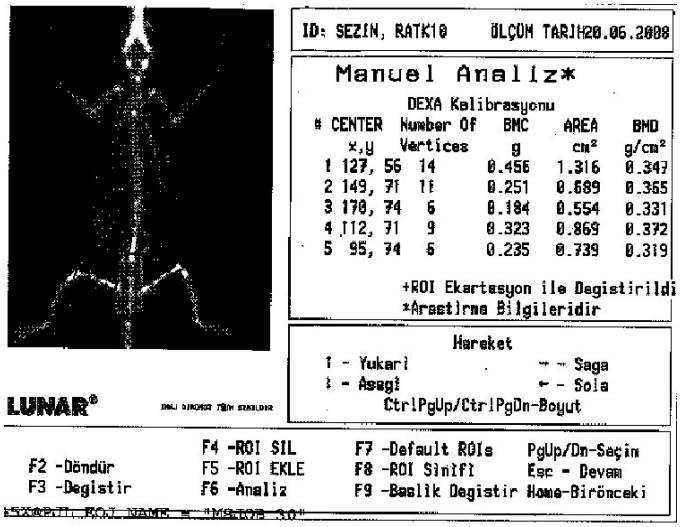

Figure 2.3: BMD analysis of rat skeleton.

The treatment of osteoporosis is currently carried out by a combination of agents that primarily target bone. Parathyroid hormones, selective estrogen receptor modulators, hormone therapy and nasal calcitonin are used for preventing bone loss and stimulating new bone formation [33].

Osteoporosis is categorized as: -Primary osteoporosis, which is resulting from hereditary factors or –secondary osteoporosis, which is resulting from environmental factors affecting bone fragility and mass. Conventionally primary osteoporosis is defined as Type I (postmenapausal) which is mainly developing due to estrogen deficiency or Type II (senile) osteoporosis which is mainly developing due to aging of skeletal system and calcium insufficiency [34].

Postmenapausal Osteoporosis develops after dysfunctioning of ovaries abandoning the female sex hormone estrogen production. During menopause, after the disappearance of estrogen's positive effects on bone anabolism, bone remodeling rate increases creating a bone remodeling imbalance. Bone tissue loss impairs skeletal architecture and increases fragility fractures [31].

2.2.2: Animal models

Osteoporosis is a complex disease; the loss of bone tissue may be age related, sex hormone deficiency associated, corticosteroid induced or secondary to unloading. Mammalian models for certain diseases provide very useful information for the understanding and preventing of the disorders. Animal models of decreased bone mass can be utilized to understand the complex molecular mechanisms regulating the bone remodeling, which is not possible with human subjects. Osteoporosis is a slowly progressing disease and animal models provide more standard experimental material and allow for extensive testing of potential therapies. Several species are used as animal models for osteoporotic bone loss such as birds, mouse, rat, dog, pig, sheep and primates [35]. Since 1994 Food and Drug Administration (FDA) requires data from both rat and a well-validated large animal model [5]. The most commonly used animal model for osteoporosis is the rat which has long provided data about skeletal behavior [36]. The advantages of rat model include inexpensiveness, easiness to house, and common use in research [5]. Previous work suggests that the biological mechanisms of growth, development and survival are similar in rats and humans so rat skeleton is defined to be a proper model for postmenopausal osteoporosis studies [37]. There are certain models mimicking osteoporosis yet the most common and reliable model for induction of osteoporosis is gonadectomy [38]. Ovariectomy meaning the excision of ovaries leads to the exact state of menopause in which ovary function is deteriorated in old women, this results in a decrease in bone mass characterized by over resorption of bone.

Ovariectomized rat model is the most preferred model for osteoporosis [5]. There are several other methods such as:-mechanical unloading, -change of diet – genetic breeding or -systemic administration of a number of compounds [38].

Mechanical unloading or disuse model is usually performed in the limbs that may include systemic immobilization, denervation or tendon resection, bandaging or suspension of hind limbs [39]. By reducing the skeletal biomechanical loading bone formation rate is reduced.

Low calcium diets are not solely adequate to generate osteoporosis in rats, but they enhance the osteoporotic process when used with other methods for generating BMD loss like ovariectomy [40].

Senescence Accelerated Mouse (SAMP6) is a genetically breeded model for severe osteoporosis, developing fragility fractures at early age and having low bone peak mass. SAMP6 mice provide a reliable model for senile osteoporosis.

Compound administration to rats such as glucocorticoids or heparin can mimic osteoporotic changes of bones in humans, yet this model requires long term treatment and fine adjustment of the proper effective dose [39,41].

WHO defines osteoporosis as having BMD that is 2.5 standard deviations below the mean of healthy young adults (T-score) [29], but use of this definition is not appropriate for animal models since there is no T-score associated with animals. Also the relative BMD decrease due to ovariectomy is lower than that of osteoporotic humans. As approximately 20% decrease in BMD of femurs is observed in humans by DXA measurements, this decrease reaches only 7% decrease in OVX rat models [42]; this is a factor that we should consider while evaluating osteoporotic animal models.

2.2.3: Estrogen

Estrogen is a sex steroid produced by ovaries in females [23]. Endogenous estrogen in women decrease suddenly at menopause and it seems that there is a

related lean body mass loss [10]. Estrogen increases BMD and protects bone loss and fractures. Following estrogen depletion bone loss accelerates in cancellous regions [35]. Therefore osteoporosis occurs more frequently postmenopausally in women, when estrogen production is ceased [30]. Decrease in estrogen levels after menopause is the main reason of BMD loss in postmenopausal women and BMD loss also causes decrease in estrogen levels in return [43,44].

Estrogen interacts positively with biomechanical sensing and strain response in bone cells and bone-muscle indicators by quantitative computerized tomography results agree with this finding [45]. There are also estrogen receptors in mammalian skeletal muscles [46].

Sugiura and co-workers have shown that estrogen administration attenuates immobilization-induced skeletal muscle atrophy in male rats which relates immobilization skeletal muscle atrophy to menopausal osteoporosis [47].

2.2.4: Ovariectomy (OVX)

Osteoporosis is a disease not only related to aging. There are two types of osteoporosis; (a) senile and (b) postmenopausal which manifests itself after loss of ovary functioning [48]. Therefore to mimic osteoporosis, removal of ovaries can be applied to generate a disease model. This is used as a model of osteoporosis in rat, mouse, rabbit, dog, sheep and primates [38]. The most commonly used organism is rats because of similarity of the bone development and remodeling mechanisms between rat and humans and their inexpensiveness. OVX rat presents most of the characteristics of human postmenopausal osteoporosis. There is broad range of literature on OVX rat and their shorter lifespan allows long–term studies on bone metabolism [5]. Also rats are unable to restore bone following OVX similar to humans. Yet animals must be older than 6 months to be included in these studies because rats reach their peak bone mass in 9 months [39,49]. After OVX osteoporotic rats have shown severe uterus atrophy proving the absence of gonad hormones [50].

Also methods like serum biochemistry, histomorphometry and densitometry used in humans are applicable in rats [39].

Following OVX, local bone loss and strength loss is observed in spongeous bones of rats mimicking postmenopausal musculoskeletal changes in women [49]. Efficiency of OVX in rats is also confirmed by BMD measurements by DXA which is also the approved method for BMD measurements by National Institute of Health [39].

2.3: Skeletal Muscle and Analysis Techniques

There are three types of muscles: (a) Skeletal muscle, (b) Smooth muscle and (c) Cardiac muscle. Skeletal muscles, a major component of the musculoskeletal system, constitute the single largest tissue mass in the body making up to 40% of the body weight [51]. They are under voluntary nervous control and responsible for locomotion and interaction of organism with its environment [52]. The mass and composition of skeletal muscle are fundamental for its function [17]. The basic structural unit of skeletal muscle is muscle fiber. Muscle fibers are surrounded by sarcolemma, the plasma membrane. Each fiber contains multiple nuclei which are situated around the periphery of the cell. A cell may include Golgi apparatus, sarcoplasmic reticulum, multiple mitochondria and a sarcoplasm containing lipid droplets, glycogen and myoglobin [51].

Sarcomeres are the basic contraction units of the muscle including A band (thick and overlapping filaments), I bands (thin filaments), Z band (connecting adjacent sarcomeres). The interaction between actin and myosin filaments in the A-band of the sarcomere is responsible for the muscle contraction [53]. Skeletal muscles provide the posture, the joint movement and locomotion of the body. They provide the contraction needed for the movement by motor units. A motor unit includes a single alpha motor neuron axon and the muscle fibers it innervates [52]. In a single

motor unit all the muscle fibers have the same contractile and metabolic properties [51]. There are different fibers of motor unit types (Table 2.1).

Table 2.1: Muscle fiber types and properties.

	Type I	**Type IIA**	**Type IIB**
Other Names	Red, Slow-Twitch Slow oxidative	White, Fast-Twitch, Fast oxidative, glycolytic	Fast glycolytic
Speed of Contraction	Slow	Fast	Fast
Strength of Contraction	Low	High	High
Fatigability	Fatigue-resistant	Fatigable	Most Fatigable
Aerobic Capacity	High	Medium	Low
Anaerobic Capacity	Low	Medium	High
Motor Unit Size	Small	Larger	Largest
Capillary Density	High	High	Low

Type I fibers contracts and relaxes more slowly than Type II fibers and requires lower frequencies of electrical stimuli to generate tetanic response and they are smaller in size. They have more myoglobin and hold higher amount of oxygen with increased activity of cytochrome oxidase system responsible for aerobic respiration. Type II fibers lack this system and are more efficient in anaerobic respiration using glycogen sources [52]. Different muscle fiber Types can be identified by histochemical stains allowing the differentiation of muscle fibers based on reactivity of muscle structural proteins and metabolic pathways.

The **soleus** (SOL) muscle causes plantar flexation of the foot at the ankle and stabilizes the tibia on the calcaneus limiting forward sway. Type I fibers are dominant

in SOL muscle, which makes them prone to rapid atrophy. It is used as a slow-twitch muscle model in muscle physiology studies [54].

The **extensor digitorum longus** (EDL) muscle origin is found in the lateral condoyle of the tibia and extends the toes of the foot. It is mainly composed of Type 2 fibers in rats and humans [54].

The SOL muscle of adult Sprague-Dawley rats contains 83% of Type I and 17% of Type II fibers whereas the EDL muscle contains mainly Type II fibers [55]. They are the routinely used in electrophysiological studies to assess muscle function. These muscles were used in our study to evaluate function alterations after OVX.

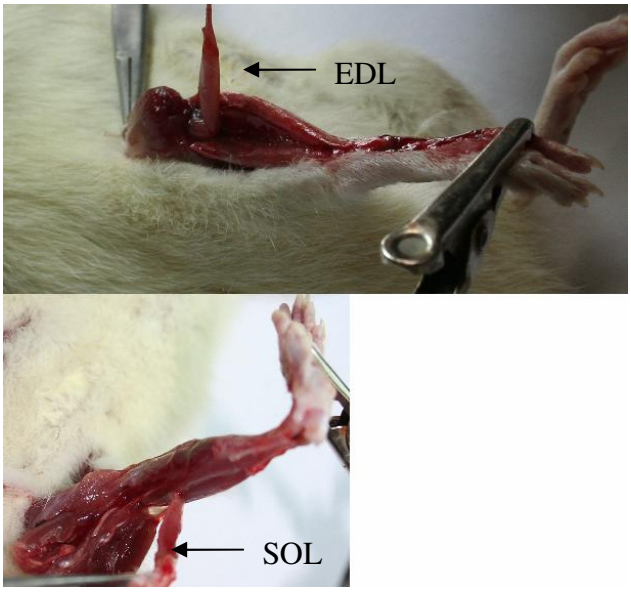

Figure 2.4: EDL and SOL muscles of rats.

Electron Microscopy is an advanced screening technique which gives the fundamental ultra-structural cellular information of the muscle. By electron microscopy, the abnormalities seen in the light microscopy level can be

characterized, localized and observed at the organelle level. However it gives little information about the overall condition of the muscles. The muscle can be analyzed for its sarcolemma, myofibril organization and associated cytoskeleton, Z lines, intermediate filaments, nuclei, mitochondria, membrane systems, deposits and particles [56].

Histological stains are used to observe histological structure. The most important stain used routinely is haematoxylin and eosin stain clearly showing the overall structure of the tissue in relation to fibers, nuclei, fibrous and adipose tissue, the presence of inflammatory cells, vascular and neural components. It is sometimes easier to observe minor increases in endomysial connective with Masson Trichrome technique in which muscle fibers stain a red color and collagen is a lighter distinguishable blue-green color. Also oxidative enzymes are useful for histochemical staining of muscle fibers for distinguishing fiber Types. The most useful oxidative enzymes studied in muscle are NADH-TR (Nicotinamide adenine dinucleotide-Tetrozolium Reductase) Succinic Dehydrogenase and Cyclooxygenase enzymes. NADH-TR employs a colorless tetrozolium salt as an electron acceptor which is reduced to deeply colored formazan product at site of enzyme activity. Thus end product intensity reflects the number of mitochondria in a fiber revealing the fiber is fast twitch or slow twitch. Type I fibers show darkest blue color as Type II fibers are lighter in color [56].

2.4: Muscle Atrophy and Hypertrophy Mechanisms

Muscle atrophy**,** meaning muscle wasting, is characterized by decreased muscle fiber cross sectoional area (CSA) and protein content, reduced force and increased insulin resistance as well as slow to fast fiber Type transition. It can appear due to several factors such as bed rest, denervation, hind limb un-loading, disuse or immobilization [17]. Skeletal muscle atrophy has severe effects. Recent studies focus on several diverse cascades that control the activation of ubiquitin ligases [57].

Muscle usage changes are shown to activate early recruitment of several inflammatory responses too [18]. Muscle losses in both cachexia and disuse, protein degradation is mediated primarily by the ubiqiuitin-proteosome pathway [58]. The reasons leading to atrophy can be counted as: cachexia, disuse and senility. Skeletal muscle hypertrophy meaning increasing in muscle mass is defined by increase in size of the pre-existing muscle fibers but not in fiber number resulting in an increase in muscle mass [59]. Skeletal muscle atrophy and hypertrophy proceed by several molecular pathways. These often coincide with each other. Recent studies suggest that hypertrophy pathways are dominant over induction of atrophy mediators [59].

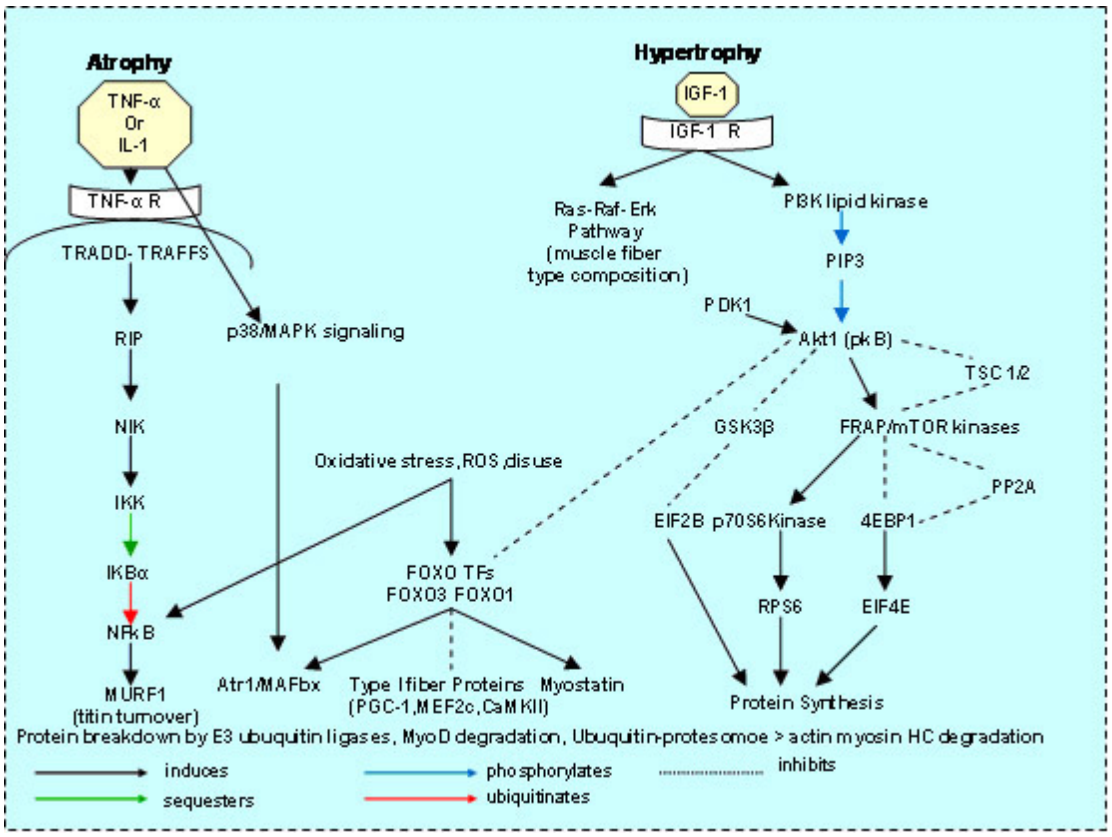

Figure 2.5: Skeletal muscle hypertrophy and atrophy molecular pathways

Syntheses of proteins are reduced and protein degradation ratio is increased in most of the muscle atrophy types. This response mechanism explains the rapid muscle mass loss [58]. Findings up to now point out that whatever the reason of atrophy is, it proceeds by protein degradation through the ubiqiuitin-proteosome pathway. On the other hand the upper molecular signaling pathways of cachexia and disuse atrophy are different from each other [15,16,17].

A study [15] has shown that during disuse atrophy NF-kB pathway is induced by over-expression of p50, C-Rel and Bcl3 proteins whereas the p65 protein expression has not changed. However during cachectic atrophy of muscles, only p50 and p65 proteins have shown over-expression.

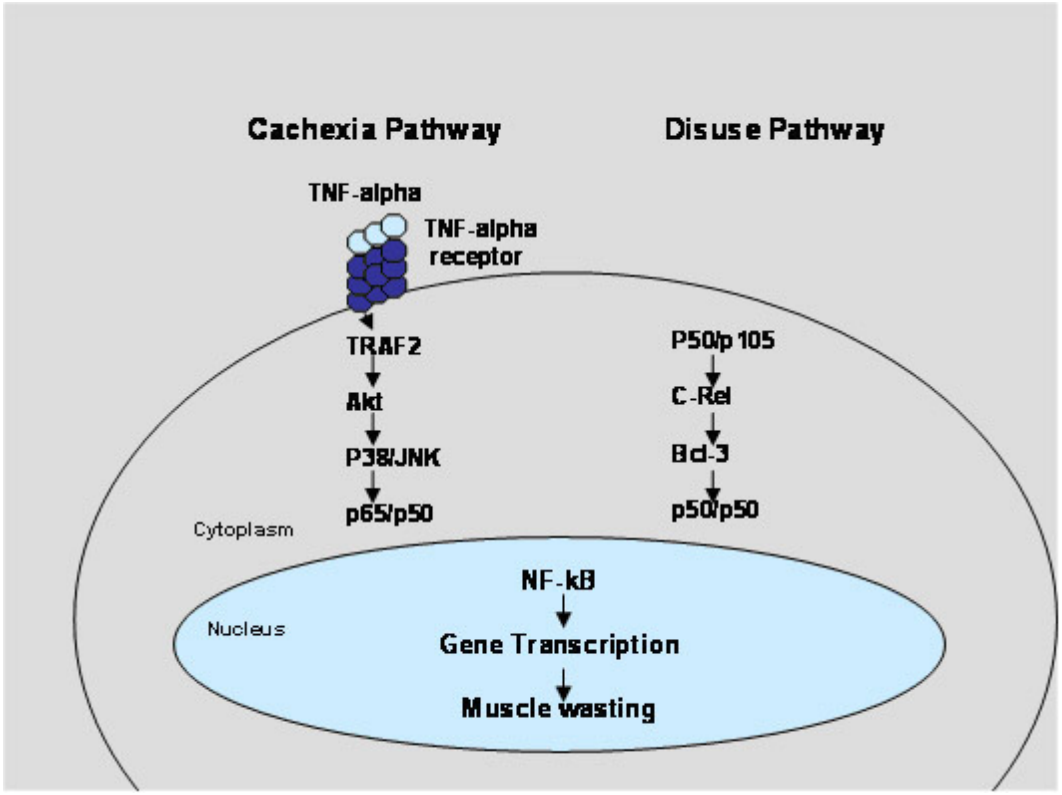

Figure 2.6: Molecular signaling during cachectic atrophy and disuse atrophy

Previous research suggests that cachexia uses TNF-alpha induction to activate the NF-kB pathway leading to atrophy whereas in disuse atrophy TNF-alpha induction is not in the picture. Figure 2.6 represents the different proteins taking place in different kind of muscle atrophies.

Microarray chips designed for rats contain transcripts of over 30000 genes and results are quantitatively available for expression analysis. Previously microarray analysis was carried out in disuse atrophy and hypertrophy of rat skeletal muscles [60,61]. These studies have shown several changes in expression of many genes involving energy, catabolism, and lipid storage process up to 2 fold. Ubiqiuitin-proteosome pathway gene activation also gives us major clues on molecular changes in disuse atrophy and hypertrophy of skeletal muscles.

2.5: Skeletal Muscle in Osteoporosis

Skeletal muscle strength and BMD are observed to be in correlation in osteoporotic male and female patients, and exercise is advised for the patients to slow down bone mineral loss. [62,63]. Since skeletal muscle is in close interaction with the bones, it is affected during postmenopausal period where BMD falls. Decrease in muscle strength is previously recorded in postmenopausal women [9]. Also postmenopausal women exhibited lower muscle force per unit cross-sectional area compared with age matched premenopausal women [64].

OVX rat is used to mimic postmenopausal osteoporosis for more extensive research on animal models. In OVX rats, greater extensor muscle atrophy and declined contraction times are reported [10]. OVX is also reported to cause deterioration in force generating capacities of EDL and SOL muscles and impairment in actin myosin interactions. [11] Myofibril growth, regeneration and extracellular matrix remodeling are recorded after estrogen replacement at recovery from disuse atrophy [13].

Estrogen hormone which disappears after OVX is a key hormone regulating recovery from the atrophy [65,66]. In agreement with this, lack of estrogen after OVX causes greater muscle atrophy [11] and estogen replacement reverses OVX induced declines in hindlimb muscle contractility and myosin interactions. [67]. Estrogen administration also recovered skeletal muscle size changes after OVX in rats in a previous study [12]. The dysfunction in OVX rat is not related to calcium metabolism, since no change in Ca sensitivity of isometric tension is observed despite an approximately 20% decrease in maximum isometric force in SOL muscles [68].

In a comparative study of the slow (SOL) and fast (EDL) muscles of the female mice entering the menopausal period, EDL muscles became more slow-twitch like, increasing the Type I fiber content of the muscle cells whereas SOL muscles faced greater decline in muscle force generation [11]. This suggests fiber Type conversion is more dominant in fast twitch muscles due to OVX. In a study OVX caused a mass increase in all organs including the muscle but this is suggested to be related with the lipid metabolism changes in all organs, not the hypertrophy of skeletal muscle specifically [10].

Skeletal muscle atrophy is not only limited to the OVX rats. Atrophy, tendon and periosteum degenerations and changes in the mitochondria number is also defined in SAMP6 male osteoporotic models [14].

Estrogen-deficient mice as another model of menopausal osteoporosis had lower maximum isometric contraction forces than the estrogen treated mice, and estrogen-deficient mice exhibited a strong correlation between bone and muscle strength. [69,70]

As BMD loss after menopause is a factor that could lead skeletal muscle weakness, skeletal muscle weakness is also a factor leading to BMD loss in osteoporosis in return. Assessment of skeletal muscle weakness in computerized simulation models and animal models point out that muscle weakness may actually lead to osteoporosis [28]. Molecular mechanism and functional pathways of skeletal muscle atrophy and dysfunction after OVX which are defined in the literature,

however are seldom investigated. Most of the research defines a dysfunction or atrophy in osteoporotic animal skeletal muscles physiologically or morphologically but none of them suggests a reason for the condition. If skeletal muscle atrophy really exists in osteoporotic rat muscles, then it must be caused by either the disuse or the cachectic atrophy pathway since they are the two main mechanisms of muscle atrophy. In disuse atrophy inflammatory cachectic molecules are not observed. If skeletal muscle atrophy after OVX is caused by a cachectic inducement, it must be a consequence of loss of BMD and hormonal level changes and is expected to progress as a disease state developed related to the osteoporosis. To determine the progressing pathway of this pronounced atrophy in osteoporotic rat skeletal muscles we chose to block the differentiating molecule TNF-alpha in the treatment group to see if this blocking would have any effect on the condition.

2.6: TNF-alpha Antagonists

Tumor Necrosis Factor-alpha is a cachectic cytokine involved in molecular processes. It is a potent activator of NF-kB, causing it to translocate to the nucleus and bind to promoters and enhancers of genes involved in inflammatory and proliferative responses [20]. TNF-alpha is an important mediator of skeletal muscle degeneration associated with cachexia. This molecule was recently shown to inhibit skeletal myogenesis in vitro [20].

TNF-alpha may trigger skeletal muscle apoptosis and muscle atrophy and it may inhibit myogenesis [71,72]. There are several TNF-alpha antagonists in usage as pharmaceuticals in autoimmune diseases like rheumatoid arthritis. Infliximab is a monoclonal antibody used as a TNF-alpha antagonist. Remicade (Schering-Plough) contains infliximab as the active substance [21,22]. Infliximab can be used to block the TNF-alpha pathway to a certain extent. The positive effect of infliximab on dystrophic muscle is previously defined [73].

CHAPTER 3

PURPOSE AND EXPERIMENTAL DESIGN

3.1: Purpose

The primary purpose of this study was to analyze skeletal muscle in OVX rats to identify (1) molecular, (2) functional and (3) structural changes by measuring (a) twitch responses, (b) assessing histology, (c) morphology, (d) immunohistochemistry, (e) electron microscopy and (f) gene expression. The role of TNF-alpha was furthermore assessed as the potential cause of TNF-alpha linked muscle atrophy and the effects of TNF-alpha antagonist infliximab injection were compared to normal and OVX rats. The research questions of this study were whether (a) molecular, structural and functional changes will occur in skeletal slow-twitch (SOL) and fast-twitch (EDL) muscles that are reported to exhibit muscle atrophy and (b) TNF-alpha antagonist administration will recover skeletal muscle atrophy and dysfunction in OVX rats?

3.2: Hypothesis

Following OVX, (1) rats will develop muscular atrophy and structural changes, (2) functional impairment will take place in the skeletal muscles, (3) TNF-alpha will be involved in skeletal muscle changes and (4) administration of the TNF-alpha antagonist infliximab will improve the functional and structural deterioration of skeletal muscles.

3.3: Experimental Design

A prospective, randomized controlled and longitudinal interdisciplinary (orthopedics, histology, pharmacology, and molecular genetics) study was designed.

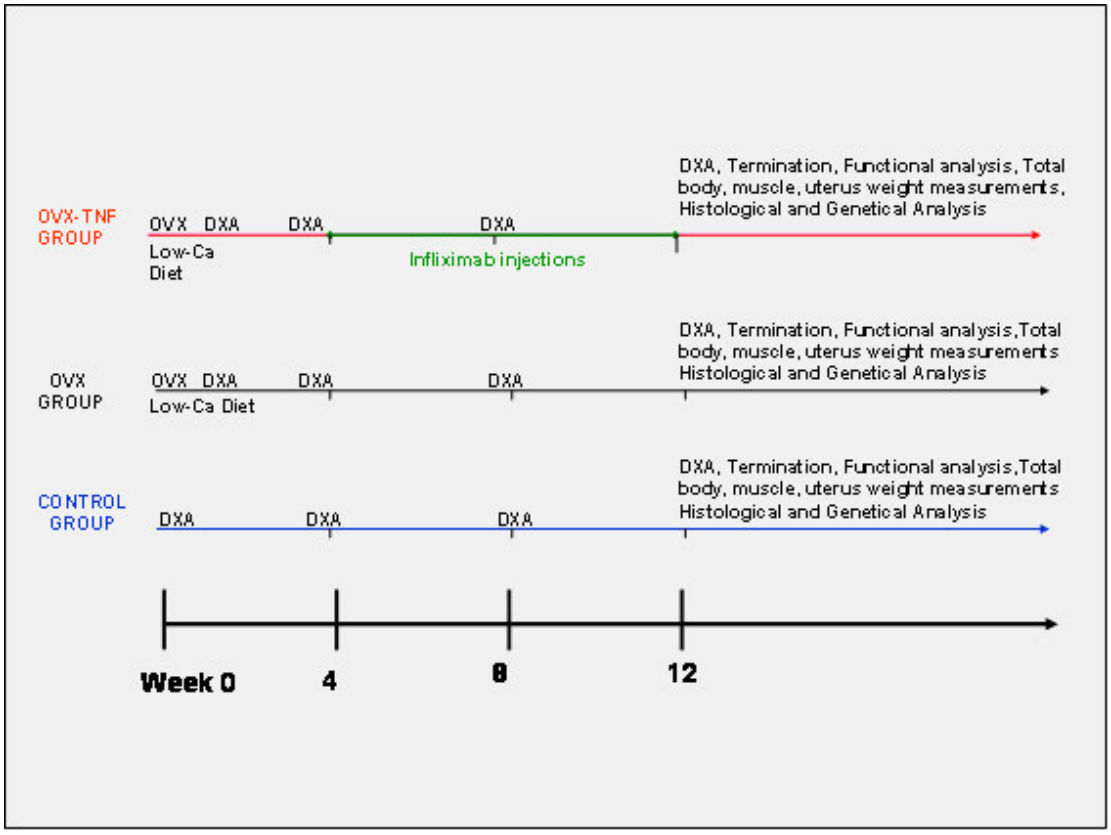

Figure 3.1 : Experimental design.

Thirty weeks old female Sprague–Dawley rats were randomly assigned into the (a) Control, (b) OVX and (c) OVX-TNF groups. Each group contained nine rats. Ovariectomy was carried out in the OVX and OVX-TNF groups. Four weeks after

the operations the OVX-TNF group was intraperitoneally injected with the TNF-alpha antagonist infliximab (10μg/g/week; Remicade, Schering-Plough Co, Ireland) for 8 weeks. Twelve weeks after the operations the skeletal muscles of rats were excised and analyzed functionally, histologically, ultra-structurally, immunohistochemically and genetically.

3.3.1: Dependent and independent variables

The groups (n=3) compromised the independent variable. Every group had 9 rats. The criteria for a rat to be included in the experiment were defined as having no bone abnormalities prior to the experiment as evidenced by x-ray pictures of the skeleton. Dependent variables were: (1) Morphological analyses of skeletal muscle histology was performed by light and electron microscopy. Fiber–type specific immune staining was performed to define fiber type changes, immunohistochemistry of selected NF-kB pathway proteins was performed to define molecular changes. Immune-reaction intensity in skeletal muscle cells during histological observations was scored by two observers independently and scoring was made on common scores. (2) TWITCH test were performed for functional analyses. During skeletal muscle contraction force measurements by pharmacological techniques (a) standard maximum isometric twitch response measurement and (b) tetanic contraction amplitude-frequency relationships were calculated. (3) Microarray gene expression analyses were carried out based on muscle and bone catabolism related gene expressions. Apart from these variables, to prove BMD changes and osteopororsis development (a) DXA measurements and (b) uterus weight measurements after terminations were carried out.

3.3.2: Assumptions

(a) OVX and low calcium diet will develop osteoporosis in rats.

(b) Muscle atrophy will occur in skeletal muscles of the OVX rats.

(c) Skeletal muscle atrophy will develop by the NF-kB final pathway.

(d) If the muscle atrophy proceeds by the cachectic pathway which is induced by the TNF-alpha upper pathway, the condition will recover with TNF-alpha antagonist infliximab injection

3.3.3: Ethics:

Hacettepe University Medical Faculty Animal Experiments Ethics Committee (14.05.2008-2008/7/40-8) approved the study. Veterinary Deontology Law Sentence 6343/2 and Helsinki Animal Rights Declaration regulations were strictly followed during the experiments.

CHAPTER 4

MATERIALS AND METHODS

4.1: Animals

Seven and a half months old female Sprague-Dawley rats weighing 220-250 g were used. Rats were housed in a temperature-controlled room (22-24°C), with a 12-12 h light-dark cycle and were given free access to food. Free movement was allowed. Twenty-seven rats were assigned randomly into one of three groups: the Control Group (n=9), the Ovariectomized Group (OVX) (n=9) and the OVX and Infliximab Treated Group (OVX-TNF) (n=9). While the control group was fed with a standard diet, the OVX and the OVX-TNF Groups were fed with the low-calcium diet which was specifically produced for this experiment by a private prey company (Bil-Yem, Ankara, Turkey). After a four week recovery period after OVX, the OVX-TNF group animals were intraperitoneally injected with Infliximab (10μg/g/week; 10mg Infliximab/1 ml solution, Remicade, Schering-Plough Co., Innishanon, County Cork, Ireland), a TNF-alpha antagonist, for 8 weeks. The dose of infliximab was determined according to previous studies [73,74]. The dosage of infliximab is clearly related to the nature of the disease. We have therefore chosen using the dosage that is proven to have positive effects on skeletal muscle of rats in skeletal muscle dystrophy model [73].

4.2: Radiography, Ovariectomy and Bone Mineral Density Measurements

4.2.1: Radiography

To confirm that rats had no bone deformities prior to the experiments, X-ray pictures of the rats were obtained. The X-ray device (Multix-X, Siemens G, Germany) in the Middle East Technical University Medical Center, the Agfa Crurix X-ray film (Agfa-Gevaert N.V, Belgium) and the Agfa Crurix 60 (Agfa-Gevaert N.V, Belgium) automatic film developer were used. The rats were anesthetized (ketamine/xylazin: 80/8 mg/kg; Alfamine %10, Alfasan International, Netherlands, Xylazin Alfazyne %2, Alfasan International, Netherlands) before the evaluation. The distance between the rats and the X-ray source was fixed at 100 cm. Whole-body X-ray pictures were obtained at an instrument setting of 41 kV and 2 mA/s. Bone deformity was not defined in any of the rats prior to the experiments and all rats were assigned to groups (Figure 4.1).

Figure 4.1: Whole body X-Ray picture of the rat.

4.2.2: Ovariectomy and Uterus Weight Measurements

Ovariectomy operations were carried out in Hacettepe University Animal Experiments Laboratory. After anesthesia (ketamine/xylazin: 80/8 mg/kg; Alfamine %10, Alfasan International, Netherlands, Xylazin Alfazyne %2, Alfasan International, Netherlands) the surgical site was shaved and cleansed with antiseptics (Betadine, Purdue Pharma, Wilson, NC, USA) for the ovariectomy operation [75]. A midline abdominal incision was made and the intersection between the ovaries and uterus was tied with 2.0 silk sutures (Doğsan, Turkey). Ovaries were then removed bilaterally (Figure 4.2,4.3).

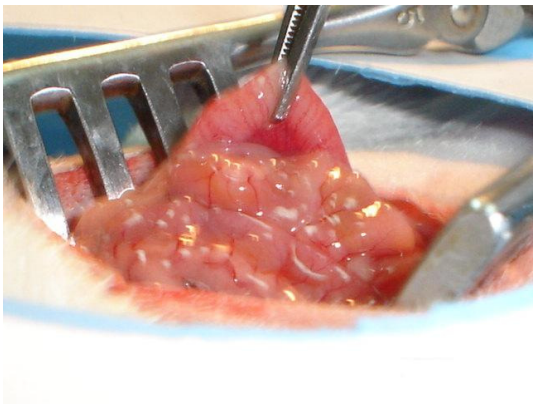

Figure 4.2: Ovariectomy operation; allocating the ovaries

The incision was sutured and prophylactic antibiotics (Cefozin 100mg/kg, Bilim İlaç San, İstanbul, Turkey) were intramuscularly administered to prevent postoperative infection. The surgical site was cleansed with antiseptics (Betadine, Purdue Pharma, Wilson, NC, USA) and the area was isolated with a spray film (Opsite, Smith&Nephew, England). To avoid post operational pain, a single dose of

non-steroidal analgesic and antiinflammatory medicine (20mg/kg phenylbutazone) was administered (Devaljin, Deva İlaç Sanayi, İstanbul, Türkiye).

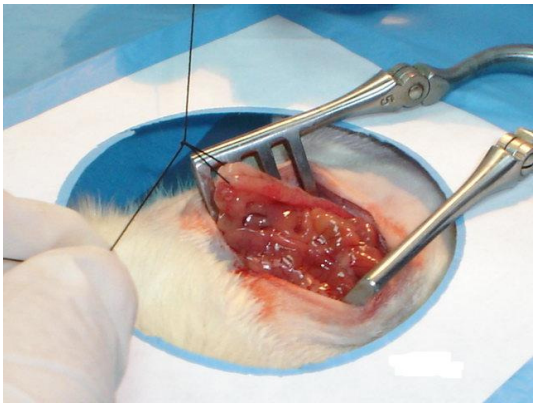

Figure 4.3: Ovariectomy operation; finding and knotting the ovary ends.

Efficacy of ovariectomy was confirmed by measuring the wet uteri weight after termination. An approximately 5 fold decrease in the wet weight of the uteri was observed (Figure 4.4, Figure 4.5).

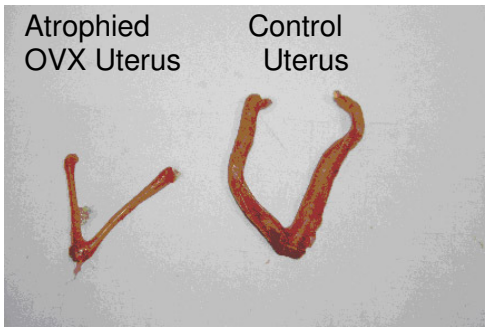

Figure 4.4: Atrophied compared to normal uterus 3 months after ovariectomy.

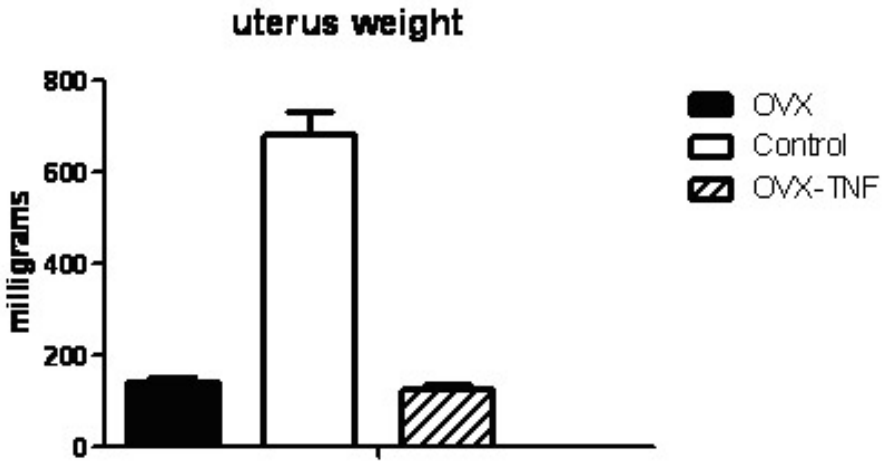

Figure 4.5: Wet uterus weights of all groups.

4.2.3: Bone Mineral Density (BMD) measurements using the Dual Energy X-Ray Absorptiometry (DXA) Device.

The efficacy of the OVX related BMD loss was defined by DXA measurements. The BMD measurements were carried out in Midddle East Technical University Medical Center. Rats were anesthetized prior to the measurements (ketamine/xylazin 0.2/0.1 ml/rat; Alfamine %10, Alfasan International, Netherlands, Xylazin Alfazyne %2, Alfasan International, Netherlands) and gently fixed to the device. DXA measurements were carried out prior to OVX and at 8 and 12 weeks after OVX. The Lunar DPX (Lunar Radiation Corp. Madison, USA) device equipped with the small animal software was used with a setting of 140/170 kV and 2.0 mA at 60 Hertz was used. The approximate measurement time was 7 minutes per rat (Figure 4.6,4.7).

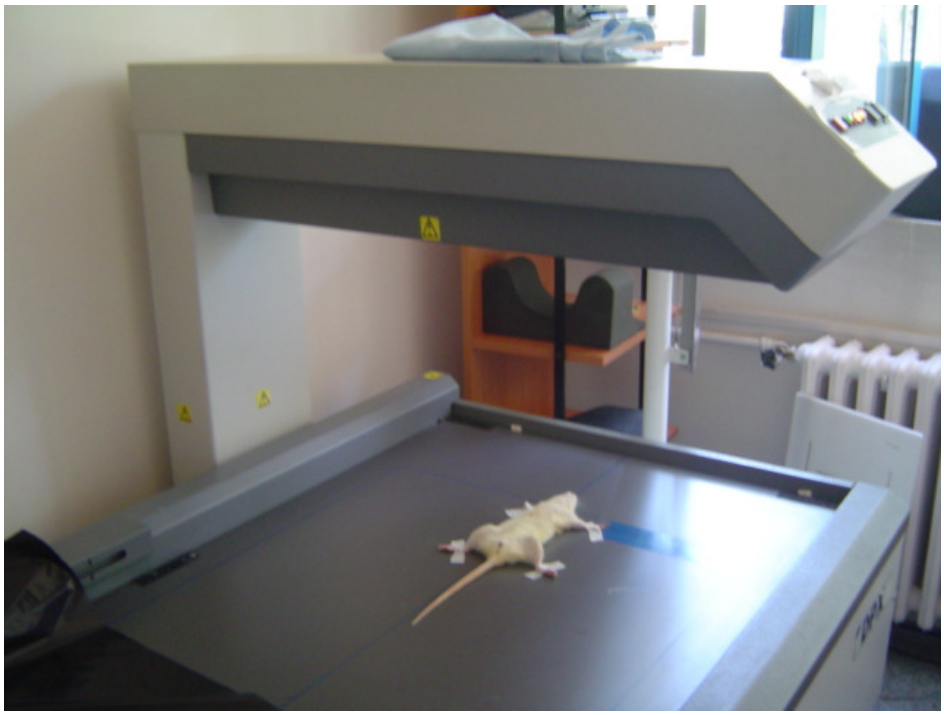

Figure 4.6: Bone mineral density measurements using the DXA device.

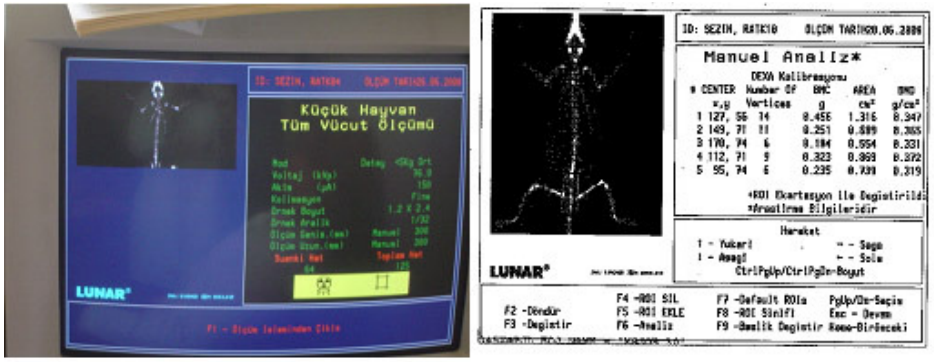

Figure 4.7: BMD calculation using the small animal software.

The BMD of the femur of the rats before OVX and at 3 months after OVX were as follows:

Table 4.1: Bone mineral densitometry measurements of the left femurs before and 12 weeks after OVX (g / cm^3) (p=0.05 *Mean ±SEM , *OVX vs. control, ¥ OVX-TNF vs. control)

BMD of the left femurs (g / cm^3)	**Control**	**OVX**	**OVX-TNF**
Week 0 (OVX)	336± 8.9	349± 7.4	351 ± 9.9
Week 12(post-ovx)	368± 7.4	345± 7.0 *	340± 6.7 ¥

Bone mineral densities of the left femurs of the OVX and the OVX-TNF groups were significantly lower (P=0.021) than that of the control rats at the end of 3 months. (One-way ANOVA and post Hoc Duncan test).

4.3: Skeletal Muscle Preparations, Contractility Studies and Body & Muscle Weight Measurements

4.3.1: Skeletal Muscle Preparations

Skeletal muscle preparations and contractility studies were carried out in Hacettepe University Pharmacology Department Labortatory. All animals were weighed in sensitive scales prior to the experiments to record total body weights. In order to analyze the structural and the functional differences in both fast twitch and slow twitch skeletal muscles of rats, the SOL (slow-twitch) and Extensor Digitor

Longus (EDL) (fast-twitch) muscles were studied in all groups. Under ketamine/xyzlazine anesthesia (80/10 mg/kg; Alfamine %10, Alfasan International, Netherlands, Xylazin Alfazyne %2, Alfasan International, Netherlands) the right leg skeletal muscles of rats were exposed by a incision extending from the ankles to the pelvis [10]. The tibialis anterior muscle at the anteromedial part of the leg was detached from its tendon and it was retracted towards the knee joint. At the ankle joint, the distal tendon of the EDL was transected at the level of the dorsal channel. The EDL muscle was isolated by holding its end with a forceps and gently dissected from its location. Isolated muscles were laced into a 20 ml tissue bath containing the Krebs-Henseleit (KH) solution (in mM): NaCl, 118.4; KCl, 4.69; $MgSO_4$ 1.18; $CaCl_2$ 2.5;KH_2PO_4 1.17;$NaHCO_3$ 25.0; glucose 11.1). The Achilles tendon was transected at the calcaneus to isolate the SOL muscle. The gastrocnemius muscle was dissected and the SOL muscle was exposed. The muscle was gently released from its attachment at the proximal tibia. The isolated SOL muscles were also transferred into the KH solution. The excised muscles were constantly perfused with a physiological solution during and after dissections.

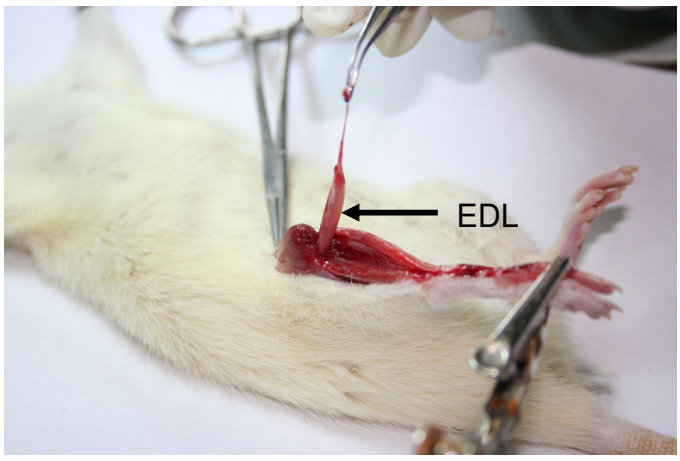

Figure 4.8: Excision of the EDL muscle.

Figure 4.9: Excision of the SOL muscle.

4.3.2: Contractility Studies and Body and Muscle Mass Measurements

After isolation of the EDL and the SOL muscles they were placed into and attached from their ends to 50 ml organ baths. Organ baths were temperature fixed at 37ºC and were filled with KH solution at pH 7.4 which is per fused with 95% O_2 and % 5 CO_2. The muscles were stimulated by rectangular electrical pulses *via* platinum electrodes which were connected to a stimulator (Model S88 Grass Instruments, MA, USA) and a stimulus isolation unit (SIU5 Grass Instruments, MA, USA) and the isometric contractions were recorded by an isometric force transducer on a computer based data acquisition system (FT03, Commat, Ankara, Turkey, Biopac version:3.7.0). Two g of resting tension was applied to produce maximal twitch force and muscles were stimulated at a frequency of 0.1 Hz and pulse width of 0.5 ms. Tetanic stimulation was applied at 1, 10, 20, 40, 60, 80 and 100 Hz with trains of 500 ms duration. An interval of 5 min was allowed between each train. Tension

production in response to electrical stimulation at 1-100 Hz with 5 min interval was measured after the optimal muscle length and stimulus intensity were adjusted. Also wet tissue weights of muscles were measured and recorded by sensitive scales (Figure 4.10,4.11,4.12,4.13).

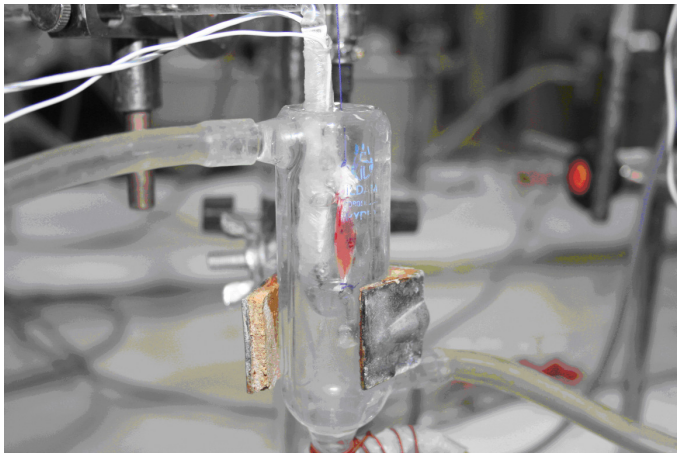

Figure 4.10: Muscles placed into the organ bath.

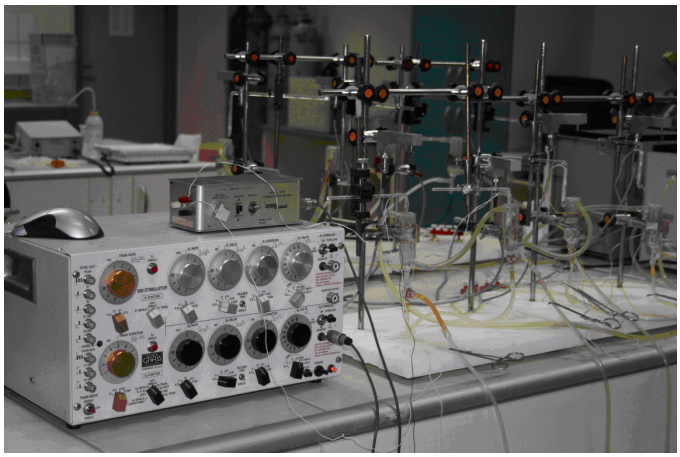

Figure 4.11: Organ baths system and measurement setting containing the SOL muscle and stimulator.

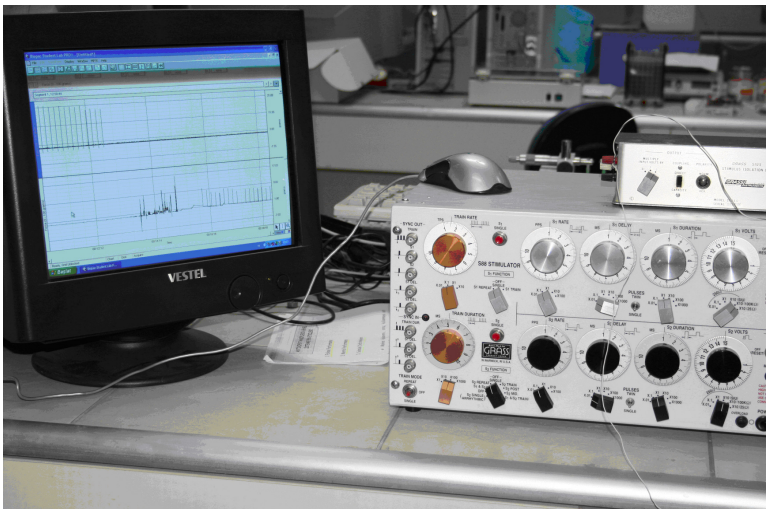

Figure 4.12: Transducer and computer screening of contraction responses.

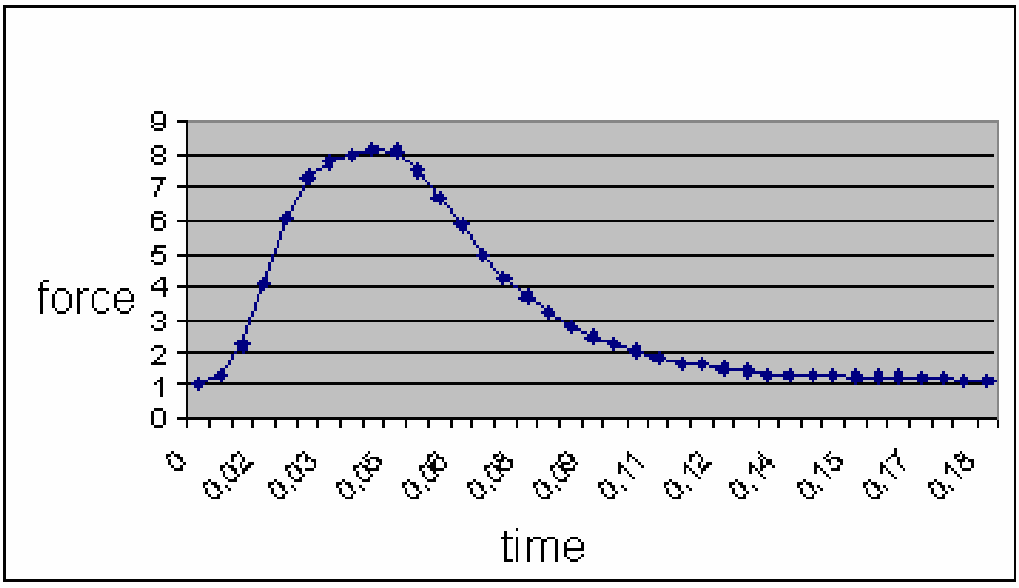

Figure 4.13: A sample contraction force (g force) vs. response time (seconds) graph of a muscle.

4.4: Histological Study

4.4.1: Muscle Preparations

The SOL and the EDL muscles of the left legs were excised for histology and genetic assessment in the same way as they were excised for functional studies. The samples were immersed in formalin for histology and histochemistry. They were placed in separate cryovials and kept at liquid nitrogen tanks (-196°C) for immunohistochemistry.

4.4.2: Light Microscopy

4.4.2.1: Histology

Tissue samples were divided into two and immediately fixed by immersion in %10 neutral buffered formalin. Formalin fixed tissues were dehydrated through graded alcohols and embedded in paraffin wax by standard method. In order to optimize the process, tissue processor with constant vacuum was used (Leica, TP1020, Germany). Five-micrometer thick sections were cut and were stained with hematoxylin-eosin and Masson's trichrome according to standard protocols.

4.4.2.2:NADH Fiber Type Specific Histochemistry

4.4.2.2.1: Staining Procedure

Seven to ten micrometer thick frozen sections were incubated with NADPH stain solution (10ml Gomori Tri HCl :10mg nitroblue tetrazolium:5mg beta-nicotinamide adenine dinucleotide) for 30 minutes at 37°C in the incubator and

washed with distilled water and 90% acetone. After that the slides were cover slipped by using glycerol and kept at 4°C until quantitative examination

4.4.2.2.2: Quantitative Evaluation of Fiber Type Specific Histochemistry

The digital images were captured using the Leica DC500 digital camera (Germany). Quantitative image analysis for fiber type scoring was carried out by using Leica Qwin Plus computer image analysis system (Germany) by modifying the literature [76,77,78]. In brief, lesser diameters and cross sectional areas of the type I and type II fibers were measured at 200x and 400x magnifications. A minimum of 100 fibers were measured at one or two nonoverlapping areas The data was interpreted as a result of fiber-specific staining and fiber size variations (Figure 4.14).

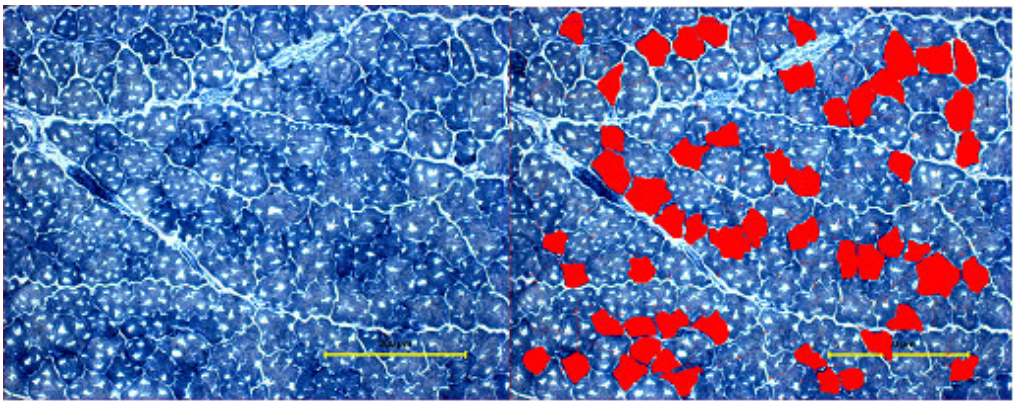

Figure 4.14: Micrographs show NADH-TR stained EDL muscle of a control rat. Red areas belong to lesser diameter and cross sectional area measurements of chosen fiber types 200x.

4.4.2.3: Immunohistology

4.4.2.3.1: Immune Labeling Procedure

The second piece of the tissue samples was immediately frozen in liquid nitrogen for immunohistochemistry procedure. Frozen tissue samples were kept in liquid nitrogen until the sections were cut. Five to seven micrometer thick cryomicrotome sections were placed on adhesive (polyL lysin) coated or electrostatic slides; and kept at room temperature overnight at least for one night in moisture-free boxes and immune labeling was performed the following day. The sections were fixed in acetone at +4 C^0 for 10 minutes and air-dried for at least 30 minutes. Anti-mouse and anti-rabbit HRP-DAB staining kits (CTS002, CTS005 R&D, Minneapolis, USA) were used according to manufacturers' protocol. Unspecific binding was blocked using rat serum at a dilution of 1:10 for 30 minutes at room temperature. Sections were incubated in a humidified chamber for an hour at room temperature with monoclonal antibodies, which are listed in Table 4.2. After washing in 0,01 M phosphate buffered saline (PBS) at pH 7.4, the sections were incubated with biotinylated anti mouse or anti-rabbit secondary antibodies for 30 min at room temperature, washed in PBS. After washing with PBS, slides were covered with HSS-HRP for 30 minutes at room temperature. The sections were washed with PBS and incubated with 3.3'-diaminobenzidine-tetrahydrochloride (DAB) for 2 minutes following suppliers' written steps. After washing with tap water, sections were stained with Mayer's haematoxylin and dehydrated through graded alcohols and cleared in xylene prior to mounting with Entellan (Merck, Darmstadt, Germany). For immunofluorescent labeling sections, which were incubated with primary antibodies under the same conditions and same time, washed with PBS 3 times for 5 minutes and then incubated with anti-mouse or anti-rabbit FITC conjugated secondary antibodies (Alexa flour 488, 546 Moleculer Probes, USA) at room temperature for 30 minutes. The sections were washed with PBS 3 times for 5 minutes and counterstined

with DAPI (D9542, Sigma,Germany) and mounted with fluorescent mounting medium (#S3025, Dako, Denmark).

All antibodies were diluted in a background reducing buffer solution consisting of 0.05 M TrisHCl containing 0.1% tween 20 (#S3022, Dako, USA). Negative control staining was performed by omitting the initial primary antibody incubation step and by using a control mouse IgG (immunoglobulin G). Positive control staining was performed by using appropriate control tissue samples provided by the manufacturer.

All sections were examined and photographed by using Leica DM6000B (Wetzlar,Germany) with a DC490 digital camera (Leica, Wetzlar,Germany).

Table 4.2: Antibodies used for immunohistochemical labeling.

Antibody	Clone	Isotype	Catalog Number	Source	Dilution
NFκB p50	NLS	Rabbit IgG	Sc-114	Santa Cruz	1:20
NFκB p65	F-6	Mouse IgG_1	Sc-8008	Santa Cruz	1:20
C-rel	B-6	MouseIgG1	Sc-6955	Santa Cruz	1:20
Bcl3	H-146	Rabbit IgG	Sc-13038	Santa Cruz	1:20
MyoD	5.8A	Mouse IgG1	Sc-32758	Santa Cruz	1:20

4.4.2.3.2: Quantitative Evaluation of Immune Labeling

All sections were examined and photographed by using Leica DM6000B (Wetzlar,Germany) with a DC490 digital camera (Leica, Wetzlar,Germany). The digital images were captured using the Leica DC500 digital camera (Wetzlar, Germany). Quantitative image analysis was carried out by using Leica Application Suit and Qwin Plus computer image analysis system (Wetzlar, Germany) by modifying the literature [79,80].

Maximum staining intensity was determined from the positive control tissue sections by using the image analysis system. Accordingly each EDL and SOL muscle section were graded for cellular immune reaction on a scale of 0 to +++ with DAB. 0 was given to no immune reactivity, + to weak but continuous reactivity, ++ for moderate but continuous reactivity and +++ to intense but continuous immunostaining. The number of immune positive cells was expressed as a percentage of positive cells over total cells at 200x magnification. In every specimen the average of screened/analysed 3 non over-lapping fields was reported. Staining intensity was combined with the percentage of stained cells by using the HSCORE that was calculated with the following equation:

H score = $\Sigma\rho$ (i+1), where i = intensity of staining with a value of (1 for +), (2 for ++) or (3 for +++) and ρ is the percentage of positive cells stained with each intensity, varying between 0-100. Σ: The sum of stained cells at different intensities.

4.4.: Transmission Electron Microscopy

Tissue samples were fixed in 2.5% gluteraldehyde solution in 0.01M phosphate buffer, pH 7.4 for 4 hours and post-fixed for 1 hour in 1% osmium tetroxide in 0.01M phosphate buffer. After washing in phosphate buffer, tissues were dehydrated in a graded series of ethanols to absolute ethanol, treated with propylene oxide and embedded in Epon812 (EMS, PA,US). Sections were cut using an ultramicrotome (Leica ultracut R Wetzlar,Germany) after heat polymerization. Semi-thin sections were stained with methylene blue–azure II and examined using the Leica DM6000B (Wetzlar,Germany) light microscope with a DC490 digital camera (Leica, Wetzlar,Germany). Ultrathin sections were double-stained with uranyl acetate and lead citrate (Leica EM AC20, Germany). These sections were examined in JEOL-JEM 1400 (Tokyo, Japan) model transmission electron microscope and digitally photographed by Gatan Orius CCD camera (CA,USA).

4.5: Microarray

All GeneChip experiments were conducted in the Hacettepe University Transcriptomics Laboratory as recommended by the manufacturer of the GeneChip system (Affymetrix, Inc., San Diego, CA, United States). The GeneChip array used was the Rat Genome RAE_230 2.0 expression probe array (Affymetrix, Inc., San Diego, CA, United States), which allows for analysis of more than 30,000 transcripts.

Skeletal muscles isolated from rats during terminations were cut from 1.0x1.0x1.0 mm cubes and kept in 1.0 ml vials filled with Trizol RNA stabilization agents (Qiagen N.V., Berlin, Germany) at -80°C. Tissue samples up to 30 mg were mortared and homogenized in RLT buffer (Qiagen N.V., Berlin, Germany) and RNA isolation was conducted due to the recommended protocol of RNeasy Fibrous Tissue Kit (Qiagen N.V., Berlin, Germany) by manufacturers. Total RNA amount was measured as an absorbance unit at 260nm coincides to 40 µg/ml RNA by spectrophotometric equipment. The ratio of absorbencies at 260nm/280nm was verified to be ~1.9-2 by UV spectrometric methods. Samples not appropriate for this protocol were eliminated. RNA isolation was also verified by gel electrophoresis using the Eukaryotic Poly-A RNA Control Kit (Qiagen N.V., Berlin, Germany) and poly-A RNA controls were prepared.

Double stranded cDNA was synthesized with a starting amount of approximately 100 µg full-length total RNA using the 3'IVT Express System in the presence of a T7-(dT)24 DNA oligonucleotide primer. Following synthesis, the cDNA was purified by sample cleanup module. The purified cDNA was then transcribed in vitro using the High Yield RNA Transcript Labeling Kit in the presence of biotinylated ribonucleotides form biotin labeled cRNA. The labeled cRNA was then purified on an affinity resin, quantified and fragmented. An amount of approximately 10 µg labeled cRNA was hybridized for approximately 16 hours at 45ºC to an expression probe array. The array was then washed and stained twice with streptavidin-phycoerythrin using the GeneChip Fluidics Workstation (Affymetrix,

Inc., San Diego, CA, United States). The array was then scanned twice using a Confocal laser scanner (GeneArray Scanner, Affymetrix, Inc., San Diego, CA, United States) resulting in one scanned image. This resulting ".dat-file" was processed using the GCOS program (Affymetrix, Inc., San Diego, CA, United States) into a ".cell-file" which was captured and loaded into the Affymetrix GeneChip Laboratory Information Management System (LIMS, Affymetrix, Inc., San Diego, CA, United States). Raw data was converted to expression levels using TMEV software. After checking for quality, data were exported to the Microarray analysis suite software for analysis.

Data analysis was performed by the transcriptomics and expression profiling researchers using the gene array tools package. Principle component analysis (PCA) was used to identify outliers (defined as samples with potential technical flaws such as tissue contamination by other surrounding organs) based upon overall gene expression values prior to continuing with analysis.

Individual experiment groups were analyzed separately, with the gene expression levels for all samples from each time point normalized to the median of their respective control samples prior to statistical analysis. Filtering was performed to remove low or non-expressing genes using the following criteria: raw expression value of >50 and a present call in at least two-thirds for any treatment group within a time point. One-way analysis of variance (ANOVA) by treatment was performed on this filtered list of genes with a p-value of 0.05, which would result in 5% of the genes identified as being expected by chance. To further refine the resulting gene list, only those genes that demonstrated at least a 2-fold difference in expression levels between the controls and the individual treated group were included for subsequent investigation. Other genes and probe sets which do not fulfill the ANOVA mentioned criteria are also taken into account according to the scientific relevance.

The information content of these data sets is a conjunction of numerical changes and biological information. The decision to consider a specific gene relevant was based on a conjunction of numerical changes identified by comparative and statistical

algorithms and the relationship to other modulated genes that point to a common biological theme. The value of that relationship was assessed by the analyst through a review of the relevant scientific literature. Any hypothesis generated from this analysis would need further validation with other analytical and experimental techniques.

4.6: Statistical Analysis

Several statistical methods were used for different sets of data in order to evaluate the hypothesis that OVX rat skeletal muscles exhibit functional loss and atrophy and this deteroriations are caused by TNF-alpha related pathways. Parametric and nonparametric tests (Student t, one way ANOVA, Post Hoc, nonparametric Kruskar-Wallis, Nonparametric Mann- Whitney, Mauchliy's test of sphericity) were used for statistical analysis by running the SPSS 18.0 statistics software (SPSS Inc, IBM, USA) on a personal computer. Data were presented as median or mean ± S.E for all the parameters measured. P values less than 5% were considered as significant.

CHAPTER 5

RESULTS

5.1: Contractility Studies and Body and Muscle Mass Measurements

Body weights of control rats were significantly ($p<0.001$) lower than those of the OVX groups; body weights of the OVX rats increased approximately 21% from surgery to termination. There was no significant difference between the OVX and the OVX-TNF groups body weights. Antagonist treatment did not alter body weights (Table 5.1).

Table 5.1: The total body weight (in gram); the SOL and EDL muscle weights (in mg) of all groups are presented. (*Mean ±SEM, *OVX vs. control, ¥ OVX-TNF vs. control, † OVX vs. OVX-TNF).

	Control	**OVX**	**OVX-TNF**
Body weight (g)	117±7,3	167±4,9 *	137±9,3 ¥
SOL Weight (g)	103±8,4	176±9,4 *	125±11,6
EDL Weight (g)	117±4,3	167±7,8 *	137±5,1 †

EDL muscle weights of the OVX group was significantly higher ($p<0.001$) than that of the control group. TNF-alpha antagonist administration partly though not significantly prevented this increase. SOL muscle weights of the OVX group was significantly higher ($p<0.001$) than that of the control group and TNF-alpha administration reverted this situation (Table 5.1).

EDL and SOL muscle weights to body weight ratios (mg muscle/g body weight) of the OVX group were significantly higher ($p=0.001$) than that of the control group and this increase recovered in the OVX-TNF group (Figure 5.1).

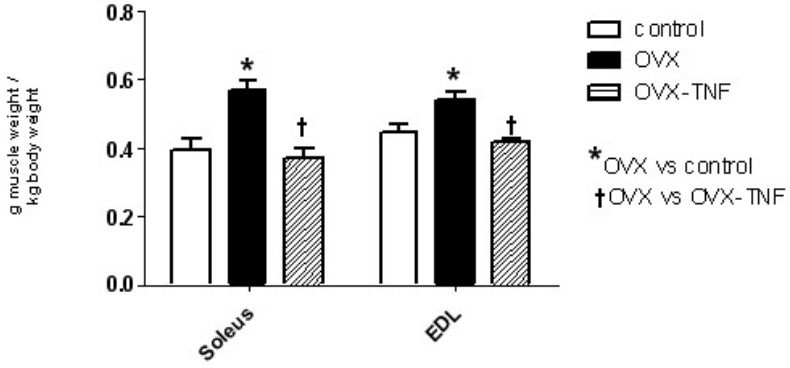

Figure 5.1: Muscle weight (g) to body weight (kg) ratios of the SOL and the EDL muscles (P=0.05, *Mean±SE; OVX vs. control, † OVX vs. OVX-TNF). (Muscle weight to body weight ratios of both the SOL and the EDL muscle increased significantly in the OVX group compared to the control group. This increase recovered in the OVX-TNF group.)

EDL and SOL muscles isometric twitch amplitude significantly (p=0.005) decreased in the OVX group when compared to the control group. This decrease was recovered in the EDL muscles of the OVX-TNF group (Figure 5.2).

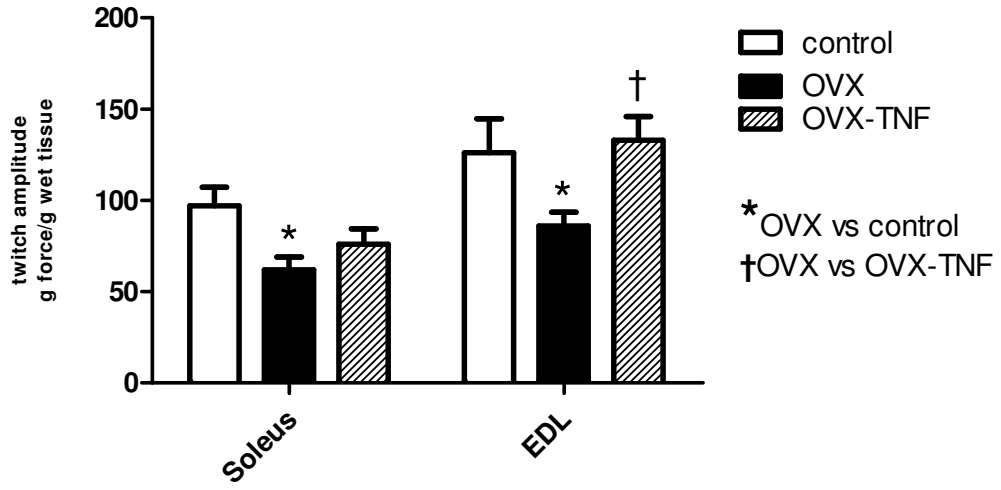

Figure 5.2: Maximum isometric twitch amplitude levels of all groups at 0.1 Hertz stimulation frequency (g/g wet tissue). (P=0.05, *Mean±SE, *OVX vs. control, †OVX vs. OVX-TNF). (Isometric contraction responses in the EDL muscle were significantly lower in the OVX group which recovered in the OVX-TNF group. In the SOL muscle, the OVX group's responses were lower than that of the control group. OVX-TNF group responses were not significantly different from OVX and control groups.)

In the course of tetanic train stimulation (increasing frequencies of stimulation) the EDL muscles of the OVX group presented lower contraction force responses than

that of the control group whereas in the OVX-TNF group this decrease was recovered (Figure 5.3).

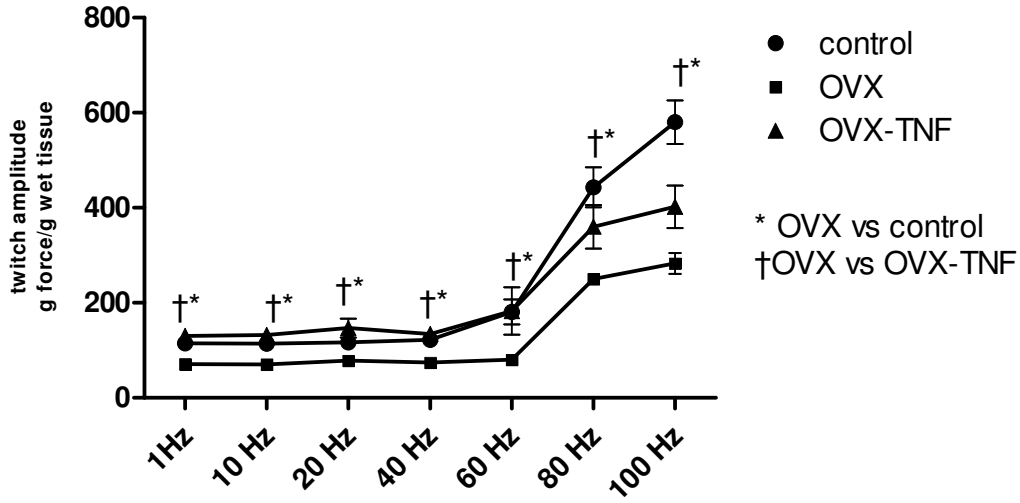

Figure 5.3: Train test of tetanic twitch amplitudes at 1, 10, 20,40,60,80 and 100 Hz stimulation frequencies of the EDL muscles of all groups (G force/g wet tissue) (P=0.05, *Mean±SE, *OVX vs. control, †OVX vs. OVX-TNF). (Contraction responses to increasing frequencies of stimulation were significantly lower in the OVX group than the control group. This functional decrease recovered in the OVX-TNF group.)

During tetanic train stimulation, when the SOL muscles were subjected to lower frequencies of stimulation (1 Hz and 10 Hertz) the OVX and the OVX-TNF groups gave lower responses ($p \leq 0.05$) than the control group. At higher frequencies however the OVX-TNF group contraction forces were well recovered giving responses

approximately equal to the control group and much higher than the OVX groups (Figure 5.4).

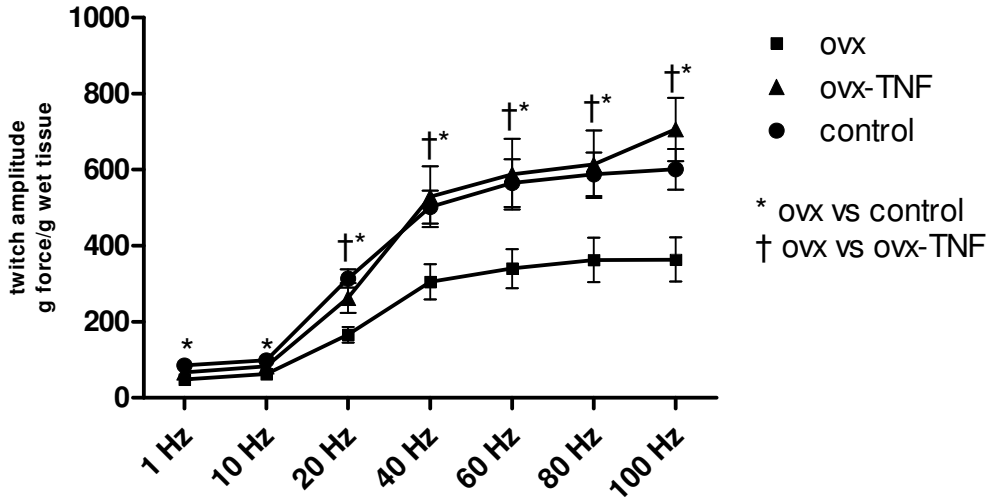

Figure 5.4: Train test of tetanic twitch amplitudes at 1,10,20,40,60,80 and 100 Hz stimulation frequencies of the SOL muscles of all groups. (G force/g wet tissue) (p=0.05, *Mean±SE, *OVX vs. control, † OVX vs. OVX-TNF). (Contraction responses to increasing frequencies of stimulation were significantly lower in the OVX group than the control group. This functional decrease recovered in the OVX-TNF group at high frequencies (>10 Hertz).)

5.2: Light Microscopy

5.2.1. Histology:

The overall muscular morphology was assessed at low magnification in haematoxylin eosin (HE) stained sections. Changes in cellular/myofibrillar shape

(loss of the polygonal shape, rounding) and size (small or large cells), changes in nuclear position (normally sarcolemmal, abnormally central location) were also analyzed on HE stained sections (Figures 5.5 and 5.6). Degeneration or regeneration, fibrosis and adipose tissue formation were assessed in Masson's Trichrome stained slides (Figures 5.7 and 5.8).

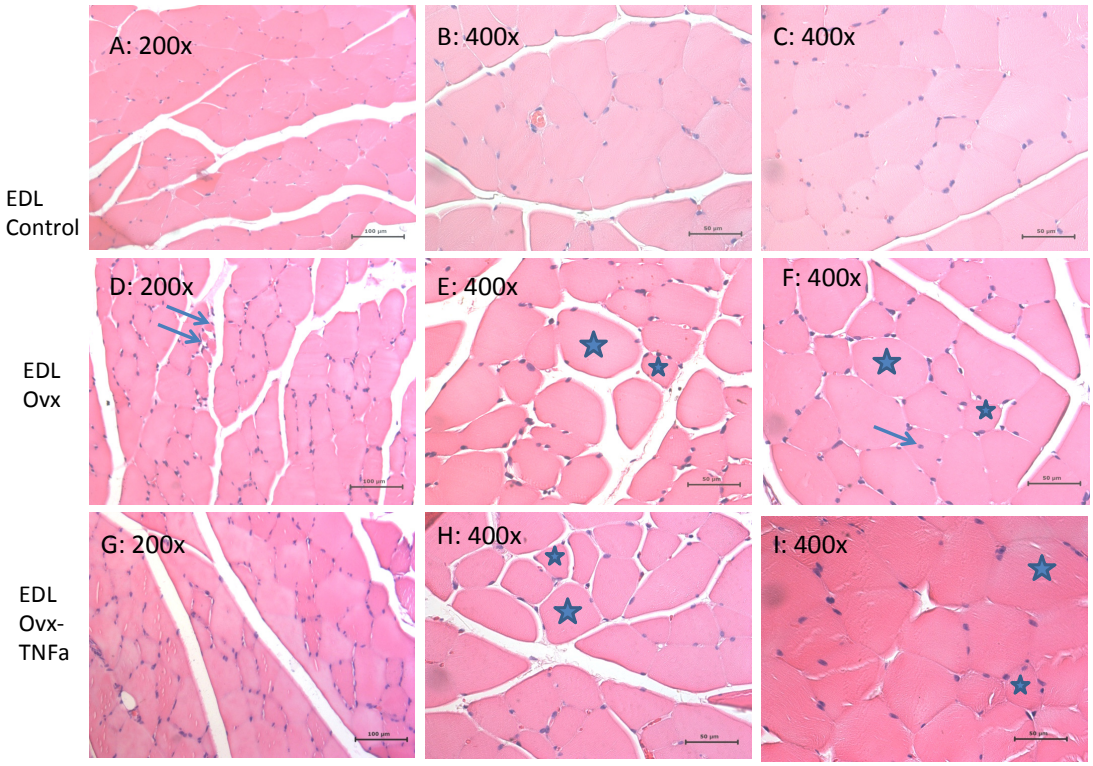

Figure 5.5: HE stained cross sections of EDL muscles from control, OVX and OVX-TNF antagonist applied groups. (Note splitting of fibres in E, F, H and I. Big and small stars show different sized fibres respectively in E, F, H and I. Arrow: Central nucleus, Double arrow: a small cluster of atrophic fibers.)

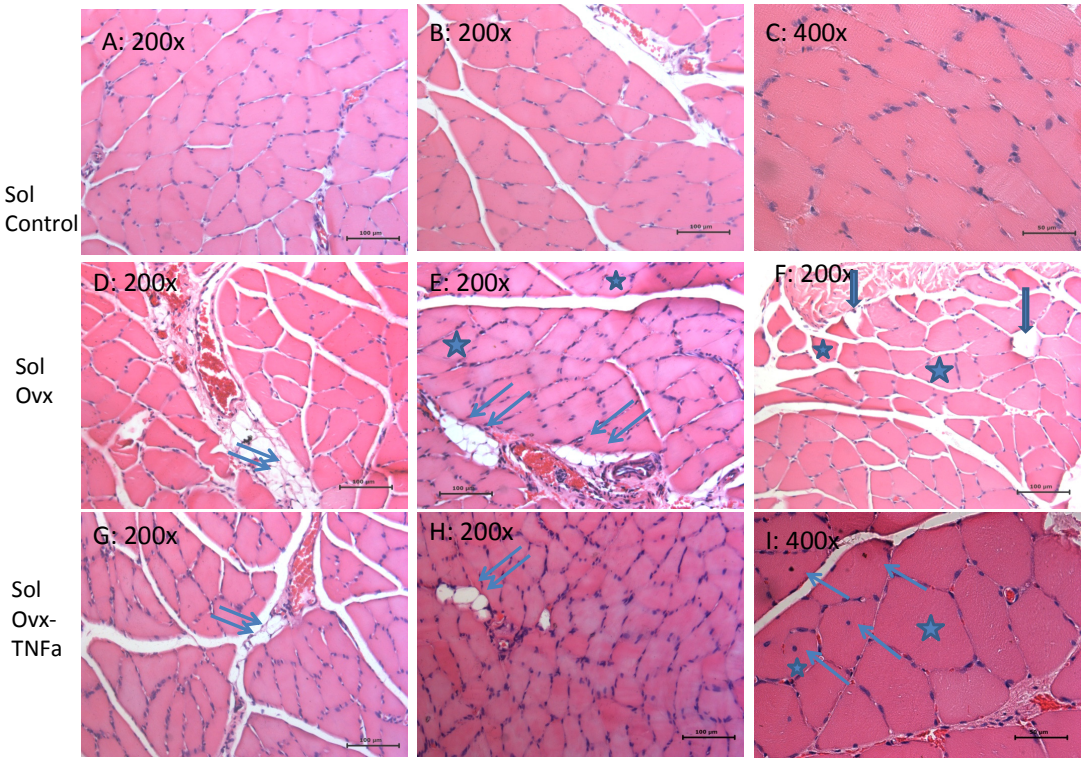

Figure 5.6: HE stained cross sections of SOL muscles from control, OVX and OVX-TNF antagonist applied groups. (Note splitting of fibres in D, and F. Big and small stars show different sized fibres respectively in E, F and I. Arrow: Central nucleus, Double arrow: Fat cells, Block arrow: Degenerated cells.)

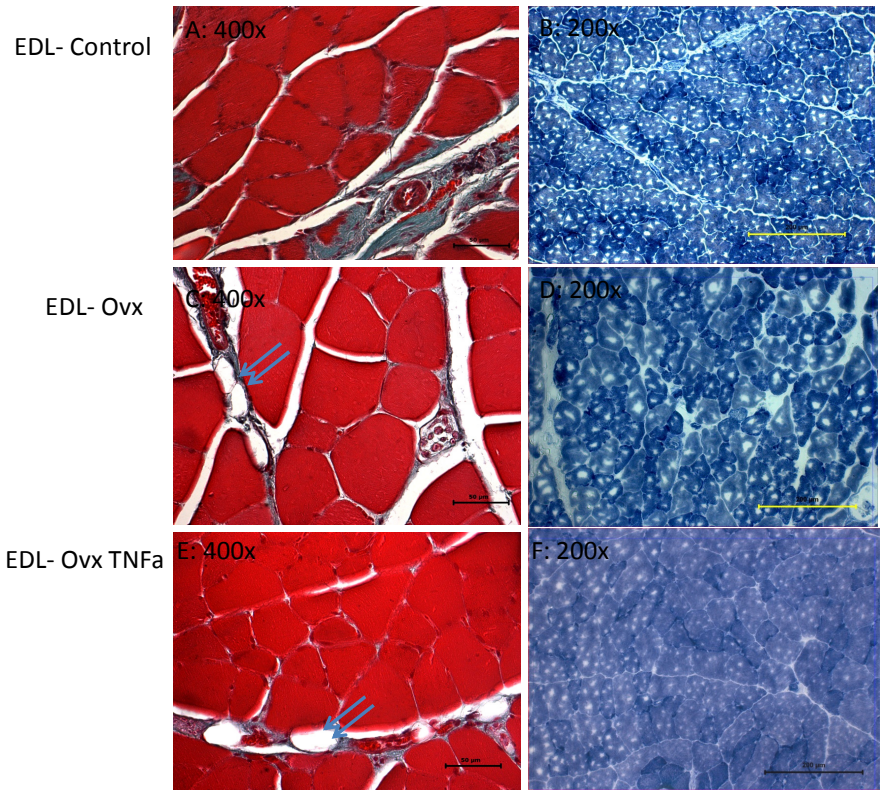

Figure 5.7: Masson's trichrome (A, C, E) and NADPH (B, D, and F) stained sections are presented for the EDL muscle. (Note the light and dark blue colours of different fiber types in B, D and F. In A, C and E the connective tissue content of the EDL muscle belonging to different groups are obvious. Double arrow: Fat cells.)

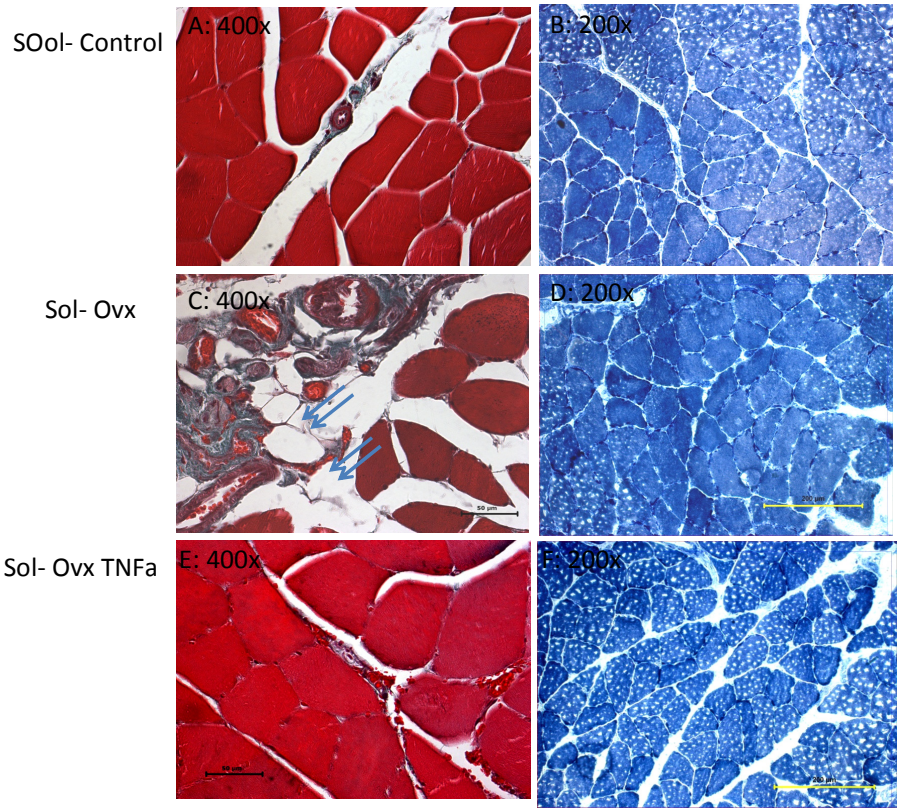

Figure 5.8: Masson's trichrome (A, C, E) and NADPH (B, D, F) stained sections are presented for the SOL muscle. (Note the light and dark blue colours of different fiber types in B, D and F. In A, C and E the coonective tissue content of the SOL muscle belonging to different groups are obvious. Double arrow: Fat cells.)

Variability and change in size of the muscle cells were observed in small clusters or single cells belonging to both the EDL and the SOL muscles of the OVX and OVX-TNF groups. In some specimens this small sized cells were accompanied by hypertrophic cells in the OVX and OVX-TNF groups. Scattered fat cells were noted in all groups, but they were much more numerous in the OVX group, compared to other groups and some degenerated or necrotic fibers were noted in this group (Figure 5. 6f). Muscle lesser diameters and the changes of the fiber type patterns were

quantitatively assessed in the following section. Splitting of myofibers was also observed in some OVX groups (Figures 5.5, 5.6, 5.7, 5.8).

5.2.2. NADH Fiber Type Specific Histochemistry

NADH-TR staining gave different color intensities for the Type I and the Type II fibers (Figures 5.7 and 5.8). The results of lesser diameter and cross-sectional area measurements revealed that type I fiber ratio to total number of fibers were higher in the EDL muscles of the control group comparing to that of the OVX ($p=0.043$) whereas no significant difference was observed between the Control and the OVX-TNF groups ($p=0.115$) and OVX-OVX-TNF groups ($p=0.732$) (Table 5.2). The SOL muscle ratios were not quantified because of the insufficient of type II fiber amount for statistics.

Table 5.2: Ratios of Type I and Type II fibers to total fiber number in all groups.

	Control Group EDL	**OVX Group EDL**	**OVX-TNF Group EDL**
Type I %	45.3%±3.5	55.3%±3.8	53.5%±3.2
Type II %	54.7%±3.5	44.7%±3.8	46.5%±3.2

There was a significant ($p=0.043$) difference between the control and the OVX groups and the control and the OVX-TNF groups in fiber type percentages. Significant difference was not observed between the OVX and the OVX-TNF groups (Table 5.2).

Type I lesser diameter and Type I cross-sectional areas of the EDL muscles were significantly different between groups (p=0.024 for diameter and p=0.034 for CSA). (Table 5.3, Figure 5.9, 5.10)

Table 5.3: Mean rank values of Type I and Type II fiber lesser diameter and CSA in the EDL muscles of groups.

Mean Ranks	**Control**	**OVX**	**OVX-TNF**
Type I Diam (µm)	3.6	10.8	9.6
Type I CSA (μm^2)	4.4	9.2	10.4
Type II Diam (µm)	3.8	10.6	9.6
Type II CSA (μm^2)	4.4	9.2	10.4

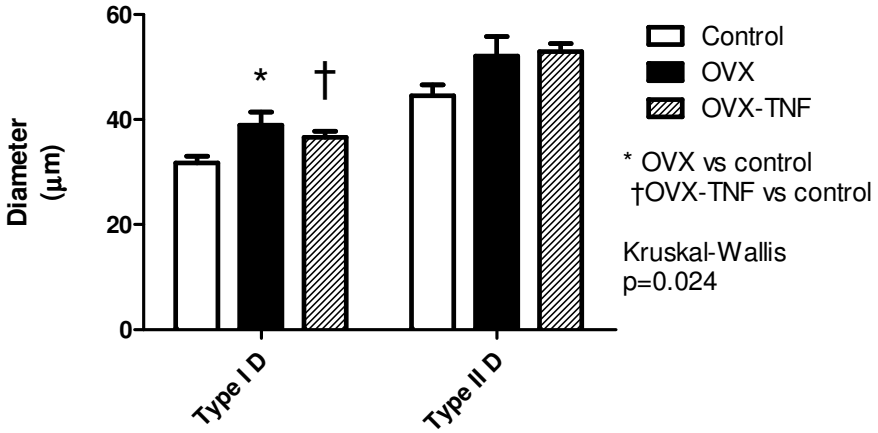

Figure 5.9: Type I and Type II fiber lesser diameter values of the EDL muscles of the control, the OVX and the OVX-TNF groups.

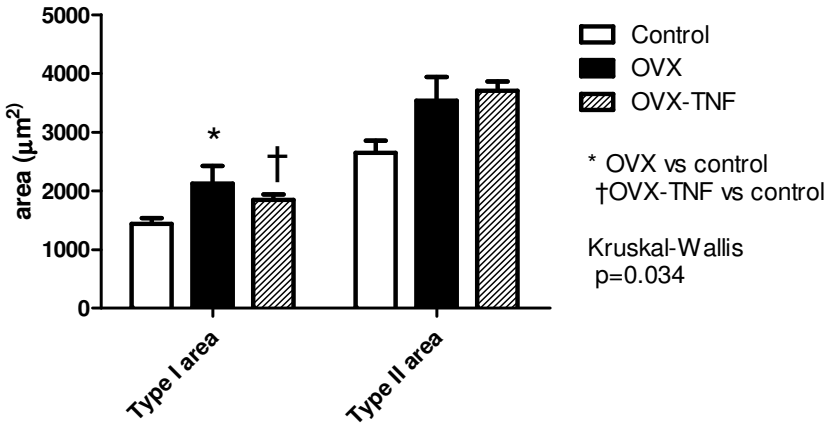

Figure 5.10: Type I and Type II fiber areas of EDL muscles of the control, the OVX and the OVX-TNF groups.

In the SOL muscles of the rats, there was no significant difference in fiber diameters and areas between groups (Table 5.4, Figures 5.11 and 5.12)

Table 5.4: Mean rank values of Type I and Type II fiber lesser diameter and CSA in the SOL muscles of groups.

Mean Ranks	**Control**	**OVX**	**OVX-TNF**
Type I Diam	6.1	10.6	10.5
Type I CSA	7.1	9.6	10.3
Type II Diam	6.6	10.8	9.8
Type II CSA	10.6	8.8	7.5

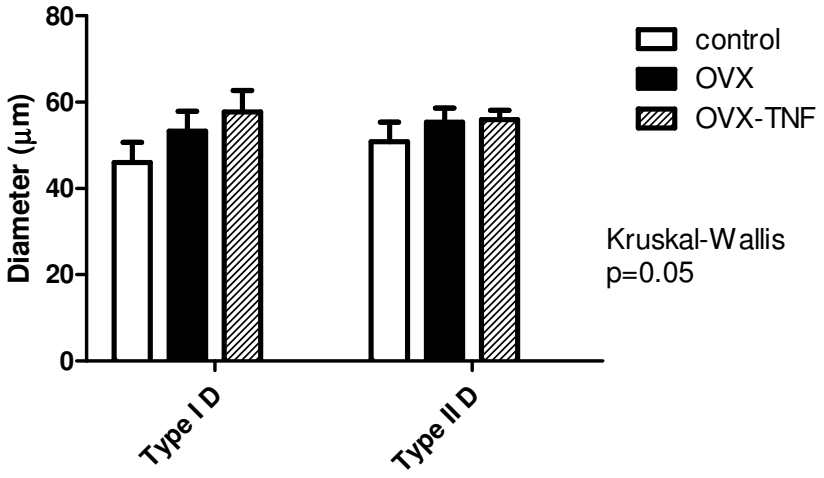

Figure 5.11: Type I and Type II fiber lesser diameter values of the SOL muscles of the control, the OVX and the OVX-TNF groups.

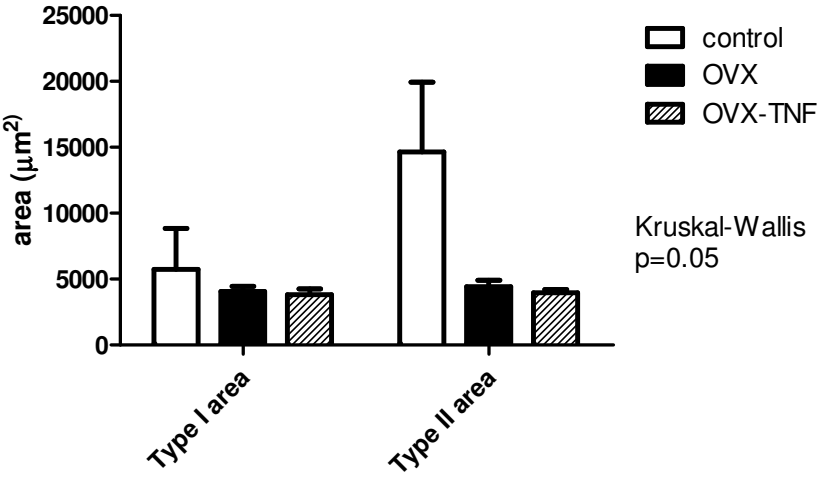

Figure 5.12: Type I and Type II fiber areas of the SOL muscles of the control, the OVX and the OVX-TNF groups.

5.3: Immunohistology

5.3.1: p65 Immune Labeling

P65 exhibited cytoplasmic and/or nuclear labeling patterns. It exhibited a very low or no immune reaction in the the control and the OVX-TNF of the EDL muscles.

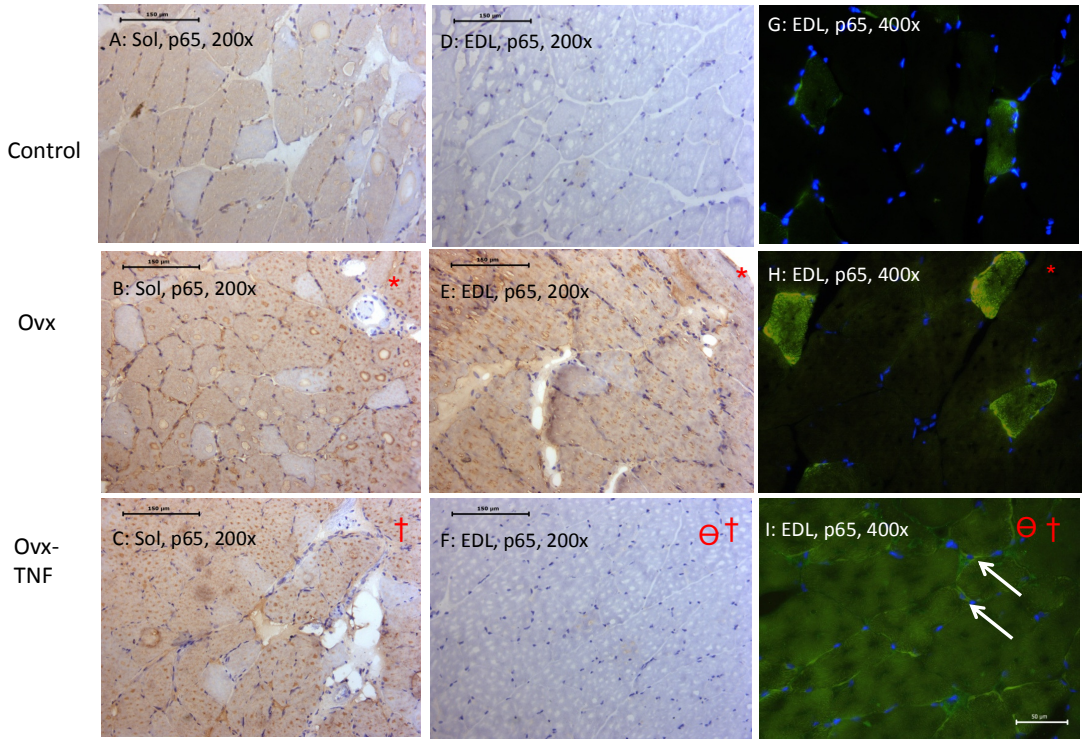

Figure 5.13: p65 immunolabeled cross sections of the SOL and the EDL muscles of the control, the OVX and the OVX-TNF groups. (p65 exhibited diffuse and strong labeling patterns in the SOL (A-C); it had very low or no immune reactivity in the EDL muscles of the OVX and the OVX-TNF groups (D-I).. A-F: Immune peroxidase gave brown, G-I: FITC labeled immune fluorescent method gave green colour to reactive cells. The nuclei were purple and blue, respectively.)

The p65 distribution was much more diffuse and its staining intensity was stronger in all groups for the SOL muscle. The cytoplasmic p65 immune reactivity in the control groups shifted towards the nucleus in the OVX and the OVX-TNF groups in both the EDL and the SOL muscles (Figure 5.13).

The p65 immunoreactivity was significantly higher in the OVX group comparing to that of the control and the OVX-TNF groups in the SOL muscles ($p<0.001$). P65 immune reactivity of the control and the OVX-TNF group muscles were not significantly different from each other in the SOL muscles. All three groups were significantly different in the OVX>OVX-TNF>Control order in the EDL muscles ($p<0.001$) (Figure 5.13).

5.3.2: MyoD Immune Labeling

The MyoD D presented a nuclear and/or cytoplasmic immune reaction pattern in the scattered cells in all groups. The H scores reflecting the staining intensity and labeled cell percentage were vey low or negative in the control groups. The MyoD immunolabeling significantly increased with OVX group when compared to the control group in both the EDL and the SOL muscles ($p=0.046$ and $p=0.001$, respectively). Results of the OVX-TNF group were not statistically different from both groups in the EDL muscle. In the SOL muscle, MyoD immunolabeling significantly increased in the OVX-TNF group compared to that of the control group (Figure 5.14).

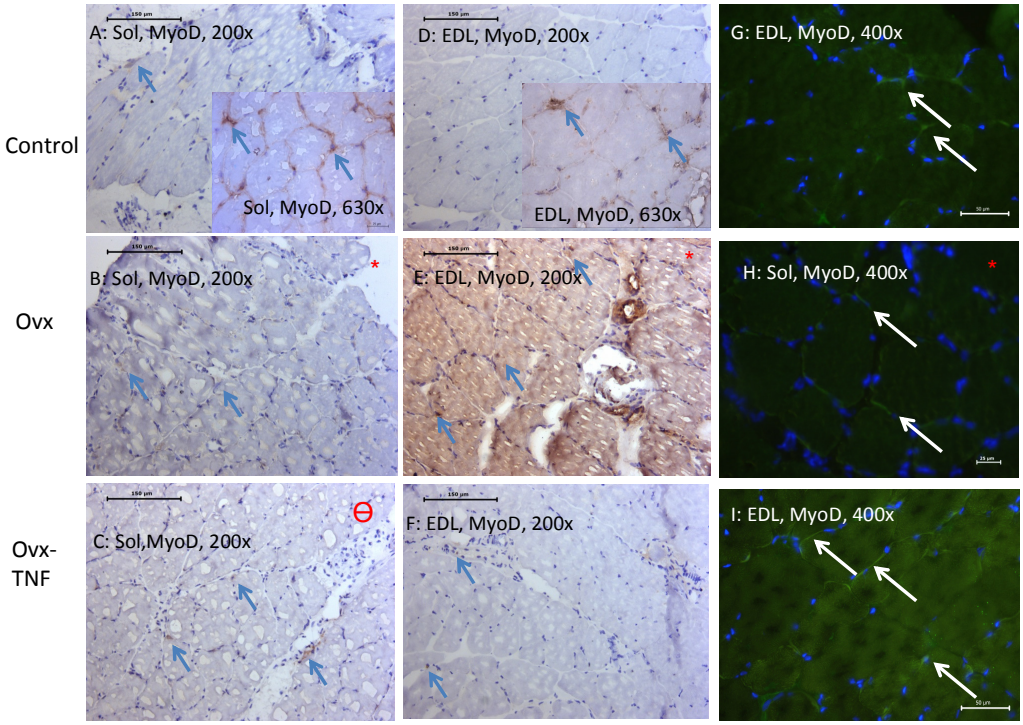

(Kruskal Wallis-Connover: * ovx vs control Θ ovx-TNF vs control Sol P=0,001, EDL P=0,046)

Figure 5.14: MyoD immunolabeled cross sections of SOL and the EDL muscles from the control, the OVX and the OVX-TNF groups. (MyoD exhibits low intensity nuclear labeling pattern in the SOL and the EDL in all groups; it has an enhanced immune reactivity in the OVX EDL muscle(E). Nuclear staining : Arrow. A-F: Immune peroxidase gives brown , G-I: FITC labeled immune fluorescent lmethod gives green colour to reactive cells. The nuclei are purple and blue respectively.)

5.3.3: p50 Immune Labeling

The p50 exhibited cytoplasmic and/or nuclear distribution patterns in all groups. P50 immune reactivity was lower in the OVX-TNF group when compared to that of the control and the OVX groups in the SOL muscles (P=0.033). The OVX and the control group intensities were statistically not different from each other in the SOL

muscles. In the EDL muscles statistical difference was not found between the groups. (Figure 5.15).

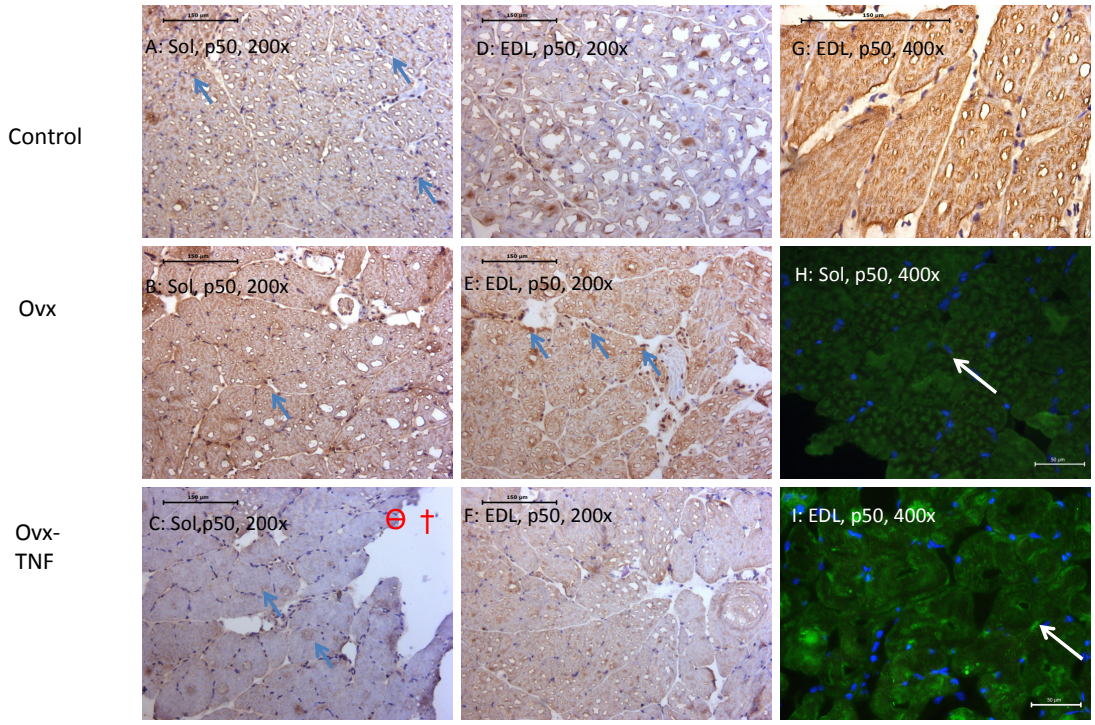

Figure 5.15: p50 immunolabeled cross sections of the SOL and the EDL muscles of the control, the OVX and the OVX-TNF groups. (p50 exhibited diffuse cytoplasmic myofilamentous-like labeling pattern in the SOL and the EDL in all groups; it has a nuclear immune reactivity in some samples. Nuclear staining: Arrow. A-G: Immune peroxidase gave brown, H-I: FITC labeled immune fluorescent method gave green colour to the reactive cells. The nuclei were purple and blue, respectively.)

5.3.4: C-Rel Immune Labeling

The C-Rel exhibited nuclear distribution patterns on scattered cells in all of the groups. C-Rel immune reactivity was higher in the OVX-TNF group when compared to that of the control and the OVX groups in the EDL muscles (P=0.01). Reactivity differences was not observed in the SOL muscles between the groups (Figure 5.16)

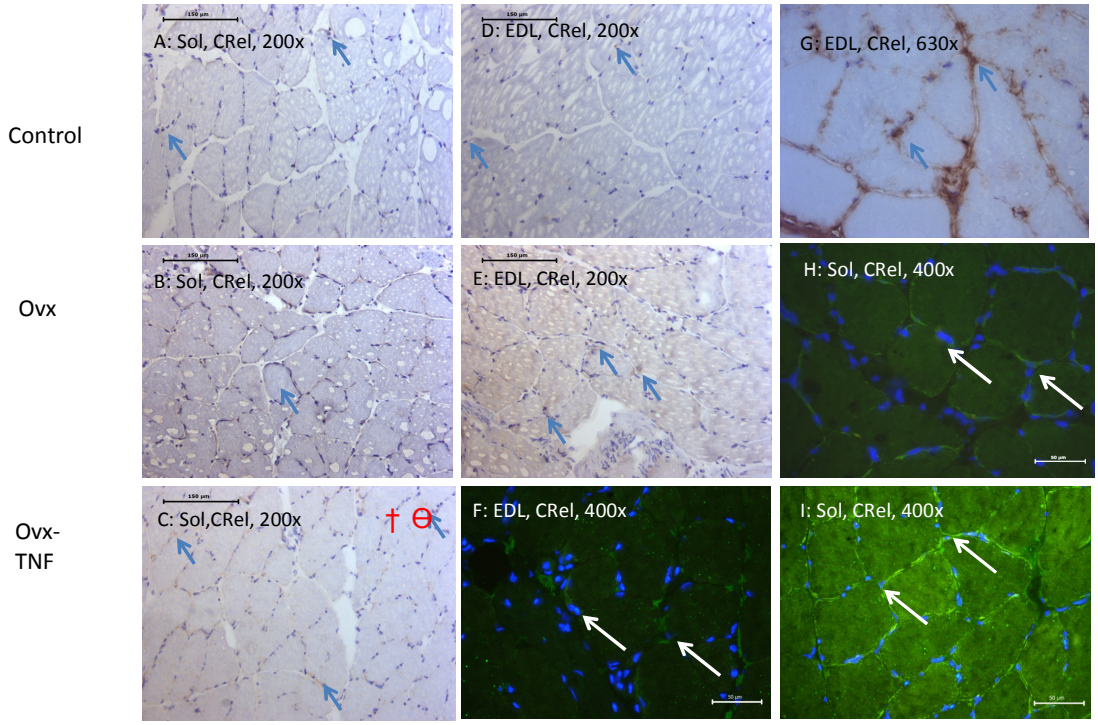

Figure 5.16: C-Rel immunolabeled cross sections of the SOL and the EDL muscles of the control, the OVX and the OVX-TNF groups. (C-rel exhibits nuclear labeling pattern in scatterered cells of the SOL and the EDL muscles in all groups; Nuclear staining: Arrow. A-G: Immune peroxidase gives brown, H-I: FITC labeled immune fluorescent method gives green colour to reactive cells. The nuclei are purple and blue respectively.)

5.3.5: Bcl3 Immune Labeling

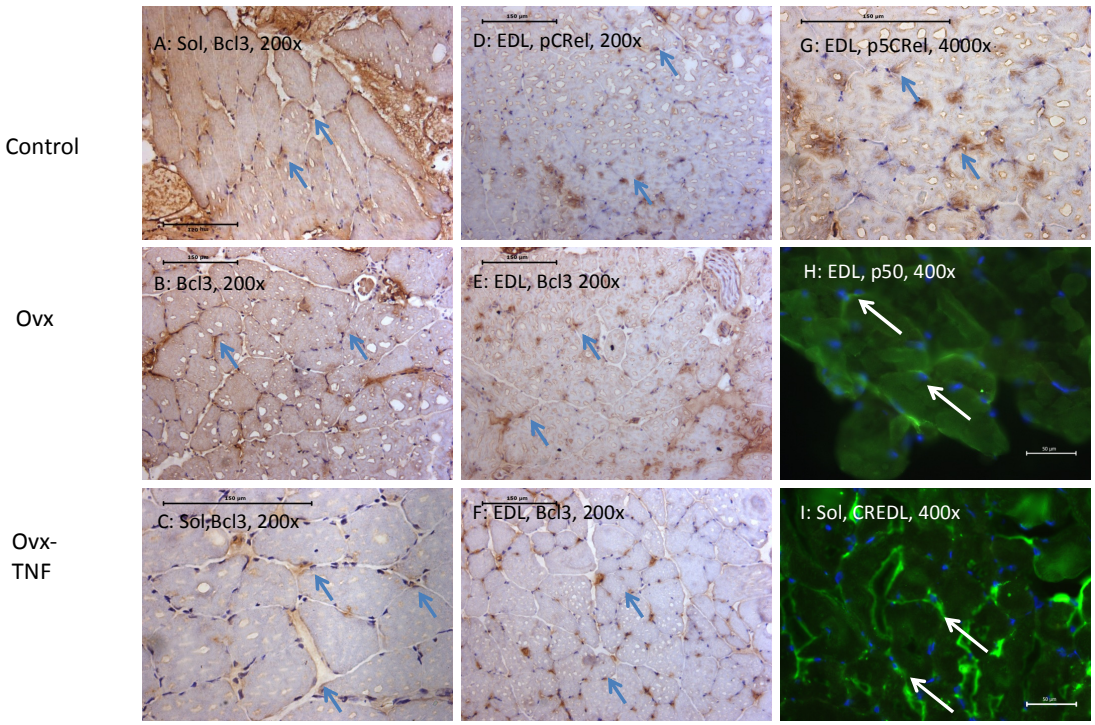

Figure 5.17: Bcl3 immunolabeled cross sections of the SOL and the EDL muscles of the control, the OVX and the OVX-TNF groups. (Bcl 3exhibited nuclear labeling pattern in the scatterered cells of the SOL and the EDL muscles in all of the groups; Nuclear staining: Arrow. A-G: Immune peroxidase gave brown, H-I: FITC labeled immune fluorescent method gave green colour to the reactive cells. The nuclei were purple and blue, respectively.)

The Bcl3 immune reaction was mainly nuclear and the labeling intensity was generally low in all of the groups for the EDL and the SOL muscles. The Bcl3

immune reaction was not different between the groups in the EDL and the SOL muscles (Figure 5.17).

5.4: Transmission Electron Microscopy

The number of mitochondria was normal in the fast-type EDL muscles of the control group rats. Some mitochondria undergoing lyses were also noted in this group (Figure 5.18).

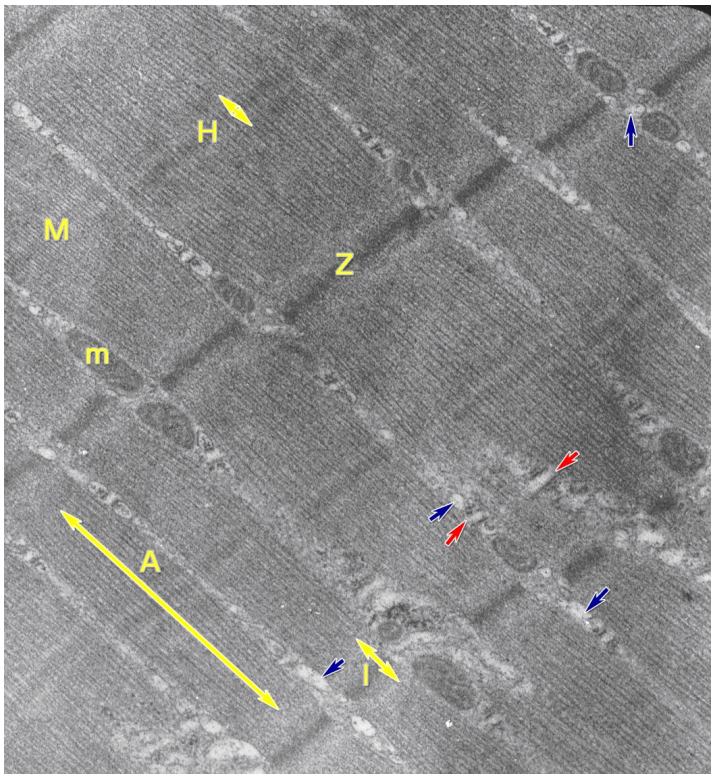

Figure 5.18: Electron microscopic image of control group rat EDL muscle under X21560 magnification. (A bands, Z bands, H bands I bands, mitochondria are seen. Blue arrows represent sarcoplasmic reticulum as red arrows represent T-tubulus.)

The slow type SOL muscles of the control group were containing immense amount of mitochondria under the sarcoplasmic reticulum and they had well-defined Z bands (Figure 5.19).

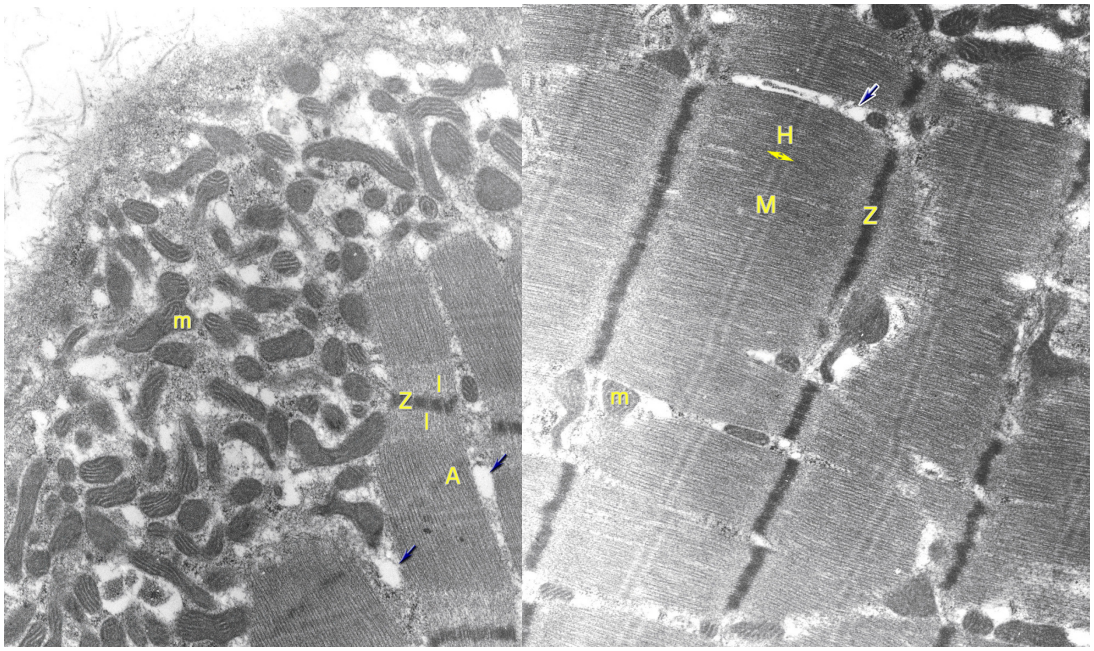

Figure 5.19: Electron microscopic image of control group rat SOL muscle under X12360 magnification. (On the left side, large cluster of mitochondria are seen, on the right Z and H bands are observed. M=m bands m=mitochondria.)

The sarcomeres were slightly disrupted in the fast EDL muscles of the OVX group. The overall condition of the muscle fibers seemed normal. The mitochondria were slightly swollen and less in number than that of the control group (Figures 5.20 and 5.21).

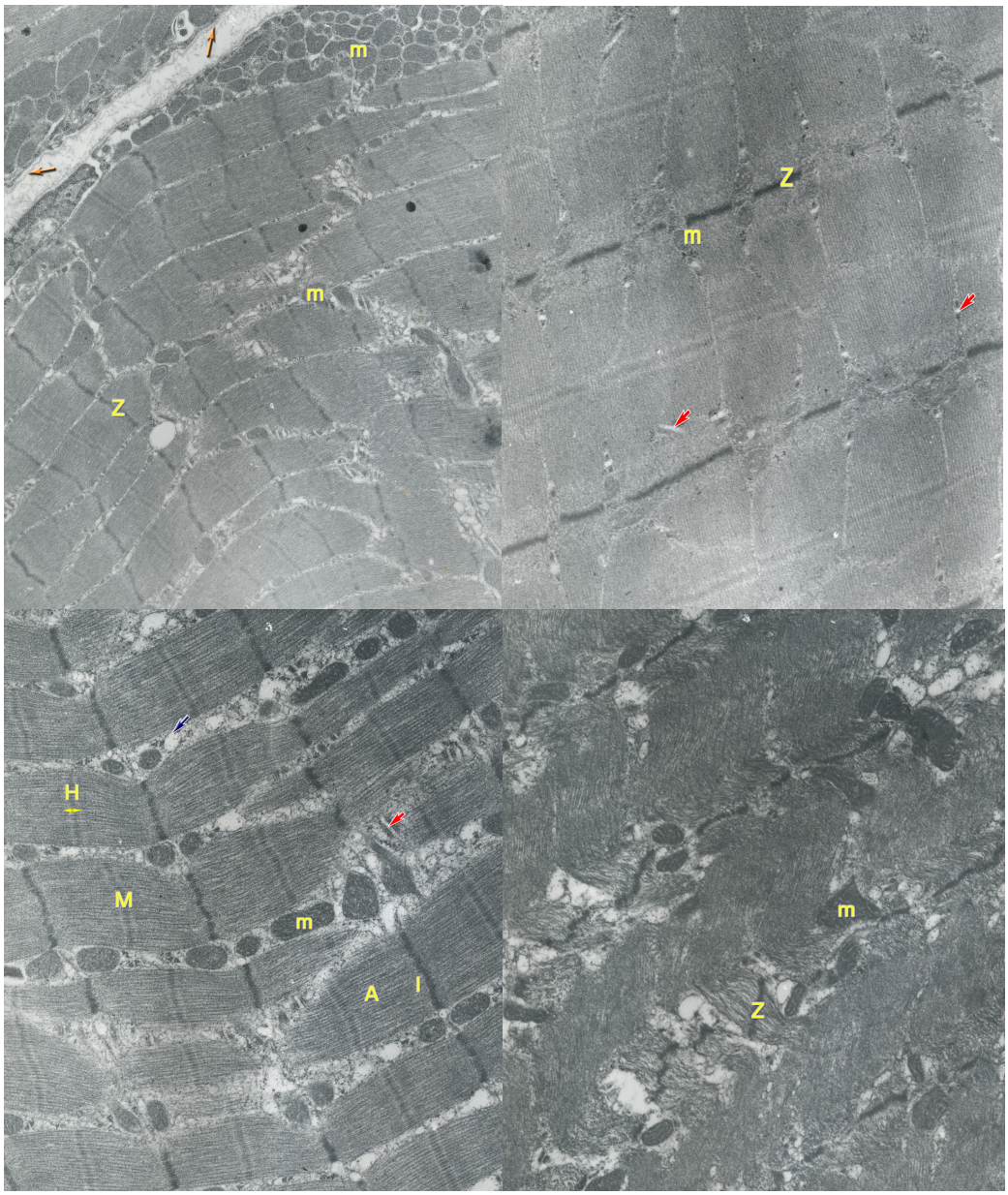

Figure 5.20: Electron micrographof the OVX group EDL muscle. (M=mitochondria, Z=Z bands, M=M bands, H= H bands, I=I bands, Orange arrows=sarcolemma, red arrows=t-tubulus. Uranyl acetate lead citrate, 12930x, 7750x)

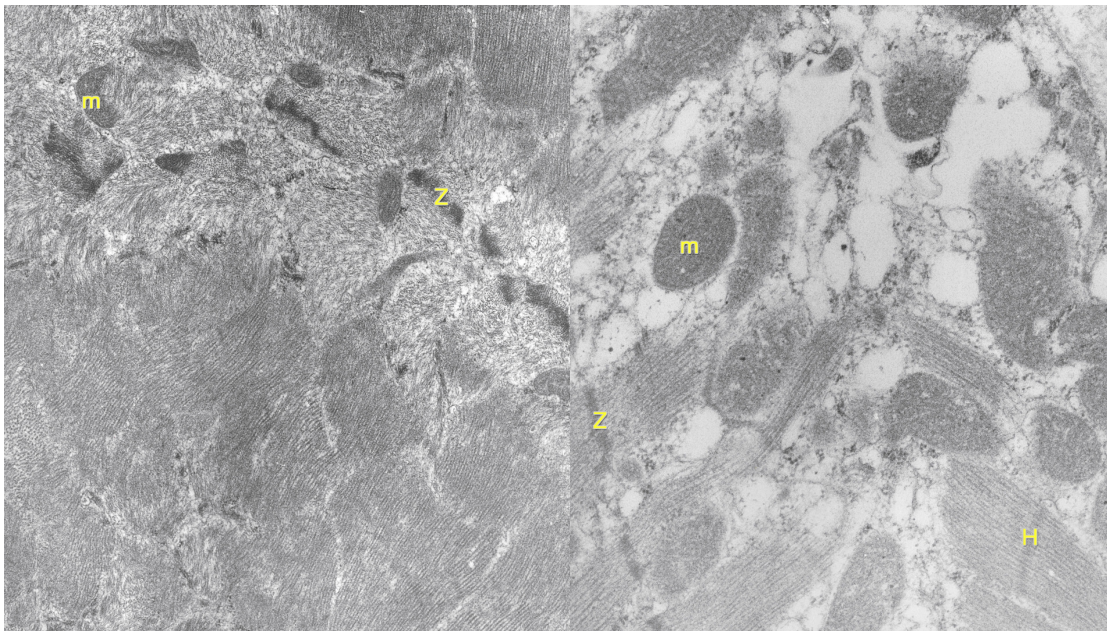

Figure 5.21: Electron microscopic image of the OVX group rats EDL muscle under X12930 and X21560 magnification (M=mitochondria, Z=Z bands, H= H bands).

The slow SOL muscles of the OVX group rats contained less number of mitochondria than that of the control group. The overall condition of the muscle fiber seemed normal but fibers were slightly thicker than normal (Figures 5.22 and 5.23).

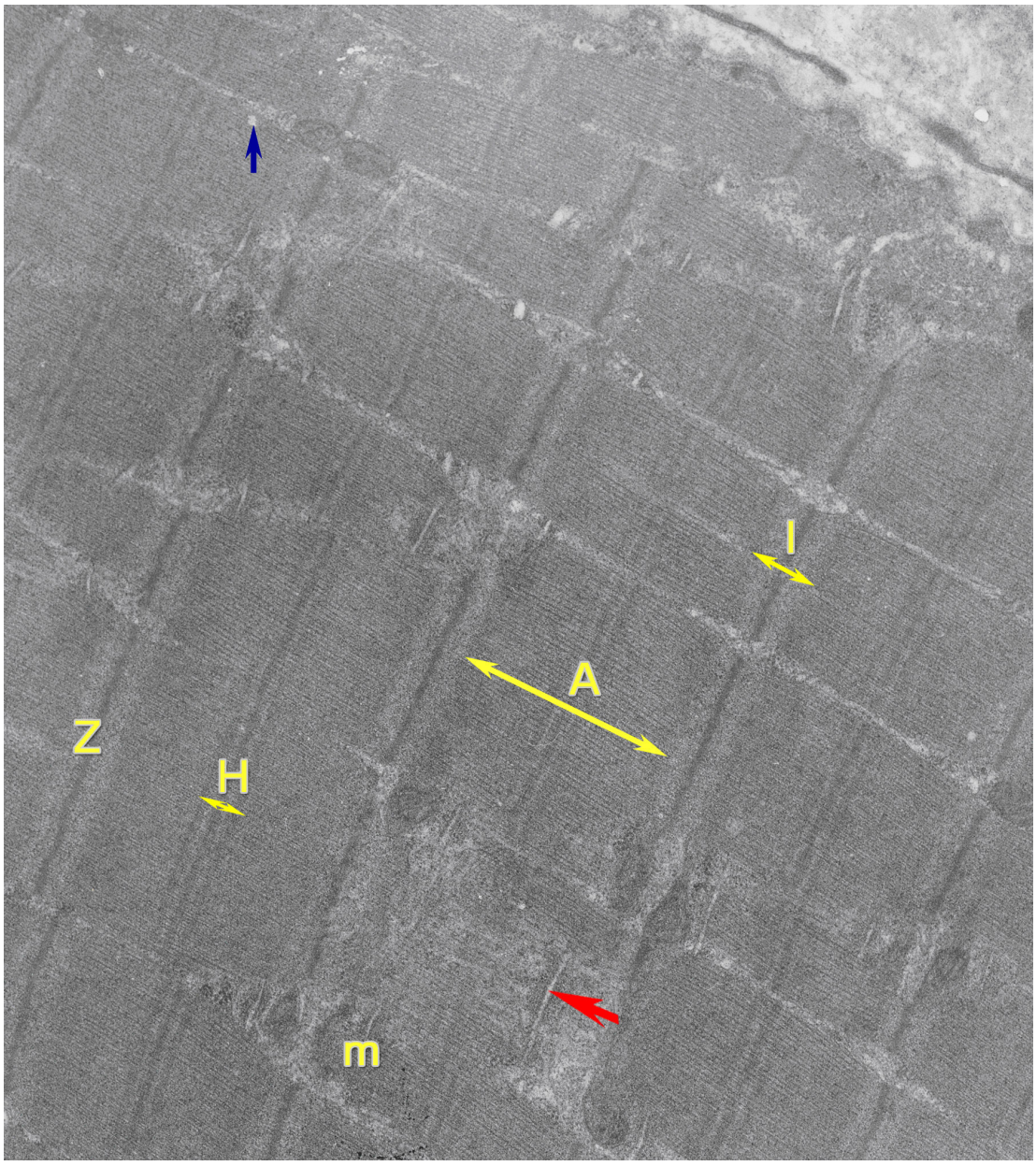

Figure 5.22: Electron micrograph of the OVX group SOL muscle (m=mitochondria, Z=Z bands, H= H bands, A=A bands, I=I bands, blue arrow=sarcoplasmic reticulum, red arrow=t-tubulus. Uranyl acetate lead citrate, 10000x).

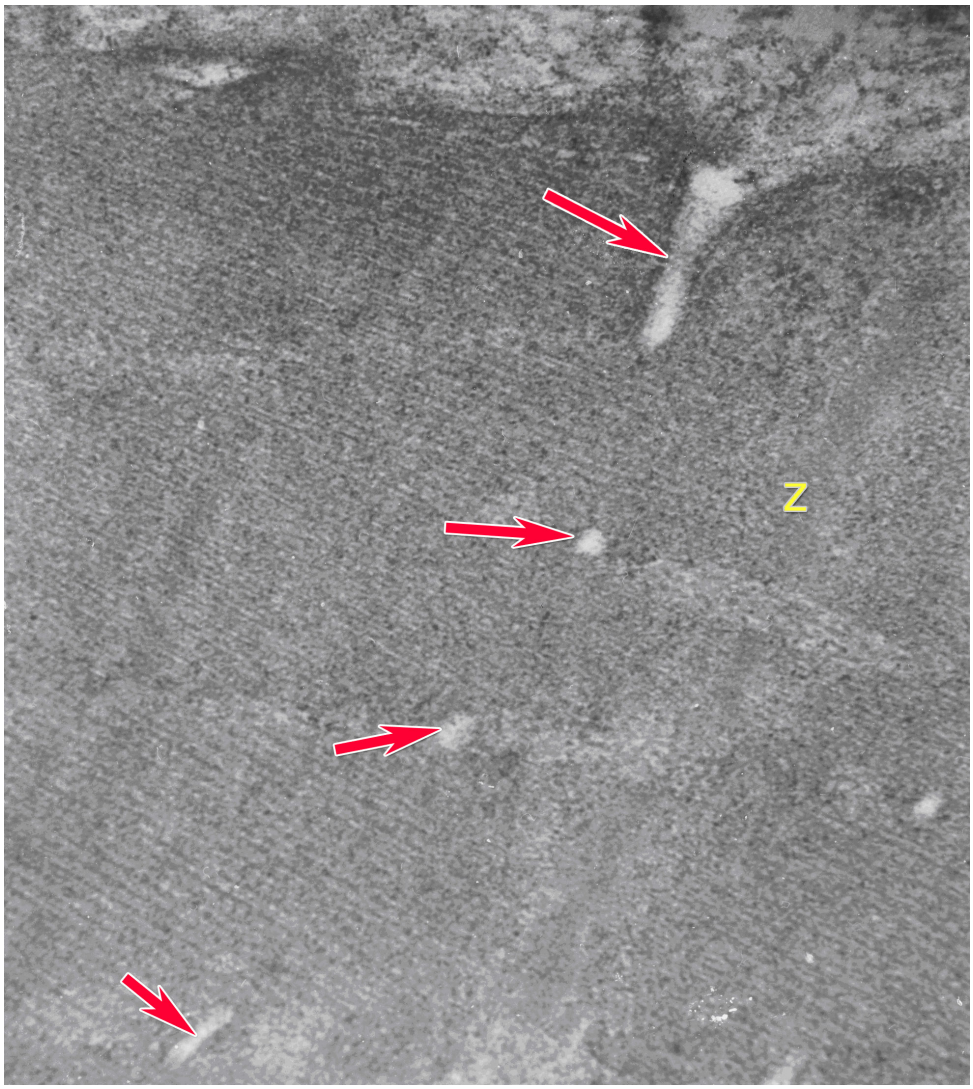

Figure 5.23: Electron micrograph of the OVX group SOL muscle (Z=Z bands, red arrow=t-tubulus). Note the presence of spaces between the myofibers. The fibers were like in a bow-tied shape (arrow). Uranyl acetate lead citrate 16460x

The fast EDL muscles of the OVX-TNF group contained even amount and distribution of mitochondria and glycogen and they were revealing a healthy state. (Figures 5.24 and 5.25)

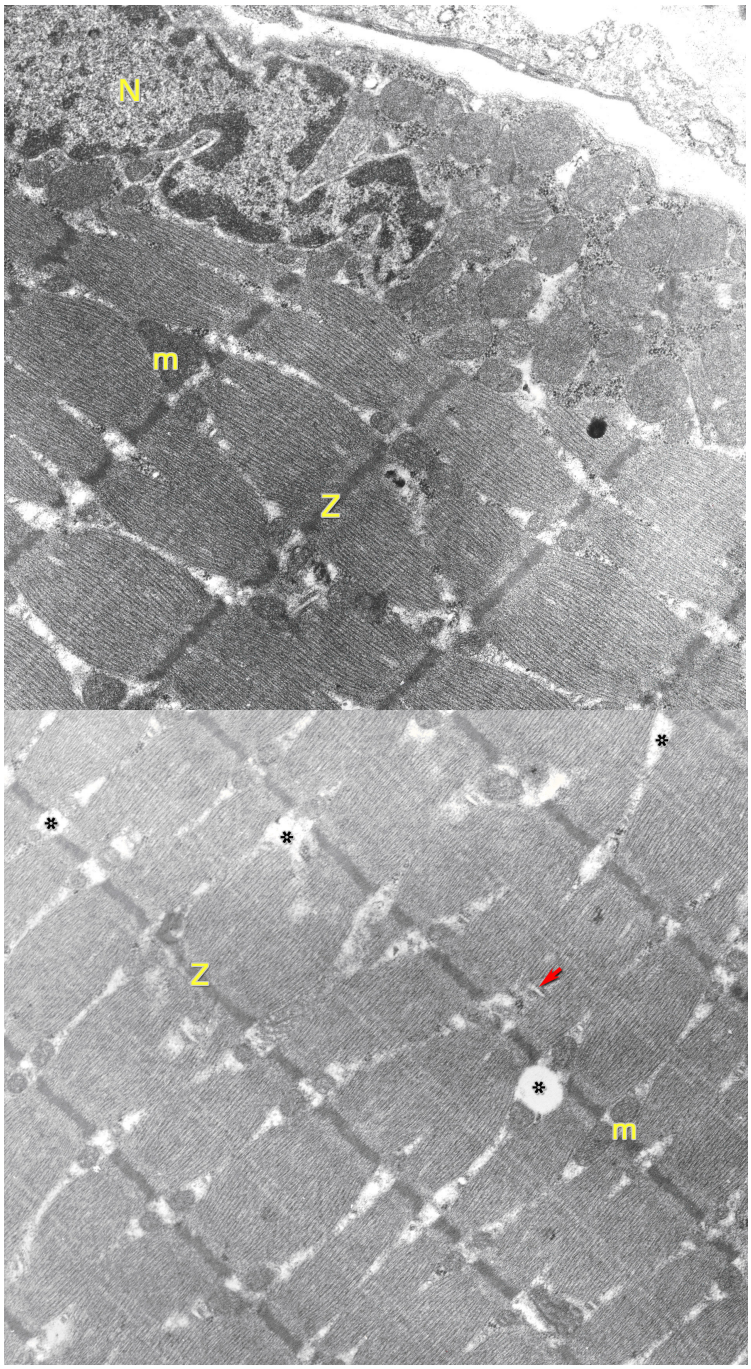

Figure 5.24: Electron micrograph of the OVX-TNF group EDL muscle (Uranyl acetate lead citrate 10000x., Arrow: splitting Z=Z bands, m=mitochondria N=nuclei, asterix=spacing of fibers)

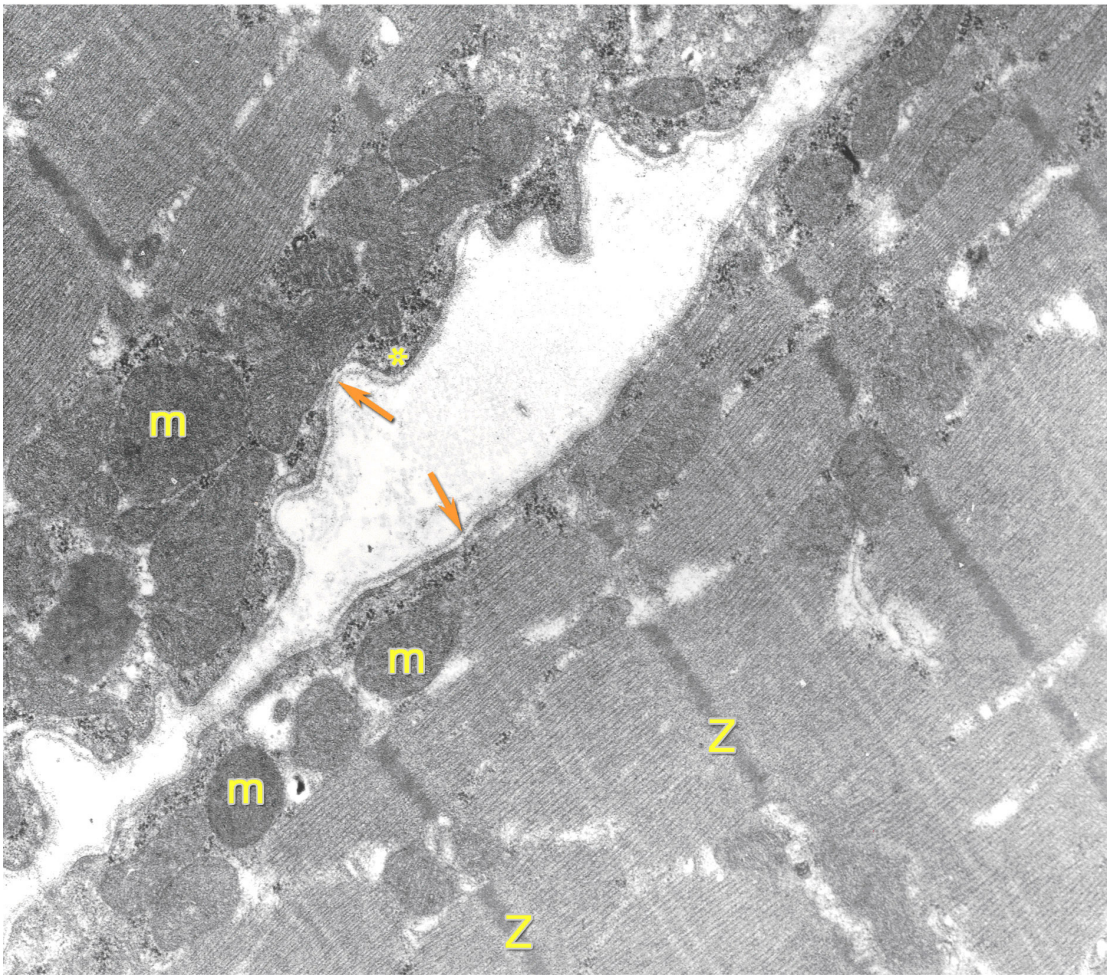

Figure 5.25: Electron micrograph of the OVX-TNF group EDL muscle. (Z=Z bands, m=mitochondria, orange arrows=basal lamina. Uranyl acetate lead citrate 10000x)

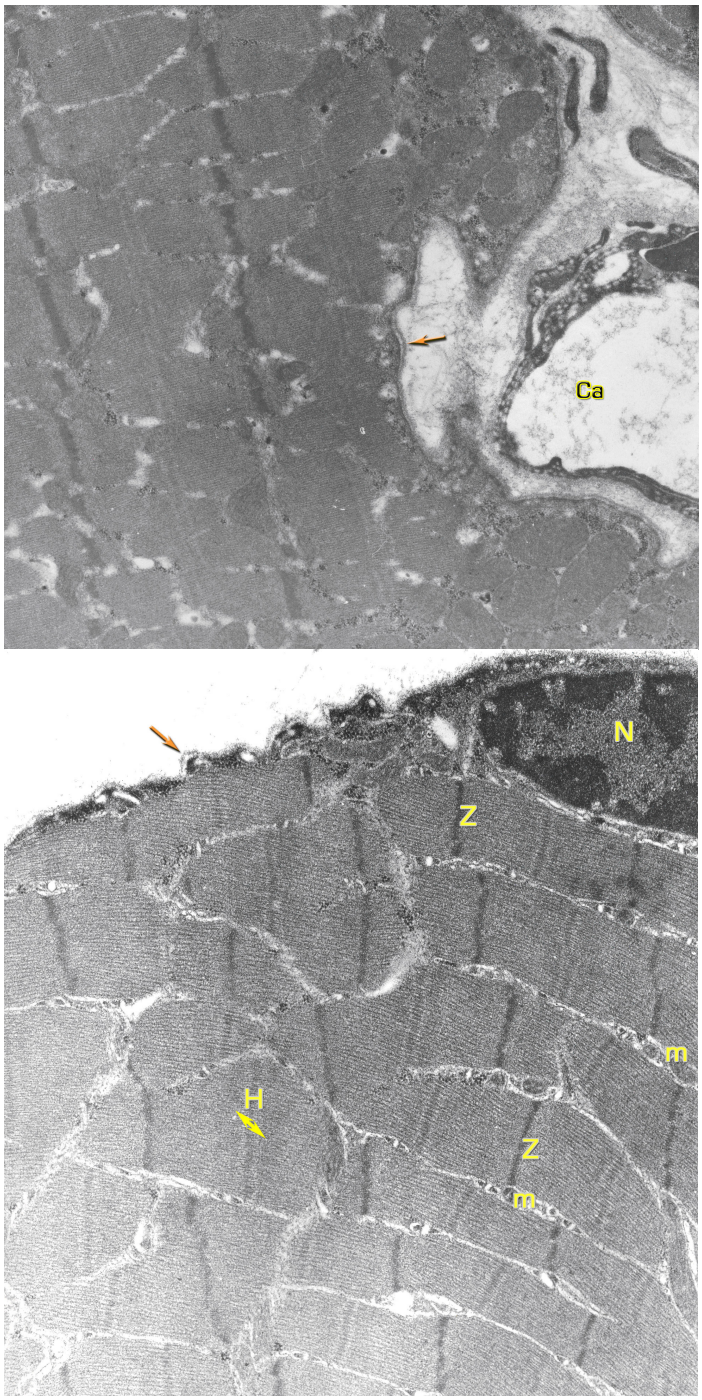

Figure 5.26: Electron micrograph of the OVX-TNF group SOL muscle (Z=Z bands, m=mitochondria, Ca=calcium Uranyl acetate lead citrate 12930x).

The slow SOL muscles of the OVX-TNF group contained large amount of mitochondria and glyogen. The mitochondirial cristae and the T-tubulus were well-defined (Figures 5.26 and 5.27).

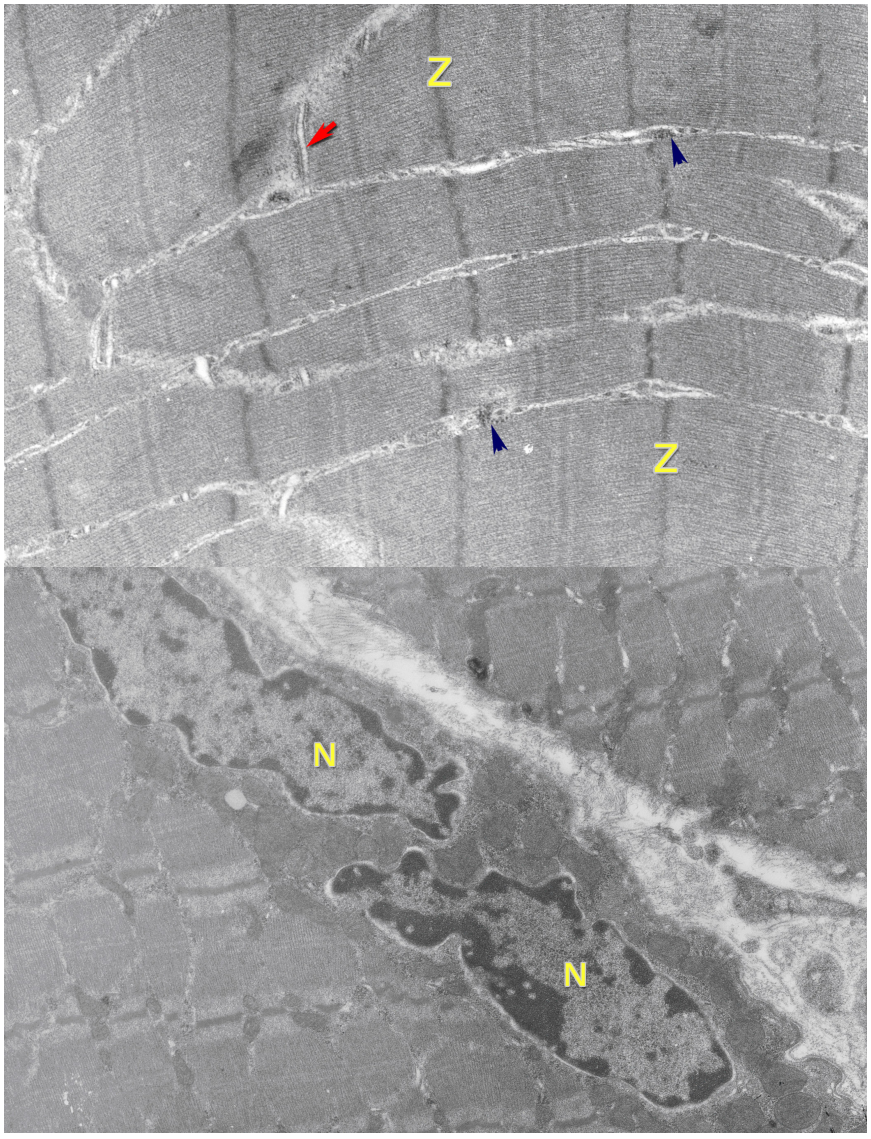

Figure 5.27: Electron micrograph of the OVX-TNF group SOL muscle (Z =Z bands, m=mitochondria, N=Nuclei. Uranyl acetate lead citrate, X6000, X10000).

5.5 Microarray:

Microarray analysis revealed significant changes in several gene expressions. The expression differences in groups were statistically analyzed for 61 genes and 42 unidentified transcripts out of 31.000 genes that were significantly altered in their transcription level at the OVX and the OVX-TNF groups at the nominal 0.001 level of the univariate test. An additional 39 genes were altered at 0.01 level. A hundred of these genes were named whereas several of the up and down regulated transcripts were unidentified transcripts. The identified genes showing expression differences are presented in Tables 5.5 to 5.9.

Table 5.5: The gene that shows expression difference between the groups in the EDL muscle.

	Control	**OVX**	**OVX-TNF**	**P-value**	**FDR**
protein phosphatase 1, regulator	130,381	92,360	33,068	0,000379	0,969

In the EDL muscle, only the protein phosphatase 1 gene showed a significant difference in expression levels in between groups which has a role in the insulin signaling pathway (Table 5.6). A significant decrease in protein phosphatase 1 regulator was observed in the OVX group when compared to the control group.

Table 5.6: The genes that show expression difference between the groups in the SOL muscle.

	Control	OVX	OVX-TNF	P-value	FDR
talin 1	26,134	23,133	54,487	2,51E-05	0,354
similar to homeobox-containing transcription factor	13,040	26,939	11,743	0,000132	0,588
chemokine (C-C motif) ligand 2	20,373	26,410	51,680	0,000182	0,708
R-spondin 3 homolog (Xenopus laevis)	235,075	141,723	138,499	0,000226	0,727
homeo box D9	60,600	108,382	58,855	0,000296	0,744
cytoplasmic polyadenylation element binding protein 2	14,774	19,950	28,621	0,000321	0,744
methionine adenosyltransferase II,	586,467	539,76	910,668	0,000451	0,815
myb-like, SWIRM and MPN domains 1	18,332	19,199	30,883	0,000464	0,815
Jun oncogene	192,154	333,133	217,276	0,000632	0,845
similar to lipid droplet associated protein	67,604	107,594	40,114	0,000707	0,845
CDW92 antigen	45,828	52,930	71,212	0,000792	0,879
chemokine (C-C motif) ligand 7	8,8966	9,2681	16,125	0,000879	0,887
nuclear receptor subfamily 4, group A, member 1	195,909	122,942	344,655	0,00097	0,887

In the SOL muscle, genes showed significant differences in expression in between groups (Table 5.7).

Processes that these genes are related in are: Apoptotic signaling in response to DNA damage, the integrin signaling pathway, mCalpain in cell motility, Rho cell motility signaling pathway, uCalpain and friends in cell spread, focal adhesion, Msp/Ron receptor signaling pathway, pertussis toxin-insensitive CCR5 signaling in macrophage, cytokine-cytokine receptor interaction, development methionine metabolism, selenoamino acid metabolism, immunology agrin in postsynaptic differentiation, angiotensin II mediated activation of JNK pathway *via* Pyk2 dependent signaling, ATM signaling pathway, BCR signaling pathway, D4-GDI signaling pathway, EGF signaling pathway, EPO signaling pathway, FAS signaling pathway (CD95), Fc epsilon receptor I signaling in mast cells, IGF-1 signaling pathway, IL 2 signaling pathway, IL 6 signaling pathway, IL12 and Stat4 dependent signaling pathway in Th1 development, inhibition of cellular proliferation by Gleevec, insulin signaling pathway, keratinocyte differentiation, MAPKinase signaling pathway, METS affect on macrophage differentiation, nerve growth factor pathway (NGF), oxidative stress induced gene expression *via* Nrf2, PDGF signaling pathway, Pertussis toxin-insensitive CCR5 signaling in macrophage, repression of pain sensation by the transcriptional regulator DREAM.

Table 5.7: The genes that showed expression difference between the groups for the pooled SOL and EDL muscles.

	Control	**OVX**	**OVX-TNF**	**P-value**	**FDR**
Empty spiracles homeobox 2	23,356	39,330	39,46	0,0002	0,983
KH-type splicing regulatory protein	14,287	20,012	24,2142	0,0002	0,983
SPEG complex locus	11,524	13,485	19,022	0,0006	0,983

Table 5.8: The genes that shows expression difference in between groups for the pooled SOL and EDL muscles (P=0.01).

	Control	OVX	OVX-TNF	P-value	FDR
asparaginase like 1	210,702	159,538	136,291	0,008507	0,983
bone morphogenetic protein 1	27,093	28,632	39,847	0,00924	0,983
coiled-coil domain containing 95	21,014	19,914	15,162	0,008206	0,983
chemokine (C-C motif) ligand 7	8,366	8,392	15,884	0,00646	0,983
CD248 molecule, endosialin	14,925	14,965	11,698	0,009805	0,983
cartilage intermediate layer protein 2	23,821	37,012	41,852	0,001319	0,983
chymase 1, mast cell	47,259	28,876	59,476	0,00743	0,983
cartilage associated protein	14,237	10,928	9,827	0,004771	0,983
dermokine	31,321	25,813	20,783	0,002022	0,983
empty spiracles homeobox 2	23,357	39,331	39,461	0,000213	0,983
GATA zinc finger domain containing 2B	48,069	51,623	31,330	0,004172	0,983
glycolipid transfer protein domain containing 1	60,735	58,950	41,865	0,004524	0,983
interferon (alpha, beta and omega) receptor 1	6,582	4,922	5,544	0,006989	0,983
inner membrane protein, mitochondrial	40,986	30,834	58,169	0,00516	0,983
KH-type splicing regulatory protein	14,287	20,012	24,214	0,00029	0,983
hypothetical LOC290577	16,195	13,416	10,470	0,009415	0,983
olfactomedin-like 1	50,530	55,535	81,908	0,007683	0,983
protein kinase C, beta	13,849	18,203	25,905	0,001265	0,983

Table 5.8 continued

pyridine nucleotide-disulphide oxidoreductase domain 2	17,006	19,294	28,353	0,006696	0,983
RNA binding motif protein 12B	34,921	31,675	59,208	0,006104	0,983
similar to 2810022L02Rik protein	25,849	39,779	40,124	0,008567	0,983
similar to 2810022L02Rik protein	50,077	75,937	77,958	0,009822	0,983
similar to HSPC288	12,137	12,793	16,964	0,006897	0,983
similar to UDP-glucose: glycoprotein glucosyltransferase 2	8,862	9,499	13,810	0,00243	0,983
similar to Docking protein 5 (Downstream of tyrosine kinase 5) (Protein dok-5)	95,908	69,562	46,952	0,009334	0,983
similar to MYST histone acetyltransferase monocytic leukemia 4	79,127	93,446	108,622	0,006356	0,983
Rho family GTPase 3	11,827	8,605	14,646	0,002357	0,983
ribosomal protein S6 kinase, 70kDa, polypeptide 1	72,750	64,690	39,604	0,002775	0,983
Rtf1, Paf1/RNA polymerase II complex component, homolog (S. cerevisiae)	110,329	152,196	115,450	0,009686	0,983
SH3 domain and tetratricopeptide repeats 1	9,035	14,058	14,797	0,000675	0,983
SPEG complex locus	11,524	13,486	19,023	0,007139	0,983
supervillin	43,662	45,542	25,491	0,00835	0,983
thymine-DNA glycosylase	6,806	7,027	9,154	0,006721	0,983
toll-like receptor 4	14,105	9,485	20,151	0,008964	0,983
tocopherol (alpha) transfer protein-like	7,322	7,195	10,839	0,003454	0,983
ubiquitin-conjugating enzyme E2, J1	171,689	142,267	119,972	0,007852	0,983
WW domain binding protein 2	20,571	20,577	15,588	0,008284	0,983
xylosyltransferase II	25,810	31,840	37,345	0,004738	0,983
zinc finger protein 143	59,825	42,626	40,216	0,007683	0,983

When the SOL and the EDL muscles of each group of rats were pooled, the intensities of only 3 genes showed significant difference in between groups. They were routine regulatory proteins belonging to the non-specific muscle-related processes (Table 5.7). However when the P value was 0.01, several expression differences in many genes were observed (Table 5.8).

Table 5.9: The genes that show expression difference between the OVX and the control groups.

Gene Name	Control	OVX	Fold Change	P value
similar to Docking protein 5 (Downstream of tyrosine kinase 5) (Protein dok-5)	27,640	16,332	1,692	0,005
cleavage stimulation factor, 3' pre-RNA, subunit 1	38,414	26,632	1,442	0,004
zinc finger protein 143	59,825	42,626	1,404	0,003
solute carrier family 30 (zinc transporter), member 9	17,688	12,671	1,396	0,005
SHC (Src homology 2 domain containing) transforming protein 2	43,626	31,331	1,392	0,007
phospholipase C, beta 2	24,105	17,937	1,344	0,01
acyl-Coenzyme A oxidase 2, branched chain	15,187	11,348	1,338	0,01
interferon (alpha, beta and omega) receptor 1	6,582	4,922	1,337	0,004
galanin-like peptide	14,011	10,691	1,311	0,006
cartilage associated protein	14,237	10,928	1,303	0,009
zinc finger and BTB domain containing 10	7,680	5,929	1,295	0,008
leucine rich repeat containing 4B	9,920	7,719	1,285	0,007

Table 5.9 continued

uroplakin 3A	12,465	9,808	1,271	0,007
salvador homolog 1 (Drosophila)	10,743	8,469	1,269	0,007
deoxycytidine kinase	5,809	4,621	1,257	0,009
adaptor-related protein complex 3, mu 1 subunit	10,823	8,661	1,250	0,009
a disintegrin and metallopeptidase domain 1a	32,305	26,524	1,218	0,008
syntaxin 1A (brain)	7,540	9,925	0,760	0,009
myosin IF	11,354	15,122	0,751	0,008
X-linked myotubular myopathy gene 1	30,425	41,725	0,729	0,002
Rtf1, Paf1/RNA polymerase II complex component, homolog (S. cerevisiae)	110,329	152,196	0,725	0,001
similar to RIKEN cDNA 2310007F12	29,028	40,615	0,715	0,005
KH-type splicing regulatory protein	14,287	20,012	0,714	0,004
ATP synthase, H+ transporting, mitochondrial F1 complex, gamma polypeptide 1	41,732	59,036	0,707	0,006
melanoma antigen, family H, 1	28,783	41,243	0,698	0,006
AT hook, DNA binding motif, containing 1	22,385	32,254	0,694	0,009
ubiquitin C	3887,136	5631,036	0,690	0,006
bone morphogenetic protein 6	36,219	53,221	0,681	0,008
heparan sulfate 2-O-sulfotransferase 1	84,409	125,260	0,674	0,001
cAMP responsive element modulator	87,989	132,525	0,664	0,003
similar to 2810022L02Rik protein	50,077	75,937	0,659	0,004

Table 5.9 continued

similar to 2810022L02Rik protein	25,849	39,779	0,650	0,007
cartilage intermediate layer protein 2	23,821	37,012	0,644	0,00
SH3 domain and tetratricopeptide repeats 1	9,035	14,058	0,643	0,006
apoptosis-inducing factor, mitochondrion-associated 2	20,385	32,871	0,620	0,006
similar to homeobox-containing transcription factor	13,987	22,570	0,620	0,004
hairy/enhancer-of-split related with YRPW motif 1	22,754	37,715	0,603	0,001
PHD finger protein 12	19,353	32,105	0,603	0,002
empty spiracles homeobox 2	27,942	46,773	0,597	0,009
doublesex and mab-3 related transcription factor 2	23,357	39,331	0,594	0,0001
similar to RIKEN cDNA 1200009O22; EST AI316813	40,020	71,375	0,561	0,007
guanine nucleotide binding protein (G protein), beta polypeptide 1	14,468	27,019	0,535	0,008
bone marrow stromal cell antigen 2	23,162	46,604	0,497	0,003

When the Control group was compared to the OVX group, the intensity of the transcripts of the genes that showed expression difference in-between groups presented differences (Table 5.10). Expression differences in several genes were observed between the control group muscles and the OVX group muscles. Some pathways that those differing genes play role in are: MAPK signaling pathway focal adhesion, insulin signaling pathway, natural killer cell mediated cytotoxicity, VEGF signaling pathway, calcium signaling pathway, Gap junction, GnRH signaling pathway, inositol phosphate metabolism, long-term depression, long-term

potentiation, phosphatidylinositol signaling system, taste transduction, Wnt signaling pathway, fatty acid metabolism, PPAR signaling pathway, IFN alpha signaling pathway, cytokine-cytokine receptor interaction, Jak-STAT signaling pathway, natural killer cell mediated cytotoxicity, toll-like receptor signaling pathway, immunology, purine metabolism, pyrimidine metabolism, gene regulation, pharmacology, transcription, ATP synthesis, oxidative phosphorylation, PPAR signaling pathway, TGF-beta signaling pathway, development, glycan structures-biosynthesis 1, heparan sulfate biosynthesis, repression of pain sensation by the transcriptional regulator DREAM.

CHAPTER 6

DISCUSSION

Skeletal muscle dysfunction and structural and molecular changes were observed following ovariectomy in the rats in this study. This finding was in line with previous studies [10, 11]. Contraction responses in slow-(SOL) and fast-(EDL) twitch muscles of the OVX rats and the effect of TNF-alpha antagonist administration to functional responses were investigated in the functional part of this study. The SOL and the EDL muscles of the OVX mice generated lower maximum twitch forces than did those of the control group. Maximum isometric twitch tension at 0.1 Hz and tetanic twitch responses of the fast-twitch EDL muscle, were lower in the OVX group compared to that of the control group. This finding pointed out a functional loss in the EDL muscles of the OVX group while TNF-alpha antagonist administration recovered this deterioration in the OVX-TNF group. This recovery against functional loss was not observed in the maximum isometric twitch tension of the slow-twitch SOL muscle at 0.1 Hertz. Tetanic stimulations of the SOL muscles of the OVX rats however provided weaker contraction responses indicating a functional loss. This loss recovered by TNF-alpha antagonist administration. TNF-alpha stimulates loss of skeletal muscle function [81]. Therefore findings of this study demonstrated a TNF-alpha pathway related muscular function deterioration in the OVX rats which recovered by TNF-alpha antagonist administration at tetanic stimulations.

Two upper muscle atrophy and functional deterioration pathways, the TNF-alpha related and the non-related one were previously defined [15,16,17,59,85]. Findings of this study concurred that the TNF-alpha pathway has a key role in

skeletal muscle functional deterioration after OVX in rats and TNF-alpha antagonist administration recovered this state. Based on the findings of this study and a previous similar study in which positive effects of infliximab was proved for dystrophic muscle [73], TNF-alpha antagonist administration can have a positive effect on both slow and fast twitch skeletal muscle function recoveries in OVX rats. In the EDL muscle, the lower maximum isometric twitch responses caused by OVX totally were recovered totally by TNF-alpha antagonist administration whereas in the SOL muscle they recovered only partially. Difference between the EDL and the SOL muscle responses could have been caused by the fiber-type compositions. The SOL muscle of adult Sprague-Dawley rats contains 83% of Type I and 17% of Type II fibers whereas the EDL muscle contains more Type II fibers than Type I fibers [55]. The TNF-alpha antagonist administration resulted in more pronounced recovery of fast-twitch muscle.

Ovariectomy is associated with increase in body fat and insulin resistance [82]. Body weight including skeletal muscle weight increased after OVX in this study. Muscle weight to body weight ratio was higher in the OVX group which recovered by TNF-alpha antagonist administration. We observed skeletal muscle weight increase in the OVX rats agreeing with previous studies [10,13]. In definition, skeletal muscle weight loss can be expected from the atrophic situation however increase of organ weights following OVX was also defined in previous studies [10, 83]. Increase in skeletal muscle weight in the OVX rats can be explained not only due to the direct effect of estrogen on skeletal muscles but due to the general increase of organ weights as in previous studies [10]. TNF-alpha antagonist administration inhibited skeletal muscle weight increase in rats. This demonstrated that the degeneration and adaptation of skeletal muscles after OVX is TNF-alpha pathway related as skeletal muscle weight changes recovered with TNF-alpha antagonist administration.

Femoral BMD decrease was recorded at the end of 3 months in the OVX groups but not in the control group. Success of OVX can be confirmed by uterus atrophy [50]. Severe atrophy of the uterus was observed in the OVX groups. Yet as a

limitation to the study we did not measure serum estrogen levels in the OVX rats. Also low-calcium diet is known to induce BMD loss [39,40]. We used a lowered calcium diet that did not interfere with skeletal muscle function. The positive effect of TNF-alpha antagonist administration in osteoporosis was previously defined in humans [84]. In this study however we were not able to observe a recovery in BMD after TNF-alpha antagonist administration. This may be a dose dependent issue as we administered weekly 10μg/g of TNF-alpha antagonist to rats. This dose was used in a previous study which proves to protect skeletal muscles from dystrophic necrosis in a rodent model [73].

In histological analyses of the HE stained sections of the OVX and the OVX-TNF group EDL muscles, splitting of fibers and different sized fibers were observed pointing out a deterioration and the initial stages of atrophy. Central nucleus was observed in the OVX group EDL muscles designating myopathies [56]. A small cluster of atrophic fibers were observed in the OVX group EDL muscles.

In the HE stained sections of the OVX group SOL muscles, splitting of fibers and different sized fibers were observed. Different sized fibers and the central nucleus was also prominent in the OVX-TNF group SOL muscles. Fat cell infiltration was also noticed in both the OVX and the OVX-TNF group skeletal muscles. These findings suggest that infliximab administration was not effective in preventing structural changes that were occurring in the OVX rat skeletal muscles.

NADH-TR staining results enabling fiber type differentiation has shown that in the EDL muscles of the control group, fast-twitch Type II fibers were dominant in percentage whereas in the OVX and the OVX-TNF group slow-twitch Type I fibers were in dominance. Atrophy and hypertrophy analyses are generally carried out with the conventional lesser diameter measurements [56] or cross sectional area (CSA) determination. In this study we calculated both lesser diameters and cross sectional areas (CSA) of muscle fibers to disclose ambiguity and found correlated diameter and CSA values. NADH-TR analysis also showed that Type I fibers of the EDL muscles which increased in the OVX and the OVX-TNF groups in numbers also

increased in fiber diameter and areas when compared to the control group. This increase in number, diameter and area was not observed statistically in the SOL muscles. Type II fiber amount was not sufficient to statistically analyze percentages in the SOL muscles. Increase in Type I areas can also be interpreted in accordance to the absence of general increase in organ weights or compensating hypertrophy in Type II fibers. This was indicating a Type II specific atrophy. Type II atrophy is a non-specific finding presenting in conditions including osteomalacia and cachectic states [52]. Hypertrophy of skeletal muscle fibers can be mixed with pseudohypertrophy in where the volume of skeletal muscle increases because of fatty infiltration; an inflammatory process that is observed in tumor cases [52].

Previous research proved that the p65 molecule activation that increased in TNF-alpha induced cachectic atrophy was not observed in disuse atrophy [15]. The p65 molecule increased in the OVX group EDL and SOL muscles. This finding supported our hypothesis that TNF-alpha related atrophy establishes in the OVX rats. The OVX-TNF group SOL muscles furthermore presented a similar more scarcely immunlabeled pattern with the control group suggesting that infliximab treatment may have an inhibitory effect on p65 related skeletal muscle deterioration. The OVX-TNF group EDL muscles p65 immune labeling was also significantly lower from that of the OVX group suggesting a protecitve effect of infliximab also in the EDL muscle.

Cytoplasmically stained p50 molecule labeling patterns have shown no difference in all groups' EDL muscles. The p50 labeling of the SOL muscle of the OVX-TNF group was lower than that of the other two groups. The p50 molecule activation and its translocation to the nucleus were observed in both the cachectic and disuse atrophies [15]. The reduction of p50 immune labeling in the OVX-TNF SOL muscles can be considered as a positive catabolism intervention effect.

MyoD molecule is important in muscle differentiation and myotube formation and MyoD was shown to be degraded by the ubiquitin ligases atrogin or MAFbx [17]. The presence of MyoD in other words represents muscle regeneration. MyoD

expression in the OVX and the OVX-TNF group SOL muscles increased whereas in the EDL muscle labeling increased only in the OVX group. This suggests a regeneration that occurs in the OVX group agreeing with the central nuclei findings especially in the OVX group but this finding disagreed with the expectation of the negative NF-kB effect on MyoD pronounced in muscle cachexia [20].

The C-Rel molecule moderately increases in disuse atrophy [15]. Staining intensity of C-Rel increased in the OVX-TNF group SOL muscles. Differences between groups in the EDL muscles were not observed. The Bcl3 molecule which is also a protein that is upregulated in disuse atrophy [15] was not different in between groups after the immune labeling of both the SOL and the EDL muscles supporting our hypothesis that muscle atrophy in OVX rats is caused by the TNF-alpha dependent cachectic pathway but not the disuse atrophy pathway.

According to the findings of the electron microscopy analyses, the number of mitochondria was normal as expected in the fast-type EDL muscles of the control group. Slow twitch skeletal muscles need many mitochondria for the aerobic process. The slow type SOL muscles of the control group contained large amount of mitochondria under the sarcoplasmic reticulum as was expected from a slow-twitch aerobic muscle and they had well-defined Z bands. The sarcomere structure was slightly disturbed in the fast EDL muscles of the OVX group pointing out a defect; mitochondria were partly swollen yet the overall condition of the muscle fibers seemed normal. The SOL muscles of the OVX group contained less amount of mitochondria compared to the control group suggesting a rationale for the functional loss due to the insufficient energy production. Nevertheless, the general condition of the muscle fibers seemed normal. The muscle fibers however were slightly thicker than normal in both the OVX and the OVX-TNF group exhibiting a swollen state that can be a result of increased fluid content as well as true muscle mass; also spaces inside the fibers pointing fiber deteroriation were observed in some parts of the skeletal muscle. The fast EDL muscles of the OVX-TNF group attained its healthy state with an even amount of mitochondria amount and distribution. The spaces

inside the fibers that were caused during muscle fiber internal splitting, however were also observed in the OVX-TNF group. This suggests ultra structural recovery was not accomplished by infliximab administration. The SOL muscles of the OVX-TNF group contained high amounts of glyogen and mitochondria and they had defined cristae and T-tubulus structures. Though rapid protein breakdown can take place during muscle fiber atrophy, morphological evidence is hardly provided and lysosomal content generally does not increase significantly [52]. Lysosomal increase in muscle fibers was not observed in this study.

Literature search [73,86,87,88,89,90,91,92] on TNF-alpha blockers in rat revealed that the dose of infliximab for intraperitoneal use is about 10 μg/g. In clinical practice the human dose of infliximab for several autoimmune diseases are defined as 5.0–10.0 mg/kg per infusion for infliximab [86,92]. There were several studies on infliximab injection of rats involving differing dosages for different conditions (0.5μg/g x5 [87] autoimmune uveitis; 1.25μg/g/week x12 [88] diabetes; 20 μg/gx1 [89] IBD; 2μg/g/week x5 [90] Hepatic Fibrosis, 5μg/gx1 [91] spinal cord injury). We chose to use the dosage that is proven to have positive effect on skeletal muscles of rats [73] and also approximately the same dosage that was used in a previous study that claims to adjust the infliximab dosage for rat metabolic rates compared to the human metabolic rates and had a dosage study in the liver showing that the positive effects start to occur at the 5-10μg/g threshold [86]. Pharmacology review of the infliximab including animal studies before entering to the market shows that a dosage study in human-TNF alpha expressing transgenic mice Tg197 indicated a theurapetic efficacy with 10μg/g dose in the presence of an induced immune response[93]. As a limitation to the study we can say that we worked on a single dose of infliximab which restrains us from making dose-dependent effects of infliximab in the skeletal muscle.

During microarray studies, infliximab did not alter the expression of TNF-alpha. Previous studies reported that anti-TNF antibody did not effect expression of mRNA levels in rats and humans [94,95]. In these studies it was suggested that an

indirect effect of the antagonist could lead to changes in other molecules interacting with TNF-alpha; this may also be the case in this study.

Though serum levels of TNF-alpha could be measured by special bioassays; two previous did not measure TNF- alpha serum levels [73,89] and two other studies presented no significance effect of infliximab tratment on serum TNF-alpha level was recorded [90,96]. Also TNF-alpha receptors in serum did not change with the treatment in humans [95]. As a limitation to this study; due to the findings of these mentioned studies we excluded the measurement of serum TNF-alpha levels of rats before and after the treatment.

During our microarray studies significant difference was not observed directly in NF-kB proteins. Yet there has been changes in other molecules that are in interactions with NF-kB pathway molecules, which may have indirect effects on the NF-kB pathway, the muscle energy metabolism and the muscle catabolism.

TNF-alpha translocates NF-kB proteins to the nucleus rather than regenerating it [97]. Therefore, higher staining of the p65 in the nucleus that was observed in immunohistochemitry, but no significant changes in the mRNA levels were reasoned. TNF–alpha stimulation is known to increase activity of redox sensitive kinases including Protein Kinase C (PKC) and enhance conjugation of ubiquitin to muscle proteins [81,98]. The increase of PKC expression in the OVX and the OVX-TNF groups suggested that a TNF-alpha activation of PKC might have occurred in the OVX rats but this activation could not be prevented by infliximab administration. There has been a slight fall in the p70s6kinase mRNA in the OVX group and a more pronounced fall in the OVX-TNF group. The p70s6kinase molecule is essential for the control of muscle cytoplasmic volume by Akt and mTOR [99]. Deletion of p70s6kinase does not affect myoblast cell proliferation but reduces myoblast size, generates smaller nuclei and its absence may result with an anti-hypertrophic condition. The low amount of p70s6kinase in the OVX-TNF group may be the reason of the lesser skeletal muscle mass in the OVX-TNF group.

UbuqitinC (UbC) expression increased in the OVX rats in our study. UbC plays a critical role in the ubuquitin-proteosome protein breakdown pathway and ubiquitinates p70s6kinase. It acts in the PPAR pathway which plays a role in lipid metabolism of skeletal muscle. The UbC mRNA is typically increased more than other ubiquitin mRNA's when there was evidence of skeletal muscle wasting and ubiquitin-proteosome system activation in catabolic patient or rat skeletal muscles [100,101]. Since there was a simultaneous increase in ubiquitin mRNA, it was suggested that UbC transcription is an integral part of the program of responses that results in muscle atrophy [100]. Besides that, UbC expression was shown to increase in disuse atrophy of rat skeletal muscles and this agrees with our description of muscle atrophy occurring in the OVX rats. Also TNF-alpha is known to increase ubiquitin mRNA levels in intact skeletal muscle [98]; this supports the probability of a TNF-alpha effect on the OVX rat muscles.

Another protein RhoE expression decreased in the OVX rats where it was normal in the control and the OVX-TNF groups. RhoE is a GTPase family protein that plays a role in muscle myogenesis and myoblast alignment; its expression increases at skeletal muscle regeneration [102]. The RhoE molecule also inhibits phosphorylation of the 4EBP1 molecule which was also shown to change expression in muscle atrophy and the hypertrophy mechanism [59,60]; thus a fall in the RhoE molecule may point out a defect in muscle regeneration in the OVX group rats.

Acyl-coenzyme A oxidase 2 (ACOX2) mRNA expression which plays a role in the lipid metabolism decreased in the OVX group rats. ACOX2 has a common regulatory role in muscle growth. It regulates re-growth of the atrophied muscle and its inhibition reduces hypertrophy [103,104]. ACOX2-dependent prostoglandin synthesis is essential during early muscle regeneration and ACOX2 pathway products have a major influence in the muscle healing process [105,106]. A fall in the ACOX2 level after OVX may therefore agree with a defect in the muscle healing process and at our atrophy definition in the OVX rats.

The two transcripts of transcription factors Nur77 and Jun oncogene gave different expression results in the OVX group than the control and the OVX-TNF groups specifically in the SOL muscles. Nur77 is down-regulated in the OVX group SOL muscles whereas Jun oncogene was upregulated. Both Jun and Nur77 mRNA expressions were shown to increase in the microarray analysis of the skeletal muscles bearing disuse atrophy [60]. By their role in JAK-STAT signaling they may have several effects on gene regulation of muscle metabolism: Nur77 is known to function by Jun phosphorylation whose expression also changed in our study [107]. They both play role in inflammatory diseases [108] suggesting an inflammatory aspect to our muscles like in the cachectic muscle. Nur77 deletion reduces skeletal muscle glucose utilization [109] and local muscle contractile activity is required for increased Nur77 [110]. Atrophy in the SOL muscles may therefore have reduced contraction and resulted in poorer glucose utilization feeding the atrophy or vice versa. The Jun molecule which is upregualted in many cancers including osteosarcoma [111] increased in the OVX group comparing to that of the control and the OVX-TNF groups. This may suggest an unhealthy growth in the OVX skeletal muscles which was prevented in the OVX-TNF group. Jun controls NF-kB p65 recruitment and this may explain us the p65 increase in OVX muscle immunohistochemistry.

Protein phosphatase 1 subunits, which was downregulated in EDL muscles of OVX and OVX-TNF groups was shown to decrease in both hypertrophy and sarcopenia microarrays previously [60,112]. Since it acts in glycogen metabolism in muscle it may be in the charge of multiple regulations of energy metabolism in muscle for adapting different conditions.

Talin which may play an important role in integrin signaling pathway, muscle contraction, apoptotic signaling and satellite cell differentiation was previously presented to decrease in disuse atrophic muscle [60]. In our experiment, in the SOL muscles, an increase in the expression of Talin is observed in the OVX-TNF group. Since its reduction was shown in atrophic muscle its increase may have an effect of atrophy prevention in the OVX-TNF group. There are up-regulated and down-

regualted other molecules whose possible effects on skeletal muscle metabolism in the OVX rats needs further discussion.

In this study changes in skeletal muscles of OVX rats as a postmenopausal osteoporosis model were investigated. Twitch responses, morphological and histological assasments, immunohistochemistry results, electron microscopy observations and mRNA expression data show that functional, structural and molecular changes occur in OVX rat skeletal muscles in agreement with the previous studies [10,11,14]. According to the results TNF-alpha antagonist administration recovered skeletal muscle dysfunction (totally in the EDL and partly in the SOL msucles) and weight gain in OVX rats. The recovery was more prominent in the fast EDL muscle. But this modulation was not sufficient enough for structural recovery. To conclude, TNF-alpha involved inflammatory pathways play a role in functional loss and partial degeneration of skeletal muscles after OVX but it is not the only pathway leading to structural deterioration, several other molecules may also be involved following a complex pathway. But it is at least can be proposed that atrophy and degeneration pronounced in OVX rat skeletal muscles is not solely related to disuse atrophy justified by a sedentary life style.

REFERENCES

1. Bonnick, S. L., Osteoporosis in Men and Women, Clinical Cornerstone, 811:28-39, 2006

2. Raisz, L. G., Pathogenesis of osteoporosis: concepts,conflicts, and prospects, J. Clin. Invest. 115:3318–3325, 2005

3. Lindsay, R., Hormone and Bone Health in Postmenopausal Women, Endocrine, 24:223-30, 2004

4. Parvez, T., Postmenapausal Osteoporosis, JK-Practitioner, 11:4:281-283, 2004

5. Turner, A. S., Animal models of osteoporosis- necessity and limitations, European Cells and Materials, 1:66-81, 2001

6. Schönau, E., Fricke, O., Muscle and Bone: a Functional Unit, Dtsch Arztebl, 103:50: :3414–9, 2006

7. Takata, K., The nature and function of mononuclear cells on the resorbed surfaces of bone in the reversal phase during remodeling, Annals of Anatomy - Anatomischer Anzeiger, 183:2:103-110, 2001

8. Weiss, A., Arbel, I., Steinhagen-Thiessen, E., Silbermann, M., Structural changes in aging bone: osteopenia in the proxmal femurs of female mice, Bone, 12:165-172, 1991

9. Heikkinen, J., Kyllonen, E., Kurttila-Matero, E., Wilen-Rosenqvist, G., Lankinen, K. S., Rita, H., Vaananen, H. K., HRT and exercise: effects on bone density, muscle strength and lipid metabolism:A placebo-controlled 2-year prospective trial on two estrogen-progestin regimens in healthy postmenopausal women, Maturitas 26:139–149, 1997

10. Fisher, J. S., Hasser, E. M., Brown, M., Effects of ovariectomy and hindlimb unloading on skeletal muscle, J.Appl Physiol, 85:1316-1321, 1998

11. Moran, A. L., Warren, G. L, Lowe, D. A., Removal of ovarian hormones from mature mice detrimentally affects muscle contractile function and myosin structural distribution, J Appl Physiol 100:2:548-59, 2006

12. Kobori, M.,Yamamuro, T., Effects of gonadectomy and estrogen administration on rat skeletal muscle, Clin Orthop Rel Res, 243:306–311, 1989

13. McClung, J. M., Davis, J. M., Wilson, M. A., Goldsmith, E. C., Carson, J. A., Estrogen status and skeletal muscle recovery from disuse atrophy, J Appl Physiol, 100:2012-2023, 2006

14. Chen, H., Yao, X. F., Emura, S., Shoumura, S., Morphological changes of skeletal muscle, tendon and periosteum in the senescence-accelerated mouse (SAMP6) : A murine model for senile osteoporosis, Tissue & Cell, 38:5:325-335, 2006

15. Hunter, R. B., Stevenson, E., Koncarevic, A., Mitchell-Felton, H., Essig, D. A., Kandarian, S. C., Activation of an altenative NF-kappaB pathway in skeletal muscle during disuse atrophy, FASEB J, 16:529-538, 2002

16. Hunter, R. B., Kandarian, S. C., Disruption of either the Nfkb1 or Bcl3 gene inhibits skeletal muscle atrophy, J Clin Invest, 114:1504-1511, 2004

17. Zhang, P., Chen, X., Fan, M., Signaling mechanisms involved in disuse atrophy, Medical Hypotheses, 69:2:310-321, 2007

18. Frenette, J., Cai, B., Tidball, J. G., Complement activation promotes muscle inflammation during modified muscle use, Am J Pathol, 156: 2103–2110, 2000

19. Ghosh, S., May, M. J., Kopp, E B., NF-kappaB and Rel proteins: evolutionarily conserved mediators of immune responses, Annu Rev Immunol, 16:225–260, 1998

20. Guttridge, D. C., Mayo, M. W., Madrid, L. V., Wang, C. Y., Baldwin, A. S., NF-kappaB-induced loss of MyoD messenger RNA: possible role in muscle decay and cachexia, Science, 289:2363–2366, 2000

21. Knight, D. M., Trinh, H., Le, J., Construction and initial characterization of a mouse-human chimeric anti TNF antibody, Mole Immuno 30:1443-1453, 1993

22. Scallon, B. J., Moore, M. A., Trinh, H., Chimeric anti-TNF alfa monoclonal antibody cA2 binds to recombinant transmembrane TNF alfa and activates immune effector functions, Cytokine, 7:251-259, 1995

23. Silverthorn, D. U., Human Physiology: An Integrated Approach, Pearson Education Inc., San Fransisco, 739-46, 2004

24. Wolff, J., The Law of Bone Remodeling, Springer Inc., New York, 1986

25. Frost, H. M., Changing concepts in skeletal physiologie:Wolff's Law, the Mechanostat and the "Utah Paradigm", J Hum Biol 10:599–605, 1998

26. Passi, N., Gefen, A., Trabecular bone contributes to strength of the proximal femur under mediolateral impact in the avian, J Biomech Eng, 127:1:198-203, 2005

27. Sinaki, M., Muscoskeletal Challanges of Osteoporosis, Aging, 10:249-262, 1998

28. Gefen, A., Be'ery-Lipperman, M., Contribution of Muscular weakness to osteoporosis: Computational and animal models, Clinical Biomechanics, 20:984-997, 2005

29. US National Institutes of Health, Osteoporosis Prevention, diagnosis and therapy, NIH Consensus statement 17:1-45, 2007

30. Iacono, M. V., Osteoporosis: A National Public Health Priority, Journal of Peri Anesthesia Nursing, 22:3:175-183, 2007

31. National Osteoporosis Foundation, Clinician's Guide to Prevention and Treatment of Osteoporosis, Washington, DC, National Osteoporosis Foundation, 2010

32. Compston, J., Cooper, A., Cooper, C., Francis, R., Kanis, J. A., Marsh, D., McCloskey, E. V., Reid, D. M., Selby, P., Wilkins, M., on behalf of the National Osteoporosis Guideline Group, Guidelines for the diagnosis and management of osteoporosis inpostmenopausal women and men from the age of 50 years in the UK, Maturitas, 62:105–108, 2009

33. Pinkerton, J. V., Dalkin, A. C., Combination therapy for treatment of osteoporosis: A review, American Journal of Obstetrics and Gynecology, 197:559-565, 2007

34. International Osteoporosis Foundation, http://www.iofbonehealth.org/patients-public/more-topics/secondary-osteoporosis.html, Last Access date: 05.31.2010

35. An, Y. H., Friedman R. J., Animal models in orthopaedic research, CRC Pres, Florida, 280-293, 1999

36. Barlet, J. P., Coxam, V., Davicco, M. J., Gaumet, N., Animal models of post-menopausal osteoporosis, Reprod Nutr Dev, 34:3:221-36, 1994

37. Atalay, A., Kutsal, Y.G., Yıldırım, M., Onur, R., Description of 'Tail Suspension' as a model of immobilization in rats, Osteoporoz Dünyasından, 8:3:134-135, 2002

38. Hau, J., Van Hoosier Jr, G. L., Handbook of Laboratory Animal Science, Second Edition: Essential Principles and Practices, Volume I, CRC Press, USA , 148-176, 2003

39. Jee, S. S., Yao, W., Overview: Animal Models of Osteopenia and Osteoporosis, J Muscoskele Neuron Interact, 1:3:193-207, 2001

40. Park, J. H., Omi, N., Estrogen defi ciency and low-calcium diet increased bone loss and urinary calcium excretion but did not alter arterial stiffness in young female rats, J Bone Miner Metab, 26:3:218-25, 2008
41. Monreal, M., Vinas, L., Monreal, S., Lavin, E., Lafoz, E., Angles, A. M., Heparin-Related Osteoporosis in Rats, Haemostasis 20:204-207, 1999

42. Egermann, M., Goldhahn, J., Schneider, E., Animal models for Fracture Treatment in Osteoporosis, Osteoporosis Int 16: 129-138, 2005

43. Gambacciani, M., Spinetti, A., de Simone, L., The relative contributions of menapause and aging to postmenapausal vertebral ostoeopenia, J Clin Endocrinol Metab, 77:1148-1151, 1993

44. Gambacciani, M., Spinetti, A., Taponeco, F., Bone loss in perimenopausal women: a longitudinal study, Maturitas, 18:191-197, 1997

45. Ferretti, J. L., Cointry, G. R., Capozza, R. F., Frost, H. M., Bone mass, bone strength, muscle- bone interactions, osteopenias and osteoporoses, Mechanisms of Ageing and Development, 124:269-279, 2003

46. Bigard, X. A., Merino, D., Serrurier, B., Lienhard, F., Guezennec, Y. C., Bockhold, K. J., Whalen, R. G., Role of weight-bearing function on

expression of myosin isoforms during regeneration of rat soleus muscles, Am J Physiol Cell Physiol, 270:C763–C771, 1996

47. Sugiura, T., Estrogen Administration Attenuates Immobilization-Induced Skeletal Muscle Atrophy in Male Rats, The journal of Physiological Sciences, 56:6:393-399, 2006

48. Riggs, B., L., Overview of Osteoporosis, West J Med, 154:1:63–77, 1991

49. Wronski, T. J., Walsh C. C., Ignaszewski, L. A., Histologic evidince for osteopenia and increased bone turnover in ovariectomized rats, Bone, 7:119, 1986

50. Hidaka, S., Okamoto, Y., Royal Jelly Prevents Osteoporosis in Rats: Beneficial Effects in Ovariectomy Model and in Bone Tissue Culture Model, Evidence-based Compl. and Alt. Medicine, 3:3:339-348, 2006

51. Garret, W. E., Best, T. M., Buckwalter, J., Orthopaedic Basic Science , American Academy of Orthopaedic Surgeons Press, USA, 2007

52. Mastaglia, F. L., Walton, J., Skeletal muscle pathology, Churchil Livingstone,1-88, 360-393, 605-621, 1992

53. University of Vermont, Department of Molecular Phsiology and Biophysics, http://physioweb.med.uvm.edu/muscle_physio/striated/striated_sarcomeres.htm, Last Access date: 05.31.2010

54. Wheeless C. R., Wheeless' Textbook of Orthapaedics, http://www.wheelessonline.com/, Last access date: 05.31.2010

55. Armstrong, R. B., Phelps, R. O., Muscle fiber type composition of the rat hindlimb. Am J Anat 171:259–272, 1984

56. Dubowitz, V., Sewry, C. A., Muscle Biopsy: A Practical Approach , Elsevier, Philedelphia, 2007

57. McKinnell, I. W., Rudnicki, M. A., Molecular Mechanisms of Muscle Atrophy, Cell, 29:119:7:907-10, 2004

58. Lecker, S. H., Solomon, V., Mitch, W.E., Goldberg, A. L., Muscle protein breakdown and the ciritical role of the ubiquitin proteosome pathway in normal and disease states, J. Nutr, 129:227-237, 1999

59. Glass, J. D., Skeletal muscle hypertrophy and atrophy signaling pathways, 37:10:1974-84, 2005

60. Stevenson, E. J., Giresi, P. G., Konsarevic, A., Kanderian, S. C., Global Analysis of Gene Expression Patterns During Disuse Atrophy in Rat Skeletal Muscle, J Physiol, 551:33-44, 2003

61. Carson, J. A., Nettleton, D., Reecy, J. M., Differential gene expression in the rat soleus muscle during early work overload-induced hypertrophy, The FASEB Journal express article, 16:207-209, 2001

62. Özdurak, R. H., Düz, S., Arsal, G., Akıncı, Y., Kablan, N., Işıklı, S., Korkusuz, F. Quantitative forearm muscle strength influences radial bone mineral density in osteoporotic and healthy males, Technology and Health Care, 11:4: 253-261, 2003

63. Cauley, J.A., Petrini, A.,M., LaPorte, R. E., Sandler, R. B., Bayles, C. M., Robertson R. J., Slemenda, C. W., The decline of grip strength in the menopause: relationship to physical activity, estrogen use and anthropometric factors, J Chronic Dis, 40:115–120, 1987

64. Phillips, S. K., Rook, K. M., Siddle, N. C., Bruce, S. A., Woledge, R. C., Muscle weakness in women occurs at an earlier age than in men, but strength is preserved by hormone replacement therapy, Clin Sci (Colch.), 84:95–98, 1993

65. McClung, J. M., Davis, J. M, Carson, J. A., Muscle: Ovarian hormone status and skeletal muscle inflammation during recovery from disuse in rats, Exp Physiol 92:219-232, 2007

66. Sitnick, M., Foley, A. M., Brown, M., Spangenburg, E., Ovariectomy prevents the recovery of atrophied gastrocnemius skeletal muscle mass, J Appl Physiol, 100:286–293, 2006

67. Moran, A. L., Nelson, S. A., Landisch, R. M., Warren, G. L., and Lowe, D. A., Estradiol replacement reverses ovariectomy-induced muscle contractile and myosin dysfunction in mature female mice, J Appl Physiol 102:1387–1393, 2007

68. Wattanapermpool, J., Reiser P. J., Differential effects of ovariectomy on calcium activation of cardiac and soleus myofilaments, Am J Physiol Heart Circ Physiol, 277:467-473, 1999

69. Warren, G. L., Lowe, D. A., Inman, C. L., Orr, O. M., Hogan, H. A., Bloomfield, S. A., Armstrong, R. B., Estradiol effect on anterior crural muscles-tibial bone relationship and susceptibility to injury, J Appl Physiol, 80:1660–1665, 1996

70. Hubal, M. J., Ingalls, C. P., Allen, M. R., Wenke, J. C., Hogan H. A., Bloomfield S. A., J Appl Physiol 98:1674-1681, 2005

71. Langen, R. C., Schols, A. M., Kelders, M. C., Wouters, E. F., Janssen-Heininger, Y. M., Inflammatory cytokines inhibit myogenic differentiation through activation of nuclear factor-kappaB, FASEB J 15:1169-1, 2001

72. Langen, R. J. C., Schols, A. M. W. J., Kelders, M. C. J. M.,van der Velden J. L. J., Wouters, E. F. M, Janssen-Heininger, Y. M. W., Tumor necrosis factor-a inhibits myogenesis through redox-dependent and independent pathways, Am J Physiol, Cell Physiol, 283:714-721, 2002

73. Grounds, M. D., Torrisi, J., Anti-TNFalpha (Remicade) therapy protects dystrophic skeletal muscle from necrosis, Faseb J, 18:6:676-82, 2004

74. Bendele, A. M., Chlipala, E. S., Scherrer, J., Frazier, J., Sennello G., Rich, W. J., Edwards, C. K., Combination benefit of treatment with the cytokine inhibitors Interleukin-1 receptor antagonist and PEGylated soluble tumor necrosis factor receptor type I in animal models of rheumatoid arthiritis, Arthiritis & Rheumatism, 43:12:264859, 2000

75. Xu, S. W., Yu, R., Zhao, G. F., Wang, J. W., Early period of fracture healing in ovariectomized rats, Chin J Traumatol, 6:3:160-6, 2003

76. Derave, W., Eijnde, B. O., Ramaekers, M., Hepsel, P., Soleus muscles of SAMP8 mice provide an accelerated model of skeletal muscle senescence, Experimental Gerontology, 40:562–572, 2005

77. Stassijns G., Gayan-Ramirez, G., de Leyn, P., Verhoeven, G., Herijgers, P., de Bock, V., Dom, R., Lysens, R., Decramer, M., Systolic Ventricular Dysfunction Causes Selective Diaphragm Atrophy in Rats, Am J Respir Crit Care Med, 158:1963–1967, 1998

78. Geyikoğlu, F., Temelli, A., Özkaral, A., Morphological Adaptation of Rat Skeletal Muscle to A Cold Environment, Turk J Vet Anim Sci, 26:1121-1126, 2002

79. Dogru, M. T., Aydos, T. R., Aktuna, Z., Korkusuz, P., Zeybek, D., Görgü, N., Korkut, O., Basar, M. M, The effects of beta-blockers on endothelial nitric oxide synthase immunoreactivity in the rat corpus cavernosum, Urology, 75:3:589-97, 2010

80. Uğur, Y., Sarı, O., Uğur, Ö., Korkusuz, P., Varoğlu, E., Arslan, N., Gürcan, N., Yıldırım, M., Sökmensüer, C., Aşan, E., Aras, T., Lack of Correlation Between Tc-99m-sestaMIBI Uptake and Cadherin Expression in Infiltrating Ductal Breast Carcinoma as Prognostic Indicators, Annals of Nuclear Medicine, 17: 281-287, 2003

81. Li, Y. P., Atkins, C.M., Sweatt J. D., Reid, M. B., Mitochondria mediate tumor necrosis factor-a/NF-kB signaling in skeletal muscle myotubes, Antiox Redox Signal ,1: 97–104, 1999

82. Ahmed-Sorour, H., Bailey, C. J., Role of ovarian hormones in the long-term control of glucose homeostasis: Interaction with insulin, glucagon and epinephrine, Horm Res, 13:396-403, 1980

83. Booth, F. W., Tipton, C. M., Effects of training and 17-b estradiol upon heart rates, organ weights, and ligamentous strength of female rats, Int Z Angew Physiol, 27:187–197, 1969

84. Seriolo, B., Paolino, S., Sulli, A., Cutolo, M., Are there any positive effects of TNF-alpha blockers on bone metabolism?, Reumatismo, 58:3::199-205, 2006

85. McKinnell, I. W., Rudnicki, M. A., Molecular Mechanisms of Muscle Atrophy, Cell, 29:119:7:907-10, 2004

86. Barbuio, R., Milanski, M., Bertolo, M. B., Saad, M. J., Velloso, .L A., Infliximab reverses steatosis and improves insulin signal transduction in liver of rats fed a high-fat diet., J Endocrinol 194:3:539-50, 2007

87. Demir, T., Gödekmerdan, A., Balbaba, M., Türkçüoglu, P., Ilhan, F., Demir, N., The effect of infliximab, cyclosporine A and recombinant IL-10 on vitreous cytokine levels in experimental autoimmune uveitis, Indian J Ophthalmol, 54:4:241-5, 2006

88. Moriwaki, Y., Inokuchi, T., Yamamoto, A., Ka, T., Tsutsumi, Z., Takahashi, S., Yamamoto, T., Effect of TNF-alpha inhibition on urinary albumin excretion in experimental diabetic rats, Acta Diabetol, 44:4:215-8, 2007

89. Cury, D. H. B., Costa, J. E., Irika, K., Mijji, L., Garcez, A., Buchiguel, C., Silva, I., Sipahi, A., Protective Effect of Octreotide and Infliximab in an Experimental Model of Indomethacin-Induced Inflammatory Bowel Disease, Digestive Diseases and Sciences, 53:9, 2008

90. Bahcecioglu, I. H., Koca, S. S., Poyrazoglu, O. K., Yalniz, M., Ozercan, I. H., Ustundag, B., Sahin, K., Dagli, A. F., Isik, A., Hepatoprotective Effect of Infliximab, an Anti-TNF-α Agent,on Carbon Tetrachloride-Induced Hepatic Fibrosis. Inflammation 31: 4, 2008

91. Kurt, G., Ergün, E., Cemil, B., Börcek, A. O., Börcek, P., Gülbahar, O., Ceviker, N., Neuroprotective effects of infliximab in experimental spinal cord injury, Surg Neurol. 71:3:332-6, 2009

92. Remicade PI, Centocor Inc.,PA, US, 2006

93. Black,L. E.,Memorandum: Pharmacology Review of the infliximab BLA. ,Clinical Trial Analysis., Centocor Inc., 1998

94. Iimuro, Y., Gallucci, R. M., Luster, M. I., Kono, H., Thurman, R. G., Antibodies to tumor necrosis factor alfa attenuate hepatic necrosis and inflammation causedby chronic exposure to ethanol in the rat, Hepatology, 26:1530–1537, 1997

95. Tilg, H., Jalan, R., Kaser, A., Davies, N. A., Offner, F. A., Hodges, S. J., Ludwiczek, O., Shawcross, D., Zoller, H., Alisa, A., Mookerjee, R. P., Graziadei, I., Datz, C., Trauner, M., Schuppan, D., Obrist, P., Vogel, W., Williams, R., Anti-tumor necrosis factor-alpha monoclonal antibody therapy in severe alcoholic hepatitis, J Hepatol. 38:4:419-25, 2003

96. Koca, S. S., Bahcecioglu, I. H., Poyrazoglu, O. K., Ozercan, I. H., Sahin, K.,Ustundag, B., The Treatment with Antibody of TNF-α Reduces the Inflammation, Necrosis and Fibrosis in the Non-alcoholic Steatohepatitis Induced by Methionineand Choline-deficient Diet, Inflammation, 31:2, 2008
97. Thanos, D., Maniatis T., NF-KB: A Lesson in Family Values, Cell, 80:529-532, 1995

98. Li, Y. P., Reid, M. B., NF-kB mediates the protein loss induced by TNF-a in differentiated skeletal muscle myotubes, Am J Physiol Regulatory Integrative Comp Physiol, 279:1165-1170, 2000

99. Ohanna, M., Sobering, A. K., Lapointe, T., Lorenzo, L., Praud, C., Petroulakis, E., Sonenberg, N., Kelly, P. A., Sotiropoulos, A., Pende, M., Atrophy of S6K1 (-/-) skeletal muscle cells reveals distinct mTOR Effectors for cell cycle and size control, Nat. Cell Biol., 3: 286-94, 2005

100. Marinovic, A. C., Zheng, B., Mitch, W. E., Price, S. R., Ubiquitin (UbC) Expression in Muscle Cells Is Increased by Glucocorticoids through a Mechanism Involving Sp1 and MEK1, The Journal of Biological Chemistry, 277:16673-16681, 2002

101. Bailey, J. L., Wang, X., England, B. K., Price, S.R., Ding, X., Mitch, W. E., The acidosis of chronic renal failure activates muscle proteolysis in rats by augmenting transcription of genes encoding proteins of the ATP-dependent ubiquitin-proteasome pathway, J Clin Invest, 15;97:6:1447-53, 1996

102. Fortier, M., Comunale, F., Kucharczak, J., Blangy, A., Charrasse, S., Gauthier-Rouvière, C., RhoE controls myoblast alignment prior fusion through RhoA and ROCK, Cell Death Differ.,15:8:1221-31, 2008

103. Bondesen, B.A., Mills, S.T., Pavlath, G.K., The COX-2 pathway regulates growth of atrophied muscle via multiple mechanisms, Am J Physiol Cell Physiol, 290:6:C1651-9, 2006

104. Novak, M. L., Billich, W., Smith, S. M., Sukhija, K. B., McLoughlin, T. J., Hornberger, T. A., Koh, T. J., COX-2 inhibitor reduces skeletal muscle hypertrophy in mice, Am J Physiol Regul Integr Comp Physiol., 296:4:R1132-9, 2009

105. Bondesen, B.A., Mills, S. T., Kegley, K. M., Pavlath, G. K., The COX-2 pathway is essential during early stages of skeletal muscle regeneration, Am J Physiol Cell Physiol, 287:2:C475-83, 2004

106. Shen, W., Li, Y., Zhu, J., Schwendener, R., Huard, J.,. Interaction between macrophages, TGF-beta1, and the COX-2 pathway during the inflammatory phase of skeletal muscle healing after injury, J Cell Physiol., 214:2:405-12, 2008

107. Han, Y. H., Cao, X., Lin, B., Lin, F., Kolluri, S. K., Stebbins, J., Reed, J. C., Dawson, M. I., Zhang, X., Regulation of Nur77 nuclear export by c-Jun N-terminal kinase and AktRegulation of Nur77 nuclear export by JNK and Akt Oncogene, 25: 2974-2986, 2006

108. Tsokos, G. C., Principles of molecular rheumataology, Humana Press Inc, NJ, 2009

109. Chao L., C., Zhang, C. Z., Pei, L., Saito, T., Tontonoz, P., Pilch, P. F., Nur77 coordinately regulates expression of genes linked to glucose metabolism in skeletal muscle, Mol Endocrinol, 21:9:2152–2163, 2007

110. Kawasaki, E., Hokari, F., Sasaki, M., Sakai, A., Koshinaka, K., Kawanaka, K., Role of local muscle contractile activity in the exercise-induced increase in NR4A receptor mRNA expression, J Appl Physiol., 106:6:1826-31, 2009

111. Dass, C. R., Khachigian L. M., Choong, P. F. M., c-Jun knockdown sensitizes osteosarcoma to doxorubicin, Mol Cancer Ther, 7:7:1909–12, 2008

112. Giresi, P. G., Stevenson, E. J., Theilhaber, J., Koncarevic, A., Parkington, J., Fielding, R. A., Kandarian, S. C., Identification of a molecular signature of sarcopenia, Physiol Genomics, 2:253–263, 2005